LBL-23916 c.2

Lawrence Berkeley Laboratory

UNIVERSITY OF CALIFORNIA

Materials & Chemical Sciences Division

To be published as a chapter in **Techniques for Characterization of Electrodes and Electrochemical Processes**, R. Varma and J.R. Selman, Eds., John Wiley & Sons, New York, NY, 1989

JUN 7 1989
LIBRARY AND DOCUMENTS SEC

Ellipsometry as an *In Situ* Probe for the Study of Electrode Processes

R.H. Muller

April 1989

TWO-WEEK LOAN COPY

This is a Library Circulating Copy which may be borrowed for two weeks.

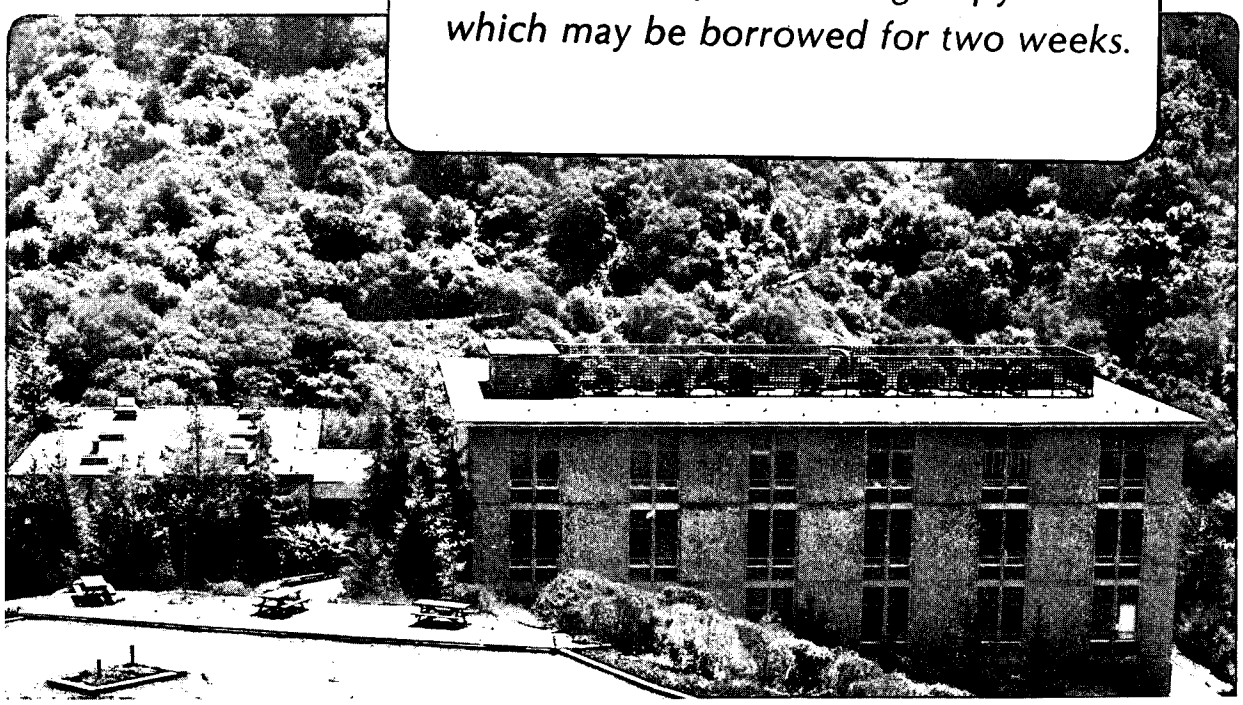

LBL-23916 c.2

Prepared for the U.S. Department of Energy under Contract Number DE-AC03-76SF00098.

DISCLAIMER

This document was prepared as an account of work sponsored by the United States Government. While this document is believed to contain correct information, neither the United States Government nor any agency thereof, nor the Regents of the University of California, nor any of their employees, makes any warranty, express or implied, or assumes any legal responsibility for the accuracy, completeness, or usefulness of any information, apparatus, product, or process disclosed, or represents that its use would not infringe privately owned rights. Reference herein to any specific commercial product, process, or service by its trade name, trademark, manufacturer, or otherwise, does not necessarily constitute or imply its endorsement, recommendation, or favoring by the United States Government or any agency thereof, or the Regents of the University of California. The views and opinions of authors expressed herein do not necessarily state or reflect those of the United States Government or any agency thereof or the Regents of the University of California.

LBL-23916

ELLIPSOMETRY AS AN *IN SITU* PROBE FOR THE STUDY OF ELECTRODE PROCESSES

Rolf. H. Muller

Materials and Chemical Sciences Division
Lawrence Berkeley Laboratory
1 Cyclotron Road
Berkeley, CA 94720

and

Department of Chemical Engineering
University of California at Berkeley

Chapter in

Techniques for Characterization of Electrodes and Electrochemical Processes

Edited by R. Varma and J.R. Selman

Published by Wiley, New York, in collaboration with
The Electrochemical Society

This work was supported by the Director, Office of Energy Research, Office of Basic Energy Sciences, Materials Sciences Division, of the U.S. Department of Energy under Contract No. DE-AC03-76SF00098.

ELLIPSOMETRY

1. INTRODUCTION 1

2. OPTICAL PRINCIPLES 3

2.1 Reflection of Light 3

2.1.1 s and p Components 3

2.1.2 Fresnel Coefficients 4

2.1.3 Optical Constants 5

2.1.4 Drude Equation 7

2.2 Polarized Light 8

2.2.1 Linear and Elliptic Polarization 8

2.2.2 Physical and Geometric Parameters of Polarized Light 9

2.2.3 Equation of Ellipsometry 10

2.2.4 Definitions and Conventions 12

2.2.5 Poincaré Sphere 13

2.2.6 Stokes Parameters 15

2.2.7 Matrix Representation 16

2.3 Optical Theory 18

2.3.1 Electromagnetic Theory 18

2.3.2 Coherence 19

2.3.3 Multiple and Inhomogeneous Films 20

2.3.4 Island Films 20

2.3.5 Composite Materials, Effective Media 21

2.3.6 Anisotropic Materials 23

2.3.7 Rough Surfaces 24

2.3.8 Spectroscopic Ellipsometry 24

2.3.9 Reflectance Ellipsometry 25

2.3.10 Multiple-Angle Ellipsometry 25

2.3.11 Transmission Ellipsometry 26

3. INSTRUMENTATION 27

3.1 Classification of Ellipsometers 27

3.2 Compensating Measurement 28

3.2.1 Incident Elliptic Polarization 28

3.2.2 Four-Zone Measurements 29

3.2.3 Alignment 30

3.2.4 Azimuth Modulation 31

3.2.5 Retardation Modulation 33

3.2.6 Achromatic Compensator 34

3.3 Photometric Measurement 34

3.3.1 Rotating-Analyzer Instruments 34

3.3.2 Other Rotating Components 36

3.3.3 Retardation Modulation 37

3.3.4 Multiple Detectors 38

3.4 Other Configurations 38

3.4.1 Return-Path and Principal-Angle Instruments 38

3.4.2 Psi Meters 39

3.4.3 Interferometric Ellipsometry 39

3.4.4 Pulse Ellipsometry 39

3.4.5 Differential Ellipsometry 40

3.4.6 Infrared and Microwave Ellipsometry 40

3.4.7 Imaging and Micro-Ellipsometry 41

4. INTERPRETATION 42

4.1 Optical Models 42

4.1.1 Surface Parameters 42

4.1.2 Measured Parameters 42

4.1.3 Optimization of Models 43

4.2 Combination and Comparison with Other Techniques 44

4.2.1 Vacuum Techniques 45

4.2.2 Radiotracer Techniques 45

4.2.3 Other Techniques 46

5. APPLICATIONS 47

5.1 Anodic Oxidation 47

5.1.1 Valve Metals 47

5.1.2 Nickel, Iron, and Manganese 48

5.1.3 Platinum and Gold 48

5.1.4 Other Metals 49

5.1.5 Semiconductors 50

5.2 Gas-Phase Oxidation 50

5.3 Corrosion 51

5.3.1 Passivation 51

5.3.2 Corrosion Layers 52

5.3.3 Corrosion Inhibitors 52

5.4 Cathodic Metal Deposition 52

5.4.1 Underpotential Deposits 52

5.4.2 Nucleation and Growth 53

5.4.3 Effect of Inhibitors 53

5.5 Reduction of Oxides 53

5.5.1 Potential Cycling 53

5.5.2 Electrochromism 54

5.6 Adsorption Processes 54

5.6.1 Double Layers 54

5.6.2 Physical Adsorption 54

5.6.3 Chemisorption 55

5.6.4 Oriented Layers 55

5.7 Mass-Transfer Boundary Layers 56

5.8 Electronic Materials 56

5.8.1 Surface Cleaning 56

5.8.2 Ion Implantation 57

5.8.3 Vapor-Phase Metal Deposition 57

5.8.4 Other Films 57

5.9 Optical Constants 58

5.9.1 Contamination 58

5.9.2 Roughness 59

5.9.3 Microstructure 59

5.9.4 Anisotropy 59

5.10 Liquid Surfaces 60

5.11 Other Studies 60

6. OUTLOOK 61

6.1 Optical Theory 61

6.2 Instrumentation 61

6.3 Interpretation 62

6.4 Applications 62

1. INTRODUCTION

Ellipsometry is an optical technique for characterizing surfaces and thin films. The technique involves the reflection of polarized (generally monochromatic) light from the surface under study and the measurement of the change in the state of polarization caused by the reflection. The measurements usually involve elliptically polarized light, a fact that is recognized in the present name of the technique, and yield two parameters that characterize the change in the state of polarization.

Ellipsometer measurements are often extremely sensitive to the presence of very thin surface layers (including fractional monolayers), to changes in their thickness (or coverage), and to changes in surface topography at an atomic scale. The range of film thicknesses that can be observed is very large (reaching to several wavelengths optical thickness), and the surfaces being studied may be immersed in any optically transparent medium, including liquids. These characteristics make the use of ellipsometry for electrochemical studies particularly attractive.

Although the reflection of polarized light has been studied for more than a century, as pointed out in the historical review by Hall (1), the term "ellipsometry" was not introduced until 1945, by Rothen (2), who described in his recollections (3) that he thought the otherwise appropriate term "polarimetry" had been given a restricted meaning by chemists for the measurement of optical rotation. Significant early work by Vašíček employs the terms "polarimetry" or "polarization spectroscopy" (4,5).

Several reviews of ellipsometry have been published. They include early publications by Rothen (3), Zaininger and Revesz (6), and Weingart and Johnston (7). An introduction to the physical principles of ellipsometry has been given by this author in a previous book chapter (8), and electrochemical applications have been reviewed in the same volume by Kruger (9). More recent review papers include those by Kinosita and Yamamato (10), who discuss the use of different types of instruments and the determination of optical constants. Reviews by Neal (11) and Paik (12) are also available. Aspnes has compared the characteristics of null and photometric measurements and has treated the determination of spectral properties of materials (13), the sensitivity to monolayers and roughness (14), and the prospects for outstanding future applications and problems (15). An earlier review of principles and performance of automatic

ellipsometers by this author (16) has been followed more recently by a comprehensive review of different types of instrumentation and their capabilities by Hauge (17). A short article in German by Haller (18) illustrates the use of a compensating instrument for Langmuir film studies, and another short article by Kutko (19) is directed toward a solid-state electronics audience.

Bashara and coworkers have published a short introduction to ellipsometry that makes use of matrix formulations (20) and a substantial review chapter that covers different types of films and measurement techniques (21). A chapter on special techniques for the study of electrode processes by Conway (22) includes a section on ellipsometry. Optical principles for the study of chemisorption from the gas phase by ellipsometry have been treated by Bootsma *et al.* (23). A recent chapter by Greef (24) includes a discussion of instrumentation, optical models, interpretation, and electrochemical applications.

The principal book about ellipsometry is the comprehensive volume *Ellipsometry and Polarized Light* by Azzam and Bashara (25). In addition, there are Neal's more recent *Ellipsometry: Theory and Applications* (26) and Archer's much earlier and shorter *Manual on Ellipsometry* (27). Collected papers are contained in the proceedings of five Ellipsometry Conferences (28–32).

2. OPTICAL PRINCIPLES

2.1 Reflection of Light

2.1.1 s and p Components

For the purposes of ellipsometry, wave models are best suited to represent optical radiation. In the electromagnetic wave theory, electric and magnetic fields are coupled. Because of this coupling, and since the electric field is primarily responsible for the interaction of light with matter, only the electric vector is considered in ellipsometry.

The electric field-strength vector E for a wave traveling in the positive z direction can be represented by (33)

$$\vec{E} = E_0 \exp\,[i(\omega t+\delta)] \exp\,(-i\vec{k}\cdot\vec{r}) \exp\,(-\alpha z) \quad , \tag{1}$$

where E_0 is the wave amplitude, i is the imaginary unit, ω is the angular frequency, t is the time, δ is the phase angle (relative to a reference, e.g., incident wave), $\vec{k}$ is the wave vector, $\vec{r}$ is the position vector, α is the amplitude absorption coefficient (equal to half the intensity absorption coefficient), and z is the distance of travel. As has been pointed out in more detail before (8), the time-independent part of the oscillating electric field at a fixed location (the complex amplitude) can be written as

$$\hat{E} = |\,E\,| \exp\,(i\varepsilon) \quad , \tag{2}$$

where the modulus $|\,E\,|$ is the real amplitude and the argument ε is the phase.

In treating optical reflection, two orthogonal components are considered separately because they incur different changes in phase and amplitude upon reflection. One component has its electric vector oriented parallel to the plane that contains incident and reflected beams (the plane of incidence) and is called the p component. The other component has its electric vector oriented normal (*senkrecht*) to the plane of incidence and is called the s component (Fig. 2.1). For the discussion of ellipsometry of isotropic media, s and p components can be treated separately (34).

2.1.2 Fresnel Coefficients

For reflection from an ideally smooth and sharp interface between two media, the ratio of the reflected field amplitude E^r to the amplitude E^i in the incident light wave is given by the Fresnel reflection coefficient r. The p and s components, indicated by the respective subscripts, are associated with different reflection coefficients:

$$\hat{r}_p = \frac{\hat{E}_p^r}{\hat{E}_p^i} \quad , \tag{3}$$

$$\hat{r}_s = \frac{\hat{E}_s^r}{\hat{E}_s^i} \quad . \tag{4}$$

The (physical) amplitudes and phases of the electric fields can be represented by complex amplitudes. Thus, complex Fresnel coefficients can be formulated, shown for the p component in Eq. 5. The corresponding expression for the s component is analogous:

$$\hat{r}_p = \frac{|E_p^r|}{|E_p^i|} \exp\,[i(\varepsilon_p^r - \varepsilon_p^i)] \quad . \tag{5}$$

With amplitude attenuation and phase change due to reflection shown for the p component in Eqs. 6 and 7:

$$|r_p| \equiv \frac{|E_p^r|}{|E_p^i|} \quad , \tag{6}$$

$$\delta_p \equiv \varepsilon_p^r - \varepsilon_p^i \quad , \tag{7}$$

the complex reflection coefficient for the p component can be more compactly written as

$$\hat{r}_p = |r_p| \exp\,(i\delta_p) \quad , \tag{8}$$

and the corresponding expression for the s component is

$$\hat{r}_s = |r_s| \exp i\delta_s \quad . \tag{9}$$

For angles of incidence and refraction and positive electric-field directions for p and s components in incident, reflected, and refracted waves defined in Fig. 2.2, the Fresnel coefficients can be formulated in

terms of angle of incidence ϕ^i and angle of refraction ϕ^t as follows:

$$r_p = \frac{\tan(\phi^i - \phi^t)}{\tan(\phi^i + \phi^t)} \quad , \tag{10}$$

$$r_s = -\frac{\sin(\phi^i - \phi^t)}{\sin(\phi^i + \phi^t)} \quad . \tag{11}$$

Alternate formulations, which contain the refractive index n^i of incident and n^t of reflecting medium, are

$$r_p = \frac{n^t \cos\phi^i - n^i \cos\phi^t}{n^t \cos\phi^i + n^i \cos\phi^t} \quad , \tag{12}$$

$$r_s = \frac{n^i \cos\phi^i - n^t \cos\phi^t}{n^i \cos\phi^i + n^t \cos\phi^t} \quad . \tag{13}$$

The angle of refraction ϕ^t is determined from the angle of incidence ϕ^i and the refractive indices of incident and reflecting media by Snell's law:

$$\sin\phi^t = \frac{n^i}{n^t} \sin\phi^i \quad . \tag{14}$$

Despite the simplicity of the formulation of the Fresnel equations, the dependence of the reflection coefficients (and the ellipsometer parameters derived from them) on optical constants and angle of incidence is quite involved, as graphs found in the literature illustrate (8,35). The Fresnel equations are derived by use of electromagnetic theory, although they were originally obtained from an elastic-solid theory of light (36). They are valid for real or complex refractive indices.

2.1.3 Optical Constants

The optical properties of a material can be characterized by its optical constants. They are expressed by the complex refractive index $\hat{n}$, which consists of the real refractive index n and an imaginary part that contains the extinction coefficient k:

$$\hat{n} = n - ik \quad . \tag{15}$$

The refractive index of transparent (dielectric) media contains the real part only, the physical meaning of which is that of a ratio of the light velocity c in vacuum to the phase velocity v in the medium:

$$n = \frac{c}{v} \quad . \tag{16}$$

The extinction coefficient k is a measure of light absorption by the medium. For normal incidence on an absorbing medium, the amplitude of the transmitted wave decays with distance z normal to the interface as

$$E = E_0 \exp(-2\pi kz/\lambda_0) \quad , \tag{17}$$

where λ_0 is the wavelength in vacuum. The amplitude absorption coefficient used in Eq. 1 is therefore

$$\alpha = \frac{2\pi k}{\lambda_0} \quad . \tag{18}$$

The amplitude penetration depth

$$z = \frac{\lambda_0}{2\pi k} \tag{19}$$

is the distance below the surface of an absorbing medium at which the amplitude is reduced to 1/e of its value at the surface.

The radiance (intensity) absorption coefficient, more often found in the literature, is twice that given in Eq. 18 because it represents the decay of the square of the amplitude (a measure of intensity). Similarly, the intensity penetration depth is half that given in Eq. 19 and is shown in Fig. 2.3.

The use of Snell's law with a complex refractive index results in a complex angle of refraction that can be used to derive complex Fresnel reflection coefficients but has no physical meaning. For this reason, the derivation of absorption coefficients and penetration depths for non-normal incidence requires the use of differently defined, alternate optical constants that involve the real propagation direction but depend on angle of incidence (8,33,36).

The optical properties of materials can also be described by the complex dielectric constant ε (relative permittivity or dielectric function, if frequency dependence is considered):

$$\varepsilon = \varepsilon_1 - i\varepsilon_2 \quad , \tag{20}$$

which is the square of the complex refractive index

$$\varepsilon \equiv \hat{n}^2 = n^2 - k^2 - 2ink \quad . \tag{21}$$

Therefore,

$$\varepsilon_1 = n^2 - k^2 \quad , \tag{22}$$

$$\varepsilon_2 = 2nk \quad , \tag{23}$$

and

$$n = \sqrt{\frac{1}{2}\left[\varepsilon_1 + \sqrt{\varepsilon_1^2 + \varepsilon_2^2}\right]} \quad , \tag{24}$$

$$k = \sqrt{\frac{1}{2}\left[-\varepsilon_1 + \sqrt{\varepsilon_1^2 + \varepsilon_2^2}\right]} \quad . \tag{25}$$

The dielectric constant is used in electromagnetic theory, where dielectric processes are represented by ε_1 and dissipative processes by ε_2.

Practical considerations for the determination of optical constants of bare surfaces are discussed in Section 5.9. The optical constants of composite and anisotropic media as well as reflection from rough surfaces will be treated in Section 2.3.

2.1.4 Drude Equation

The reflection coefficients r of a film-covered surface (for s or p polarization) are derived from the Fresnel coefficients $\hat{r}_1$ and $\hat{r}_2$ of the two film surfaces (Fig. 2.4), the angle of refraction $\hat{\phi}^t$ in the film, the film thickness L, and the refractive index of the film $\hat{n}^t$ by use of the Drude equation, given for the p component in Eq. 26 (37–39):

$$\hat{r}_p = \frac{\hat{r}_{1p} + \hat{r}_{2p}\, e^{-iD}}{1 + \hat{r}_{1p}\, \hat{r}_{2p}\, e^{-iD}} \quad , \tag{26}$$

with

$$D = \frac{4\pi}{\lambda_0} L\, \hat{n}^t \cos \hat{\phi}^t \tag{27}$$

representing the phase delay due to propagation through the film. As before, λ_0 is the wavelength in

vacuum. For an absorbing film material, with complex refractive index, the angle of refraction is complex (indicated by the caret). The Drude equation can be derived from electromagnetic theory (39) or by use of a multiple-beam model of thin-film interference (38,40).

Reflection from multiple, inhomogeneous, and island films will be discussed in Section 2.3.

Throughout this chapter, the terms "single film" and "single layer" will be used interchangeably. In the recent literature, such a system is, unfortunately, also called a "three-layer" system. A designation as a "three-media" system would be more appropriate, since the infinitely extended incident and substrate media are not really "layers" with two interfaces each.

2.2 Polarized Light

2.2.1 Linear and Elliptic Polarization

The physics of polarized light has been treated for a long time (41–46). In linearly polarized light (often simply called polarized light), the electric-field vector at a fixed position in space oscillates along a straight line. Along a wave in space, the electric-field vectors lie in a plane (the plane of polarization), with their end points showing a sinusoidal field distribution at a fixed time. The superposition of two orthogonal linear polarizations that are in phase results in another linear polarization (Fig. 2.5). Polarizers (and analyzers) are devices which convert unpolarized (or elliptically polarized) light into linearly polarized light by selective absorption (sheet polarizers, grids), birefringence (prisms), or reflection.

In elliptic polarization, the electric-field vector at a fixed position in space rotates, with its end point describing an ellipse (47). Elliptic polarization can be viewed as a superposition of two orthogonal linear polarizations, chosen here to be oriented in the s and p directions, and represented by the time-independent complex amplitudes

$$\hat{E}_p \equiv |E_p| \exp(i\varepsilon_p) \quad , \tag{28}$$

$$\hat{E}_s \equiv |E_s| \exp(i\varepsilon_s) \quad . \tag{29}$$

As shown in Fig. 2.6, the helix that results from connecting the end points of the resulting electric-field

vectors in space appears as an ellipse when projected on a plane normal to the propagation direction k. For the purpose of conventional ellipsometry, incident and reflected light are assumed to be completely polarized, and the state of polarization is described without regard for light intensity as the complex polarization ratio $\hat{\rho}$ of p to s components:

$$\hat{\rho} = \frac{\hat{E}_p}{\hat{E}_s} \equiv \frac{|E_p|}{|E_s|} \exp\,[i(\varepsilon_p - \varepsilon_s)] \quad . \tag{30}$$

Retardation plates (or compensators) introduce a known (fixed or variable) phase difference (e.g., 90° or quarter-wave) between two orthogonal components of a transmitted wave. They are usually made from crystalline birefringent materials (mica, calcite, quartz), and their operation has been examined on the basis of electromagnetic theory (48). Internal reflection can also be employed to introduce a defined retardation (49).

2.2.2 Physical and Geometric Parameters of Polarized Light

The state of polarization of completely polarized light, irrespective of intensity, can be described by two alternate sets of parameters, which can be interconverted.

The *physical parameters* ψ and Δ are based on the ratio of s and p components. The ratio of the electric-field amplitudes is expressed as the tangent of the angle ψ:

$$\frac{|E_p|}{|E_s|} = \tan\psi \ , \ 0° \le \psi \le 90° \quad , \tag{31}$$

and the difference Δ of the time-independent phases ε of the two components is

$$\varepsilon_p - \varepsilon_s = \Delta \ , \ 0° \le \Delta \le 360° \quad . \tag{32}$$

The *geometric parameters* θ and γ are based on orientation and shape of the ellipse, with

$$\theta = \text{azimuth of major axis}, \ 0° \le \theta \le 180° \quad , \tag{33}$$

and

$$\tan\gamma = \frac{\text{minor axis}}{\text{major axis}} \ , \ -45° \leq \gamma \leq 45° \ . \tag{34}$$

Positive values of γ represent left-hand (mathematically positive, counterclockwise) rotation of the ellipse, and negative values represent right-hand rotation. Physical and geometric parameters are shown in Fig. 2.6. They are related by (8)

$$\sin 2\gamma = \sin 2\psi \sin\Delta \ , \tag{35}$$

$$\tan 2\theta = -\tan 2\psi \cos\Delta \ , \tag{36}$$

$$\tan\Delta = \frac{\tan 2\gamma}{\sin 2\theta} \ , \tag{37}$$

$$\cos 2\psi = -\cos 2\gamma \cos 2\theta \ . \tag{38}$$

2.2.3 Equation of Ellipsometry

The *change* in the state of polarization caused by reflection on the specimen is determined in ellipsometry as the *ratio* of the state of polarization of the reflected light to that of the incident light. The states of polarization are characterized by the polarization ratios ρ^i and ρ^r (Eq. 30) for incident and reflected waves:

$$\rho^i = \frac{|E_p^i|}{|E_s^i|} \exp\left[i(\varepsilon_p^i - \varepsilon_s^i)\right] \ , \tag{39}$$

$$\rho^r = \frac{|E_p^r|}{|E_s^r|} \exp\left[i(\varepsilon_p^r - \varepsilon_s^r)\right] \ . \tag{40}$$

The effect of reflection on the polarization ratio can be expressed as

$$\rho = \frac{\rho^r}{\rho^i} \equiv \frac{|E_p^r| \ |E_s^i| \exp\left[i(\varepsilon_p^r - \varepsilon_s^r)\right]}{|E_p^i| \ |E_s^r| \exp\left[i(\varepsilon_p^i - \varepsilon_s^i)\right]} \ , \tag{41}$$

which, with the definition of Eq. 5:

$$\hat{r}_p = \frac{|E_p^r|}{|E_p^i|} \exp\,[i(\varepsilon_p^r - \varepsilon_p^i)] \quad , \tag{42}$$

$$\hat{r}_s = \frac{|E_s^r|}{|E_s^i|} \exp\,[i(\varepsilon_s^r - \varepsilon_s^i)] \quad , \tag{43}$$

and that of Eq. 7:

$$\delta_p = \varepsilon_p^r - \varepsilon_p^i \quad , \tag{44}$$

$$\delta_s = \varepsilon_s^r - \varepsilon_s^i \quad , \tag{45}$$

simplifies with the use of Eqs. 8 and 9 to

$$\rho = \frac{\hat{r}_p}{\hat{r}_s} = \frac{|r_p|}{|r_s|} \exp\,[i(\delta_p - \delta_s)] \quad . \tag{46}$$

With the definitions of the relative amplitude parameter ψ and the relative phase parameter Δ as

$$\tan\psi = \frac{|r_p|}{|r_s|} \quad , \tag{47}$$

$$\Delta = \delta_p - \delta_s \quad , \tag{48}$$

one obtains the basic equation of ellipsometry:

$$\rho = (\tan\psi)\, e^{i\Delta} \quad . \tag{49}$$

It is the object of ellipsometry to determine the quantity ρ; $\tan\psi$ represents the ratio of the p and s amplitude ratios before and after reflection, and Δ represents the difference of s and p phase differences before and after reflection.

A different reading of Eq. 41 used before (8) shows that for incident light of equal s and p amplitudes and zero phase difference, the state of polarization of the reflected light represents the change due to reflection.

For reflection from bare surfaces, the dependence of the ellipsometer parameters ψ and Δ on optical constants and angle of incidence is illustrated in Figs. 2.7 and 2.8.

2.2.4 Definitions and Conventions

Numerical data on the reflection of polarized light strongly depend on a large number of arbitrary choices of definitions and conventions. An analysis of the literature has shown a great variability of past usage, with at least 512 different combinations being possible and 16 different optical constants describing reflection from a given bare surface (8,33). A preferred set of nine twofold choices was established at the 1968 International Ellipsometry Conference at the University of Nebraska (33) and is used here. It was summarized later (8) and is now widely accepted (25,50). The following is a summary of the 1968 Nebraska conventions (8,33).

1. Relative amplitude parameter ψ:

$$\tan \psi = \frac{|r_p|}{|r_s|} \quad \text{(alternate: } \frac{|r_s|}{|r_p|}\text{)} \ .$$

2. Relative phase parameter Δ:

$$\Delta = \delta_p - \delta_s \quad \text{(alternate: } \delta_s - \delta_p\text{)} \ .$$

3. Complex polarization ratio ρ:

$$\rho = (\tan \psi) \exp (i\Delta) \quad \text{[alternate: } (\tan \psi) \exp (-i\Delta)\text{]} \ .$$

4. Time dependence ωt of electric-field oscillation:

$$E \sim \exp (i\omega t) \quad \text{[alternate: } \exp (-i\omega t)\text{]} \ .$$

5. Absolute phase δ:

$$E \sim \exp [i(\omega t + \delta)] \quad \text{[alternate: } \exp [i(\omega t - \delta)]\text{]} \ .$$

6. Positive coordinate directions for p component: at normal incidence, reflected beam opposite to incident beam, transmitted beam parallel (see Fig. 2.2) (alternate: reflected beam parallel).

7. Positive coordinate directions for s component: reflected and transmitted beams parallel to incident beam (see Fig. 2.2) (alternate: reflected beam opposite).

8. Complex refractive-index formulation:

$$\hat{n} = n - ik \quad [\text{alternate: } n(1 - ik)] \quad .$$

9. Complex refractive-index definition: independent of angle of incidence (alternate: dependent).

10. Sense of rotation: positive for counterclockwise rotation, looking into the beam (alternate: negative). Sign of geometric parameter γ shows sense of rotation.

While some of the choices are arbitrary, others, such as 1 and 2 or 4 and 8, are linked. As found later, the above conventions and definitions are not completely compatible with customary matrix formulations in the Mueller-Stokes calculus (51). In particular, for that use the axial ratio of the ellipse is taken to be positive for clockwise rather than counterclockwise rotation and the p rather than the s component is taken as a reference for the phase.

It has been pointed out recently (52) that the present conventions can produce difficulties for total internal reflection from a medium of refractive index $\hat{n} = n - ik$, where the evanescent wave propagates in a medium of real refractive index. The difficulty is related to the fact that some computer programming languages assign a negative sign to the imaginary square root of a negative number with a vanishingly small imaginary part; this difficulty has been overcome by the use of $\hat{n} = n + ik$.

2.2.5 Poincaré Sphere

Representation of polarized light on the Poincaré sphere provides a useful graphical device to trace the state of polarization through the components of an ellipsometer. On the Poincaré sphere, the state of polarization (irrespective of intensity) is represented as a point on a unit sphere (25,42,43,53,54). As shown in Fig. 2.9 for the set of conventions and definitions used here (33,50), "north" and "south" poles of the sphere represent left and right circular polarizations, respectively. Similarly, points on the "northern" hemisphere represent left-hand (or counterclockwise, mathematically positive) rotation of elliptic polarization, the "southern" hemisphere right-hand rotation. Points on the equator signify linear states of polarization, with pure p polarization represented by the origin H (for horizontal) of the longitudinal grid, and pure s polarization by the opposite point V (for vertical).

Coordinate grids for geometric and physical parameters of elliptic polarization are shown in the first two parts of Fig. 2.10, with a view of the sphere on the left and the corresponding stereographic projection, as seen from the "north" (L) pole, on the right. Note that all angles except phase angles appear doubled on the sphere. The effect of a compensator of retardation δ_c and fast axis F (shown at 45° azimuth) is indicated on the bottom of Fig. 2.10.

Stereographic projections are used extensively in crystallography (55) as angle-true representations of the surface of a sphere. They are obtained by projecting each hemisphere from the opposite pole on a plane tangent to the pole of the hemisphere (or a plane parallel to it, such as one through the equator). The two separate projections of both hemispheres are then superimposed. Points above the equator are designated here by circles, those below by crosses.

Stereographic projections of the Poincaré sphere are also called Carter charts (56). Two stereographic grids of the kind used here, rotated 90° against each other, have been used before for the discussion of elliptic polarization with different definitions (57).

Orthographic projections of the Poincaré sphere consist of orthogonal circles and are called Smith charts (56).

The amplitude of an elliptic polarization E transmitted by an analyzer A (with absorption direction A') can be represented inside the Poincaré sphere by the length of the chord between E and A′ (Fig. 2.11).

Among the applications of the Poincaré sphere reported in the literature are the transmission of light through birefringent and optically active media or birefringent networks (58,59), birefringent and dichroic media (60), and the analysis of polarized light by an elliptic compensator or by intensity measurements at two analyzer azimuths (61). The Poincaré sphere has also been used to discuss the accuracy of measuring intensity minima (62), and in Section 3 it will be used to follow the state of polarization through the components of different ellipsometers and to explain their operation.

Many other graphical representations of polarized light exist (25). A representation of the state of polarization by complex numbers has been used to generate equi-azimuth and equi-ellipticity contours in the complex plane as an alternate to the Poincaré spheres (63,64). The ellipsometer parameters ψ and Δ

can also be plotted in polar coordinates (65). Another graphical method used to determine the effect of retarders and rotators is based on the properties of quaternions and the use of a 2×2 matrix to represent the effect of each retarder (66,67).

2.2.6 Stokes Parameters

A more complete characterization of monochromatic polarized light requires, in addition to the two ellipsometer parameters, a measure of the light intensity (radiance) and of the degree of polarization (for partial polarization). The four Stokes parameters provide such a characterization (46,68). They are defined in terms of the time averages of two orthogonal electric-field components, chosen here to be E_p and E_s, and their associated phases ε_p and ε_s:

$$S_0 = E_p^2 + E_s^2 \quad , \tag{50}$$

$$S_1 = E_p^2 - E_s^2 \quad , \tag{51}$$

$$S_2 = 2E_pE_s \cos(\varepsilon_p - \varepsilon_s) \quad , \tag{52}$$

$$S_3 = 2E_pE_s \sin(\varepsilon_p - \varepsilon_s) \quad . \tag{53}$$

The Stokes parameters have the dimension of radiance (intensity) and can be measured directly with a combination of polarizers and retarders. Under the present definitions and conventions, the physical meaning of the Stokes parameters is: S_0 is a measure of total radiance; S_1 is a measure of the excess of linear component with 0° azimuth (p component) over that with 90° azimuth (s component); S_2 is a measure of the excess of the linear component with 45° azimuth over that with 135° azimuth; and S_3 is a measure of the excess of left-hand over right-hand circular polarization (39). Note that in the conventional definition of the Stokes parameters, S_3 is positive for right hand polarization and $\varepsilon_s - \varepsilon_p$ is used in place of $\varepsilon_p - \varepsilon_s$ (51). For complete polarization,

$$S_0^2 = S_1^2 + S_2^2 + S_3^2 \quad , \tag{54}$$

and the Stokes parameters can be represented as coordinates of points on the surface of the Poincaré sphere

(39,54,69), as shown in Fig. 2.12.

$$S_1 = S_0 \cos 2\gamma \cos 2\theta \quad , \tag{55}$$

$$S_2 = S_0 \cos 2\gamma \sin 2\theta \quad , \tag{56}$$

$$S_3 = S_0 \sin 2\gamma \quad . \tag{57}$$

For partial polarization,

$$S_0^2 > S_1^2 + S_2^2 + S_3^2 \quad . \tag{58}$$

Partially polarized light can be represented as the sum of a completely polarized and an unpolarized portion. For unpolarized light,

$$S_1 + S_2 + S_3 = 0 \quad . \tag{59}$$

The degree of polarization P is defined as the ratio of polarized to total radiance and can be formulated as

$$P = \frac{\sqrt{S_1^2 + S_2^2 + S_3^2}}{S_0} \quad . \tag{60}$$

The measurement of partial polarization to characterize a surface remains to be used to any significant extent, although instrumentation for making such measurements has been described (17,70–72).

2.2.7 Matrix Representation

Jones Calculus. For complete polarization, the state of polarization can be represented in the p, s coordinate system by the vector sum of complex p and s amplitudes, given in Eqs.28 and 29:

$$\hat{E}_p = |E_p| \exp(i\varepsilon_p) \quad , \tag{61}$$

$$\hat{E}_s = |E_s| \exp(i\varepsilon_s) \quad , \tag{62}$$

which can be represented by the complex Jones vector:

$$\hat{E} = \begin{bmatrix} \hat{E}_p \\ \hat{E}_s \end{bmatrix} ,$$

and is often used in a normalized form (24,73). The effect of a non-depolarizing optical component or system on the state of polarization can be represented by the Jones matrix T, the components of which may be complex:

$$T = \begin{bmatrix} T_{11} & T_{12} \\ T_{21} & T_{22} \end{bmatrix} . \tag{63}$$

Jones matrices for many optical components have been tabulated (25,45). The state of polarization $\hat{E}_o$ at the output of an optical system is obtained from the state of polarization $\hat{E}_i$ at the input by matrix multiplication:

$$\hat{E}_o = T\,\hat{E}_i \tag{64}$$

The effect of a series of components encountered by the light, e.g., in the order 1, 2, 3, is obtained by the multiplication of their respective Jones matrices:

$$\hat{E}_o = T_3 T_2 T_1\,\hat{E}_i \quad . \tag{65}$$

As has been pointed out (45), the Jones calculus, being based on electromagnetic theory, employs amplitudes and phases. It is suited for combining two coherent beams but is not able to handle incoherent superposition or depolarization (partial polarization). An extended Jones matrix method has been used to treat reflection and transmission under non-normal incidence on uniaxially anisotropic media (74).

Mueller Calculus. Another matrix-algebraic method used in ellipsometry is based on the Stokes parameters arranged in the form of the Stokes vector S:

$$S \equiv \begin{bmatrix} S_0 \\ S_1 \\ S_2 \\ S_3 \end{bmatrix} \tag{66}$$

for describing polarized light. The Stokes vector S_i for the incident light is multiplied by the 4×4 Mueller matrix M (73):

$$M \equiv \begin{bmatrix} M_{11}M_{12}M_{13}M_{14} \\ M_{21}M_{22}M_{23}M_{24} \\ M_{31}M_{32}M_{33}M_{34} \\ M_{41}M_{42}M_{43}M_{44} \end{bmatrix} , \tag{67}$$

which represents the effect of an optical system. To obtain the Stokes vector S_o of the outgoing light (25,45):

$$S_o = M\, S_i \quad . \tag{68}$$

The Mueller calculus is able to represent partial polarization and depolarizing systems, but it does not allow one to consider absolute phase. Of the sixteen elements of the Mueller matrix, many are zero for typical optical elements and only seven are independent (45).

As has been pointed out in Section 2.2.6, the conventional definitions of the Stokes parameters are not completely consistent with the present definition of the ellipsometer parameters (51).

2.3 Optical Theory

A few additional topics of optical theory of interest in ellipsometry are discussed here.

2.3.1 Electromagnetic Theory

The application of electromagnetic theory to the reflection of light has been treated extensively by many authors and will not be reproduced here. In addition to optical and electromagnetic textbooks (36,39,75–79) and review chapters on physical optics and reflection (44,80–82), Azzam and Bashara's book on ellipsometry (25), as well as an earlier volume on thin-film optics by Vašíček (38), are based on electromagnetic theory, as are several review chapters on thin-film optics (40,83). Energy-conservation considerations in the application of the Maxwell equations to a reflecting surface result in boundary conditions for electric- and magnetic-field components at the interface and lead to the Fresnel reflection coefficients for bare surfaces and the Drude equation for film-covered surfaces.

Use of the Maxwell equations is based on a discontinuity in dielectric properties at an interface (23), although a continuous change is physically more realistic (84). An application of electromagnetic theory to reflection from multilayers has been given earlier (85).

2.3.2 Coherence

Reflection from heterogeneous surfaces, for which optical properties vary along the surface, results in different states of polarization for reflection from different surface elements. The resulting overall state of polarization represents a superposition of these different polarizations. This superposition depends on the coherence properties of the incident light because coherent and incoherent superposition of different polarization states produces different results.

The lateral (or spatial, transverse) coherence area is the region of width w across a light beam over which the phase of the radiation is correlated. For a monochromatic beam from a thermal source, the lateral coherence depends on the angular radius ρ/R of the source (39):

$$w = \frac{0.16\, R\bar{\lambda}}{\rho} \quad , \tag{69}$$

where R is the distance between source and observer, $\bar{\lambda}$ is the quasi-monochromatic wavelength, and ρ is the radius of the circular source. The lateral coherence extends over the entire beam for light from an ideal point source ($\rho/R = 0$) or from a single-mode laser.

The longitudinal (or temporal) coherence area is the region of length along the light beam over which the phase of the radiation is correlated. The coherence length is determined by the monochromaticity of the source, described by the spread in wavelength $\Delta\lambda$ and the center wavelength $\bar{\lambda}$ (39):

$$\ell = \frac{\bar{\lambda}^2}{\Delta\lambda} \quad . \tag{70}$$

The coherence length for most laser beams is of macroscopic dimensions (meters).

For non-normal incidence, lateral and longitudinal coherence properties of the incident light have to be used to establish the size of the coherently illuminated specimen area. Surface heterogeneities smaller than the coherence area result in the coherent superposition of different polarization states, with the resulting irradiance (intensity) being the square of the sum of amplitudes. Surface heterogeneities larger than the coherence area result in the incoherent superposition of polarization states, with the resulting irradiance being the sum of the square of amplitudes.

2.3.3 Multiple and Inhomogeneous Films

Electrochemical surface layers are often not single, homogeneous films and thus require multiple-film models for the satisfactory interpretation of measurements. Reflection coefficients of multiple-film systems can be computed by a recursion process in which, beginning at the substrate, the optical effect of the adjacent single layer is computed; layer and substrate are then replaced by an effective substrate with apparent optical constants that produce the same optical effect. The computation proceeds by considering the next layer in contact with the effective substrate and treating it the same way (86).

Inhomogeneous films, in which the optical properties vary continuously with distance from the substrate, can be represented by a stack of thin homogeneous films with incrementally varying properties (87). Deriving a refractive-index profile from ellipsometer measurements has been investigated theoretically (88). A study of polishing layers on glass has shown that inhomogeneous films cannot necessarily be represented by an equivalent homogeneous film (89), although a very thin layer of graded composition has been successfully replaced by a spatial average (90). A similar simplification has been found to represent the effect of mass-transfer boundary layers (91,92).

2.3.4 Island Films

Discontinuous films have long been known to result from the vapor deposition of many metals. An island nature of such films has been suggested to account for the differences in optical constants of silver films below 20 nm from the bulk properties (93). For films consisting of very small particles, an effective-medium model (discussed in Section 2.3.5) is usually appropriate to predict optical properties. Effective-medium theories for mixtures of absorbing and transparent materials are, however, highly non-linear (Fig. 2.13), while a linear dependence of ellipsometer measurements on coverage is often found for submonolayer coverage (94–99) and aggregated films (100).

Patchwise-distributed or island films of monolayer thickness have been used to account for the observed linear behavior of underpotential layers and to avoid the use of physically unrealistic film thicknesses of fractional atomic dimensions (Fig. 2.14). The optical properties of such island films have been represented by a coherent superposition of polarization states resulting from reflection on bare and

film-covered surface elements. In this coherent-superposition model, the overall reflection coefficient $\hat{r}$ (for p or s components) is obtained by the linear combination of the reflection coefficients $\hat{r}^f$ and $\hat{r}^s$ for the film-covered and bare substrate regions, respectively, scaled by the corresponding relative surface areas θ^f and θ^s (94,101):

$$\hat{r} = \theta^f \hat{r}^f + \theta^s \hat{r}^s \quad . \tag{71}$$

For a simple system,

$$\theta^f + \theta^s = 1 \quad . \tag{72}$$

The above approach is based on the assumption that the islands are smaller than the area of coherent illumination, which was limited primarily by the lateral coherence (102). Incoherent superposition of polarization states has been found to apply to titanium hydride formation on titanium (103).

2.3.5 Composite Materials, Effective Media

Composite or heterogeneous optical materials result from the mixture of different components on a scale below the wavelength of light. Often one medium is physically dispersed in another. If the regions of the dispersed phase are large enough to retain the optical properties of the constituent material (not affected, e.g., by chemical bonding), the refractive index $\hat{n}$ of the composite can be predicted (for spherical inclusions) from the refractive indices $\hat{n}_i$ of the components, the refractive index $\hat{n}_h$ of the host material, and the volume fractions θ_i of the components by use of effective-medium theories (104). For two components, a and b,

$$\frac{\hat{n}^2 - \hat{n}_h^2}{\hat{n}^2 + 2\hat{n}_h^2} = \theta_a \frac{\hat{n}_a^2 - \hat{n}_h^2}{\hat{n}_a^2 + 2\hat{n}_h^2} + \theta_b \frac{\hat{n}_b^2 - \hat{n}_h^2}{\hat{n}_b^2 + 2\hat{n}_h^2} \quad . \tag{73}$$

Effective-medium theories differ in the choice of the host material (104,105). In the Lorentz-Lorenz theory (106,107), the host material is assumed to be vacuum; Eq. 73 therefore becomes

$$\frac{\hat{n}^2 - 1}{\hat{n}^2 + 2} = \theta_a \frac{\hat{n}_a^2 - 1}{\hat{n}_a^2 + 2} + \theta_b \frac{\hat{n}_b^2 - 1}{\hat{n}_b^2 + 2} \quad . \tag{74}$$

In the Maxwell Garnett formulation (108), the major (continuous) constituent (taken here to be medium a) is assumed to be the host medium, which leads to

$$\frac{\hat{n}^2 - \hat{n}_a^2}{\hat{n}^2 + 2\hat{n}_a^2} = \theta_b \frac{\hat{n}_b^2 - \hat{n}_a^2}{\hat{n}_b^2 + 2\hat{n}_a^2} \tag{75}$$

and applies only for small volume fractions of material b, that is,

$$\theta_a > \theta_b \quad . \tag{76}$$

In the Bruggeman theory (109), often called the effective-medium approximation (EMA), the effective medium itself is taken as the host medium. This choice results in a self-consistent expression, valid over the whole composition range:

$$\theta_a \frac{\hat{n}_a^2 - \hat{n}^2}{\hat{n}_a^2 + 2\hat{n}^2} + \theta_b \frac{\hat{n}_b^2 - \hat{n}^2}{\hat{n}_b^2 + 2\hat{n}^2} = 0 \quad , \tag{77}$$

where

$$\theta_a + \theta_b = 1 \quad . \tag{78}$$

The complex refractive index of the composite is obtained by (102)

$$\hat{n} = \left\{ \frac{1}{2} \left[-A \pm (A^2 - 4B)^{1/2} \right] \right\}^{1/2} \quad , \tag{79}$$

with

$$A = \frac{1}{2} \left[\hat{n}_a^2 (1 - 3\theta_a) + \hat{n}_b^2 (3\theta_a - 2) \right] \quad , \tag{80}$$

$$B = -\frac{1}{2} (\hat{n}_a^2 \hat{n}_b^2) \quad . \tag{81}$$

In practice, it can be difficult to select the correct root of the complex Eq. 79 if the composite consists of absorbing and nonabsorbing constituents. The root with the largest modulus has been used in the past (102). In addition, the sign of k should conform to the convention used.

The effective-medium models discussed hold for spherical, noninteracting particles (105). Relations for inclusions of more general shape and an extended effective-medium theory for ellipsoidal particles with dipole-dipole interaction between them have been presented (110). A more generally valid effective-medium theory contains an adjustable screening factor that depends on microstructure (104,105,111). Radius and shape factor of ellipsoidal particles have recently been derived by fitting real and imaginary parts of the dielectric function over the visible spectrum by use of an extended Maxwell Garnett theory (112). Such a theory has also been used to account for selective optical absorption observed with small tin spheres but not found in the bulk metal (113).

Since the optical constants of a composite material are not a linear function of composition, quite unexpected properties can be found for mixtures of absorbing and transparent media (114), such as the transparency of porous metals (101,115,116).

2.3.6 Anisotropic Materials

Although polycrystalline materials are usually well represented by isotropic optical models, anisotropic models are required in some cases that involve oriented microstructures, strain, or single crystals. Anisotropic (birefringent or dichroic) materials are characterized by the orientation of one or two optic axes and the magnitude of two or three principal refractive indices (Fig. 2.15). Transmission of light through anisotropic media can be represented on the Poincaré sphere (58,59).

Progress has only recently been made on the optical theory of reflection from anisotropic media (117–125) and birefringent multilayers (126). Although in the general case the number of unknowns is too large for practical application, the theory has been used successfully for the determination of electrostriction in dielectric films (127–130), strain-induced birefringence (131), and measurements on aggregate silver films (132).

The adsorption of oriented aromatic compounds (133–135) and macromolecules (136) has been successfully represented by uniaxially anisotropic layers, as have Langmuir films (137). The presence of surface anisotropy can be determined by measurements at two nonorthogonal azimuth orientations of a specimen (138). Treating such layers as isotropic films has been shown theoretically to result in an apparent

extinction coefficient for transparent materials (139). This result has been confirmed experimentally for the adsorption of quinolines on mercury (134).

The optical properties of stratified anisotropic media have been represented by a 4×4 matrix formalism (140).

2.3.7 Rough Surfaces

The optical theory of reflection from rough surfaces is still under active development. Extensive treatments (141–143) and a recent review (144) are available. For practical purposes, the effect of surface roughness in ellipsometry has mostly been represented by equivalent surface layers of thickness related to the depth of the surface profile and refractive index derived by an effective-medium model from the refractive indices of the two adjacent materials (114,145–153). Equivalent surface layers of optical constants uniform or gradually varying with distance from the substrate (to represent the variable volume fractions of constituents) have been employed (Fig. 2.16). Effective optical constants of rough surfaces have been used for measuring film growth on them (154). Transparent layers on rough metal substrates can appear to be absorbing if measurements are interpreted with a single-film model (154,155).

The Kirchhoff diffraction theory has been applied to ellipsometry (156,157), as have scalar and vector theories of diffraction for coherent and incoherent reflection from Gaussian and non-Gaussian rough surfaces (143). Off-specular ellipsometry has been shown to be useful for the characterization of roughness (151,158). In measurements on aluminum surfaces of controlled roughness (159), diffraction theory has been found to be applicable to bump-type (protrusion) roughness, but an equivalent surface-layer model was better able to account for the effect of pit-type (indentation) roughness. A surface-layer model has also been used to interpret measurements of the growth of a submicroscopic network of cracks during fatigue cycling of an aluminum alloy (160).

2.3.8 Spectroscopic Ellipsometry

Ellipsometer measurements at different wavelengths are of interest for two different purposes: first, they can be used to determine the wavelength dependence of optical constants in order to derive the

electronic structure and composition of substrate or film materials (161,162). Second, spectral measurements on systems with known (or small) dependence of optical constants on wavelength can be used to derive more than two unknown parameters of the reflecting surface from the two (Δ and ψ) ellipsometer measurements (102,163). A spectral scan over the visible wavelengths with 10-nm bandwidth can be considered as about 40 independent measurements from which 3–6 film parameters have been derived by multidimensional optimization (102).

2.3.9 Reflectance Ellipsometry

The measurement of reflectance during ellipsometry provides a third measured quantity that can be used to discriminate between different optical models for the interpretation of ellipsometer measurements. Changes in reflectance, which are much easier to measure than absolute reflectance, are often sufficient for that purpose and can be determined simultaneously with photometric ellipsometers. This technique has been called "three-parameter ellipsometry" (164) and has been applied to oxide formation on platinum and gold (165–167) and to the passivation of iron (168). Precision and uniqueness of solutions have been analyzed in detail (164).

Changes in the reflectance for s and p components have also been considered separately to provide greater sensitivity for the determination of the refractive index of very thin films (169).

2.3.10 Multiple-Angle Ellipsometry

Measurements of the same specimen at different angles of incidence can be used to derive additional film parameters and to resolve multiple interpretations (170–172). This approach is, however, valid only under special circumstances (87): for an absorbing film on an absorbing substrate, the optical constants of the film could be derived from measurements at different angles only for a specific film thickness. A detailed analysis of parameter correlation for multiple-angle ellipsometry has been presented (25) and applied to oxide-covered silicon (173), for which the complex refractive indices of film and substrate and the film thickness were derived. The sensitivity of the method depends greatly on the optical properties of a specific system (171,172). Four to five film parameters have nevertheless been derived from multiple-

angle measurements (171,172), although for very thin films not more than two layers can be identified, as shown by a theoretical analysis (170).

The depth and complex refractive index of ion-implanted layers in oxide-covered silicon have been derived from measurements at two angles of incidence (174). Angle-of-incidence derivative ellipsometry has been used for the same system (175). Reflectance ratios at two angles of incidence have been used in the far uv (176).

At the angle of incidence for which the reflection coefficients of the film-substrate combination are equal for s and p components ($\psi = 45°$), measurements can be conducted with a single rotating polarizer (177).

2.3.11 Transmission Ellipsometry

The simultaneous measurement of reflected and transmitted light can provide additional information about transparent specimens. This approach, including internal reflection (through a transparent substrate), has been analyzed in detail (178). Such measurements require a three-telescope ellipsometer and can be conducted by either a compensating or a photometric method.

A determination of the optical constants and thicknesses of thin gold films on glass by compensating ellipsometry at fixed wavelength has shown that the combined use of external reflection, internal reflection, and external transmission as a function of angle of incidence results in greatly reduced standard deviations compared to the individual techniques (179). Dual films of Al and MgF_2 have also been measured with this technique by the same authors (180).

Transmission ellipsometry has been conducted on a gold film optically suspended between glass and a liquid of the same refractive index as that of the glass (181).

3. INSTRUMENTATION

3.1 Classification of Ellipsometers

Ellipsometers measure the ratio of the state of polarization of light reflected from a specimen to that incident on it. This ratio ρ has been given in Eqs. 41 and 49. The principal optical elements of ellipsometers are polarizers and compensators, which have been described in Section 2.2. These elements are rotated around the optic axes of the instrument (which contain the light beam). Their position is described by the azimuth angle, which is measured from the plane of incidence (the p direction) to the transmission direction of polarizers or the fast axis of compensators in a counterclockwise direction (0–180°), looking into the beam.

Ellipsometers can be divided into compensating and photometric (noncompensating) types. Several reviews of instrumentation are available (13,16,17,25). In compensating (or nulling) instruments, the phase difference between s and p components introduced by the reflection is compensated to restore linear polarization, which can be extinguished by a polarizing element (the analyzer). In photometric instruments, the polarization ellipse is reconstructed from the response of the transmitted radiance (intensity) to a modulation of the state of polarization.

Performance characteristics of different ellipsometer types have been compared earlier (13,16). The capabilities for determination of different elements of the Jones and Mueller matrix have been compared more recently (17).

Ellipsometer designs can be further divided according to several other criteria, such as manual or automatic (computer) operation, monochromatic or spectroscopic capabilities, ability to observe small surface areas or make short-term (pulse) measurements, and ability to use transmitted light or operate outside the visual spectral range. Instruments that also measure reflectance or the degree of (partial) polarization are often called polarimeters (17).

Ellipsometers have also been classified by their use, e.g., with vacuum or high-temperature systems, but this distinction will not be applied here. Instruments have been reported that can function as several

types. One performs rotating-analyzer, principal-angle, and compensating measurements (182).

3.2 Compensating Measurement

In compensating ellipsometers, the phase change caused by reflection is counteracted by the use of a retardation device of fixed or variable retardation to restore linear polarization (8). Compensating instruments provide the greatest accuracy (13,17,183). Theoretical analyses of compensating ellipsometers have been presented (184,185). For some schemes of compensating measurements, however, the azimuth settings of adjustable components are coupled (186).

3.2.1 Incident Elliptic Polarization

The most commonly used arrangement of optical components for a compensating ellipsometer is illustrated in Fig. 3.1. It is often called the polarizer-compensator-sample-analyzer (PCSA) arrangement. Its functioning is explained by use of the Poincaré sphere, shown as a stereographic projection in Fig. 3.2. The linear polarization produced by the polarizer is represented by point P (of azimuth p) on the equator of the sphere. The action of the quarter-wave plate with fast axis F of 45° azimuth q (90° from H on the sphere) is represented by a $\delta_Q = 90°$ positive (counterclockwise) rotation of P on a small circle around F, resulting in polarization state E incident on the specimen. The location of E on the lower hemisphere is indicated by a cross (rather than a circle), and the connecting lines are dashed (rather than solid).

The effect of reflection on the specimen is shown in two separate steps in Fig. 3.2, one affecting only Δ and the other only ψ. The change in relative phase Δ results in a positive rotation of E around H by an angle Δ. This rotation brings E back to the equator at the location that happens to coincide with point F. The change in relative amplitude, which also occurs in reflection, is shown by the change (ψ) along the equator and results in the restored linear polarization A′. This polarization is extinguished by analyzer A of azimuth a with crossed (180° on the sphere) transmission direction.

Note that the combination of the polarizer of adjustable azimuth p with the quarter-wave plate of fixed azimuth q = 45° (or 135°) generates incident elliptic polarization with any relative phase and equal amplitudes of p and s components (point E lies on a great circle halfway between points H and V,

representing the p and s directions). The phase difference is chosen by rotation of the polarizer to be equal but opposite to that produced by the reflection. Thus, after reflection the light is linearly polarized, and its azimuth shows the amplitude ratio (tan ψ) of reflected p and s components.

The changes in relative phase Δ and relative amplitude tan ψ due to the reflection are related simply to the azimuths of polarizer and analyzer, as indicated in Fig. 3.2 and shown in Table 3.1 for all sixteen zones, including zone A1, which corresponds to Fig. 3.2.

3.2.2 Four-Zone Measurements

The same compensating measurement can be made by basically four different combinations of polarizer, quarter-wave plate, and analyzer azimuths, which have been called "zones" (54). The four zones are identified by the quadrant on the Poincaré sphere in which the polarizer azimuth lies and are numbered 1 to 4. The algebraic expressions for deriving ψ and Δ from the azimuth readings of polarizer, analyzer, and compensator (p, a, q) are different for the four zones. Since they also differ somewhat for different ranges of Δ values, it is convenient to further introduce four "zone groups" A to D (8). Thus, 16 zones are distinguished, which are shown in Table 3.1 with the corresponding expressions to derive the ellipsometry parameters from the azimuths at compensation. All azimuth readings are restricted to 0–180° to avoid further multiplicity.

An ideal ellipsometer would provide identical values for ψ and Δ from measurements in the four zones. In practice, however, component imperfections and alignment errors result in slightly different values. The effect of most ellipsometer imperfections is reduced by taking an average of the four-zone readings or zones 1 and 3 and zones 2 and 4 (54). The effect of cross-scattering between p and s components caused by cell windows, roughness, and optical activity of the specimen has been found to be cancelled by two-zone averaging; cross scattering in the compensator has required four-zone averaging (187).

Alternatively, the imperfection parameters of the instrument can be determined (25,188,189) and used to correct single-zone measurements. Corrections thus obtained have been found to be additive constants over ranges of ψ and Δ of only a few degrees but not over larger ranges (190).

3.2.3 Alignment

The alignment of optic axes and azimuths and the calibration of retardation are important factors in minimizing differences between zones and obtaining accurate (absolutely correct) measurements, as opposed to precise (high-resolution) measurements. It is the purpose of alignments to have the optic axes of the components for incident and reflected light positioned in the same plane (the plane of incidence, which also contains the surface normal of the specimen) and to intersect in the specimen surface; the azimuth circles should read zero for the transmission direction of polarizing elements and the fast axis of retarding elements in the plane of incidence, with azimuth readings increasing for rotation in the counter-clockwise (positive) direction, when looking into the beam.

Procedures for alignments and calibrations were described long ago (54,191) and have been discussed extensively in the literature since. Some are specific for one type of instrument. The procedures are based primarily on the fact that pure p or s linear polarization is not changed by reflection and that light of linear polarization incident parallel to the fast (or slow) axis of a compensator remains linearly polarized.

The alignment process is much simpler for instruments in which the optical components for incident and reflected light can be brought to a straight-through position (192–194) or the angle of incidence can at least be varied (188,195,196). When the angle of incidence cannot be varied, the alignment of polarizer and analyzer has to be based on transmitted-radiance (intensity) measurements at different polarizer and analyzer azimuths (197). Azimuth corrections for polarizer, analyzer, and compensator may also depend on wavelength (198).

The angle of incidence can be calibrated by autocollimation. In this technique, the image of a crosshair in an eyepiece is transmitted through the components for the incident beam and reflected back on itself by an auxiliary mirror positioned at the place of the specimen normal to the optic axis (199). The mirror is then rotated by a calibrated angle (twice the angle of incidence), and autocollimation is repeated through the components for the reflected beam. Reflection from the metallized end faces of a calibrated glass prism has also been used in place of the rotating mirror (8). Laser-beam alignment can take the place

of autocollimation (194).

Several analyses of component imperfections have been presented (25,200). Errors resulting from a 1-degree azimuth misalignment of polarizer and analyzer (without compensator) have been shown to result in 0–20% errors in n and k derived from measurements at the principal angle (138). A residual ellipticity of the polarizer of 0.003 rad has been found to cause large errors in thickness and refractive index of a SiO_2 film on Si, particularly for low film thickness (for 5-nm film, 100% error in thickness, 21% in refractive index) (201). Alignment procedures for polarizer and analyzer have been discussed (202). The sensitivity of ellipsometer measurements to errors in angle of incidence depends greatly on the properties of the reflecting surface (203). The value of $\partial\psi/\partial\phi$ is greater than unity for dielectric materials at angles of incidence above approximately 53°, but is small for metallic materials. The value of $\partial\Delta/\partial\phi$ is small for all materials at more than 10° off the principal angle of incidence. Of particular concern are errors caused by beam deviation in the polarizing elements (204).

3.2.4 Azimuth Modulation

A compensating-ellipsometer measurement typically involves finding the minimum in photodetector response as a function of polarizer and analyzer azimuth angles. Because of imperfections in optical components, depolarization in the specimen, and dark current of the photodetector, the minimum is never zero. Since the photodetector response is flat at the minimum, with the transfer curve being approximately parabolic, measurements to either side of the minimum are necessary to find the azimuth for the minimum with precision; such a measurement takes about five minutes, if done manually.

Self-compensating instruments have greatly reduced nulling time (13,16,17). An error signal, required to drive components to compensation, can be obtained by azimuth modulation. Such a modulation, analogous to the one used in manual operation, can be obtained by the mechanical rotation of polarizer and analyzer with stepping motors (130,205,206). A response time of the order of one second (based on one modulation) has been achieved by this method, with polarizer and analyzer being moved alternately.

The azimuth of the plane of polarization can also be modulated magneto-optically, by use of Faraday cells. Error signals can be derived by phase-sensitive detection from the response of the photodetector to such a modulation of the state of polarization and used for the manual nulling of analyzer and polarizer in turn (207) or simultaneously by use of servo or stepping motors (208–210). In the latter case, both modulations are applied simultaneously and can be separated by phase quadrature (190,211,212).

The mechanical azimuth rotation for nulling can also be replaced by Faraday-cell rotation, which provides higher speed, precision, and accuracy (13). An instrument of this type has been built (190,212) and is illustrated schematically in Fig. 3.3 (213). The Faraday-cell solenoids used in this instrument differ from earlier designs (211,214,215) by the use of separate concentric but magnetically decoupled windings to carry the high-frequency (10 kHz) modulation (requiring low inductance) and the lower-frequency (approximately 1 kHz) nulling currents. The modulations of polarizer and analyzer azimuths are separated by phase quadrature. The two error signals are derived by phase-sensitive detection from the photomultiplier response and integrated over 10 modulations. Polarizer and analyzer azimuths are driven to the nulling position simultaneously within about 1 ms. The exact response time depends on the change in azimuth required, since the slew rate is fixed (1600°/s).

Tests of the dynamic performance of this instrument have been conducted by the use of a segmented rotating disk to simulate a specimen with optical properties that could be reproducibly changed at different rates (216). Spectral-scanning capabilities were added later to provide a scan over the visible in three seconds (163,217). Separate Faraday cells for modulation and compensation have been used in instruments of different designs (218,219).

The design of Faraday-cell modulators has been discussed recently (220). Fused silica or different optical glasses are normally used as core materials, but benzene has been employed to avoid birefringence (221). Faraday cells have also been used for modulation and compensation in the measurement of optical rotatory dispersion (222).

Electro-optical retardation modulators can also be used to modulate the azimuth of linearly polarized light. Such devices are particularly well suited for use at high frequencies. In the simplest configuration,

an ADP (ammonium dihydrogen phosphate) Pockel cell is combined with a quarter-wave plate (223). The representation of this device on the Poincaré sphere (Fig. 3.4) shows how the action of the modulator with fast axis M and variable retardation δ_M converts the linear polarization of polarizer P into a series of elliptic polarizations between E_1 and E_2 (above and below the equator), which are converted to variable linear polarizations between P_1 to P_2 (on the equator) by the action of the quarter-wave plate with fast axis Q. That axis coincides with the azimuth of the linear polarizer P. P and Q are 45° (90° on the sphere) apart from the axis M of the modulator. Similar retardation azimuth modulators have been used to generate error signals for mechanical nulling with two servo-motors (223,224).

Another approach to rotate the plane of polarization at high rates (100 kHz) involves the use of wavelength modulation in a Mach-Zehnder interferometer design (225). This method has yet to be used in an ellipsometer.

3.2.5 Retardation Modulation

An error signal to control compensation can also be derived from a modulation of retardation (phase) (16). Variable retardations can be obtained (apart from the mechanically operated Babinet-Soleil compensator) by the application of an electric field in Pockel cells, which typically contain ammonium or potassium dihydrogen phosphate (ADP or KDP) crystals, or by the application of mechanical stress in piezoacoustic devices or in a magnetic clamp (226).

Two ADP cells, attached to polarizer and analyzer at a 45° azimuth difference (and rotating with them), have been used for retardation modulation (227). The rotation of analyzer and polarizer for compensation is accomplished with two servomotors. Two KDP plates of fixed azimuths have been used for modulation and compensation with polarizer, compensator, and analyzer at fixed azimuths (93). All 16 elements of the Mueller matrix have been determined by use of four Pockel-cell modulators, two before and two after reflection (72).

A simultaneous modulation of azimuth (with a Faraday cell) and of retardation (with a piezoacoustic device) operating at different frequencies has been used to generate error signals for manual nulling (228).

3.2.6 Achromatic Compensator

The principal shortcoming of compensating ellipsometers has been that the compensator provides quarter-wave retardation only at a single wavelength. For spectroscopic ellipsometry, deviations from quarter wave over a limited range could be taken into account in the data analysis. Alternatively, variable retardation devices, including the mechanically adjustable Babinet-Soleil compensator, can be used to provide quarter-wave retardation at selected wavelengths. However, most of these approaches are tedious and not suited for continuous spectral scanning, and they have not been used to a great extent.

A different approach consists of the use of internal reflection phase retarders, which can be designed in different forms and involve the use of transparent coatings or multilayers on the reflecting surfaces (49,229). A four-reflection device has been assembled from right-angle prisms, but the three-reflection Fresnel rhomb (Fig. 3.5) has been shown to provide remarkably constant retardation over the visible spectrum (230). Such a device has been used as an achromatic quarter-wave retarder in spectroscopic ellipsometers operated with mechanical compensation (208,210) and in two with magneto-optic compensation (163,217,218), the first of which is capable of providing a spectral scan over the visible in three seconds.

3.3 Photometric Measurement

In photometric or noncompensating ellipsometers, the irradiance (intensity) at the photodetector is measured as a function of a modulation of the state of polarization introduced before or after reflection. Because of their high optical efficiency, photometric instruments are well suited for the use of weak light sources or poorly reflecting surfaces. With most arrangements, the accuracy of photometric measurements depends strongly on the linearity and insensitivity to the state of polarization of the detector and the lack of polarization of the source (13,111).

3.3.1 Rotating-Analyzer Instruments

The photometric configuration most commonly used employs a rotating analyzer (or polarizer), often without a compensator (231–235) (Fig. 3.6). Basically, the polarization ellipse is traced in this technique as a function of analyzer azimuth a, with the shape (axial ratio) and orientation (azimuth of major axis) of

the ellipse (but not its sense of rotation) being derived from the ratio of minimum and maximum irradiance I and the azimuth associated with the maximum (Fig. 3.7):

$$\tan \gamma = \sqrt{\frac{I_{min}}{I_{max}}} \quad , \tag{82}$$

$$\theta = \theta_{max} \quad . \tag{83}$$

The variation of the amplitude from an elliptic polarization E transmitted by a rotating analyzer can be represented by the lengths of chords in the Poincaré sphere (Fig. 3.8). The irradiance I on the photodetector as a function of analyzer azimuth a can be formulated as (232)

$$I(a) = I_0 \, (1 + b \cos 2a + c \sin 2a) \quad , \tag{84}$$

where I_0 is the average irradiance over a full rotation and the Fourier coefficients b and c depend on axial ratio γ and azimuth θ of the major axis:

$$b = \cos 2\gamma \cos 2\theta \quad , \tag{85}$$

$$c = \cos 2\gamma \sin 2\theta \quad . \tag{86}$$

For linear polarization of 45° azimuth incident on the specimen:

$$b = -\cos 2\psi \quad , \tag{87}$$

$$c = \sin 2\psi \cos \Delta \quad . \tag{88}$$

The amplitude and phase of the sinusoidal photodetector response are now mostly measured by Fourier-transform detection (232,235–237).

The fact that rotating-analyzer instruments can be used without a compensator, and that polarizers operate over a wide spectral range, make such instruments well suited for spectral measurements. For precision measurements, however, a compensator may still have to be used (13), and its use is essential for the measurement of reflection from dielectric surfaces (238).

The measurement of irradiance ratios requires a photodetector with a response that is linear and (for the rotating analyzer) independent of polarization (236,239). Photometric methods offer the possibility to simultaneously measure changes in reflectance; these changes have been used as a third measured parameter for use in interpretations (164,165,167).

Systematic errors in rotating-analyzer ellipsometers have been treated in detail (232,236,240). They can be reduced by the use of different incident polarizations (241). Measurements with two polarizer azimuths 90° apart have been used to improve accuracy and have resulted in a new adjustment procedure (242).

The polarization ellipse can also be reconstructed from measurements with a partial rotation or oscillation of the analyzer (243), which can be accomplished at high frequency with a Faraday cell (25). A very high frequency of rotation has been obtained with a 1.8-MHz beat frequency between two linearly polarized components of different frequency in a Zeeman laser (244). The measurement of photomultiplier output at three predetermined analyzer azimuth angles has also been used (233). Azimuth rotation with two stepping motors or Faraday cells with four polarization-sensitive detectors can provide all the elements of the Mueller matrix (245).

3.3.2 Other Rotating Components

Many other photometric ellipsometers with rotating components are possible and have been compared in detail (17,46). Of particular interest is the rotating-compensator arrangement, which resolves the handedness of the ellipse and provides all four Stokes parameters (17,246–249). It therefore qualifies as a polarimeter, as do numerous combinations of several rotating or oscillating components (17). The Jones matrix has been derived from three measurements with a rotating compensator (247). The mechanical oscillation of a compensator can be simulated by the use of two Faraday cells surrounding a fixed compensator (250). All 16 elements of the Mueller matrix have been obtained by the synchronous rotation of two quarter-wave retarders (251).

The rotating-depolarizer ellipsometer (252) is a spectroscopic ellipsometer with a single rotating component, a calcite plate with no transverse separation between ordinary and extraordinary beams. The

optical-path difference between the two beams is larger than the longitudinal coherence. Thus, interference in the polarizer is avoided in addition to the fact that a polarization sensitivity of the detector does not introduce systematic errors.

3.3.3 Retardation Modulation

The state of polarization can also be determined from the response of the photodetector to a periodic variation of retardation, typically applied to the incident beam and determined by phase-sensitive detection. In contrast to rotating-analyzer or polarizer devices, retardation modulation is able to distinguish between circularly polarized and unpolarized light, and between left and right rotation, and the measurements are not affected by partially polarized light sources or polarization-sensitive detectors (161). The theory of retardation modulation, also called phase or polarization modulation, has been discussed on the basis of a modified Jones calculus in which component imperfections are accounted for (240).

The retardation modulation has usually been accomplished by the use of photoelastic (acousto-optic) devices (253–259) in which a strain on an otherwise isotropic material, such as fused silica, is applied by a piezoelectric driver. Retardation modulation can also be produced by electro-optic devices (Pockel cells with ADP or KDP crystals, or Kerr cells with polar liquids) (227,260–262).

The accuracy and precision of a polarization-modulation ellipsometer and the effect of alignment errors and component imperfections have been analyzed (263). The thermal stabilization of four-crystal ADP devices has been investigated (264), and microsecond response has been reported. The potentially even faster response of instruments using photoelastic devices has, however, not been realized for measurements yet. Errors resulting from the use of a photoelastic modulator in ellipsometry have been analyzed (265). For spectroscopic ellipsometry, the wavelength dependence of the retardation modulation has been accounted for (256).

A Wollaston prism dual detector has been used recently to separate phase shifts caused by reflection and by the Kerr effect (259). Four Pockel cells with two polarizers have been used for the simultaneous measurement of all 16 elements of the Mueller matrix (72).

3.3.4 Multiple Detectors

The use of two analyzing prisms of fixed azimuth and three photodetectors for measuring irradiance of azimuths 0°, 45°, and 90° has been described as one of the most simple and rugged ellipsometers (266). The application of multiple detectors is also discussed in Section 3.3. Four polarization-sensitive detectors have been proposed recently to determine the Mueller matrix (245,267).

3.4 Other Configurations

Numerous other ellipsometer configurations are possible (17). A few types that have been used in practice will be discussed briefly.

3.4.1 Return-Path and Principal-Angle Instruments

In a return-path ellipsometer, also called an autocollimation ellipsometer, the light beam, after reflection from the specimen, is made to retrace its path in the opposite direction by reflection from an auxiliary mirror placed normal to the reflected beam (268–271). Thus, the light encounters two reflections from the specimen (except for the special case of normal incidence), and the same optical elements serve as polarizer and analyzer, resulting in greater sensitivity and fewer imperfection parameters. The normal reflection from the isotropic auxiliary mirror does not change the state of polarization. Due to the double reflection on the specimen, the change in complex polarization ratio is

$$\rho = (\tan \psi \, e^{i\Delta})^2 \quad . \tag{89}$$

In the simplest configuration, illustrated in Fig. 3.9, the angle of incidence is chosen to be the principal angle at which

$$\Delta = \pm 90° \quad , \tag{90}$$

$$p = \pm \psi \quad . \tag{91}$$

To conduct a measurement, the azimuth of the single polarizer, which also serves as analyzer, and the angle of incidence are adjusted for extinction of the reflected light (268,271). This process has been automated by use of a Faraday-cell modulator and two servo-motors (272). A spherical mirror has also

been used to return the beam (273).

The circular state of polarization, resulting from the first reflection, can also be determined by a rotating analyzer instead of the return-path design (274). Such arrangements are well suited for spectroscopic measurements and are not sensitive to detector linearity. Measurements near the principal angle also provide the best accuracy for determining film thickness and refractive index or the optical constants of bare substrates (275).

If a compensator is used in a return-path ellipsometer, the angle of incidence is not restricted to the principal angle, and several different arrangements are possible (269). Normal-incidence return-path ellipsometry has been discussed for the measurement of anisotropic surfaces (270).

3.4.2 Psi Meters

Instrumentation for ellipsometry can be greatly simplified if only the amplitude parameter ψ is to be measured. With a single rotating polarizer, the ratio of the ac to the dc components of the reflected-light flux represents $\cos 2\psi$ (276). The angle of incidence may be varied until the ac component vanishes, indicating $\psi = 45°$ (177). Another form of a psi meter has been obtained by the use of an optical fiber for phase modulation and illumination, with $\tan 2\psi$ being derived from the measurement (277).

3.4.3 Interferometric Ellipsometry

An interferometric ellipsometer that requires no compensator has been based on the Michelson interferometer (278). The return-path reflection from the specimen is brought to interference with the reflection from a moving reference mirror (a corner-cube reflector). The resulting modulations in the irradiance of s and p components are measured simultaneously with a Wollaston prism and two detectors, the output of which is used to compute the ellipsometer parameters. Specimen and mirrors can be located inside a vacuum chamber, making measurements independent of window birefringence.

3.4.4 Pulse Ellipsometry

Off-null measurements of a few picoseconds time resolution have been obtained by the use of repeated picosecond optical pulses with variable delay (279). A Wollaston prism has been used for the

simultaneous measurement of two orthogonal components with submicrosecond time resolution during the cleaning of a surface with a 35-ns excimer-laser pulse (280). The use of a four-channel optical analyzer has been described for determining the ellipsometer parameters or all four Stokes parameters with a single nanosecond optical pulse (281).

3.4.5 Differential Ellipsometry

A particularly interesting type of differential ellipsometer employs the sequential reflection of light on the two surfaces to be compared (282). The angle of incidence is the same on both surfaces, but the surface normals are at right angles to each other. The p and s directions are therefore exchanged between the two reflections. In one application of this principle (comparison ellipsometer, 282,283), one of the reflecting surfaces, typically a reference surface with continuously variable properties that have been calibrated independently (e.g., a wedge-type film), is imaged (Fig. 3.10). With crossed polarizer and analyzer, extinction is observed in areas of the reference surface where the properties of the (uniform) specimen surface (e.g., the film thickness) are the same as those of the reference surface. With white-light illumination, deviations from extinction appear as interference colors.

3.4.6 Infrared and Microwave Ellipsometry

Ellipsometry has been conducted outside the visible spectral range. Although the principles of measurement are the same, many of the optical components are different.

Questions of instrument design and applications of infrared spectroscopic ellipsometers have been discussed (284,285). A rotating gold-grid polarizer between two fixed polarizers has been used to identify adsorbed species (286,287). A compensating manual ellipsometer, operating at 10.6 μm, employing wire-grid polarizers and a CdS quarter-wave plate, has been used to study shallow ion-implanted layers on Si (288). A fixed wire-grid polarizer and a rotating analyzer have been used to determine carrier profiles in silicon (289). For the same wavelength, germanium Brewster's-angle polarizers and photoelastic retardation modulation have been used to determine refractive indices (258). Wire-grid polarizers and a quartz compensator have been used at 118 μm to study epitaxial silicon layers (290). Three-reflection devices

have also been analyzed for use as infrared retarders (291).

A microwave ellipsometer, operating with a klystron source (50 GHz, 6-mm wavelength) has been used with a mica quarter-wave plate and a Faraday rotator or a twisted waveguide for conductivity measurements (292). Simpler instrumentation of this kind had been suggested earlier (293).

3.4.7 Imaging and Micro-Ellipsometry

Surfaces with locally varying optical properties can be observed with ellipsometers that restrict the measurement to a small surface element. The spatial selection can be made before or after reflection. In the former case, the illuminating beam is focused to a small spot on the specimen (typically 25 μm). Such a converging beam results in a continuous range of angles of incidence, which should be taken into account in the evaluation of measurements. The problem can be alleviated by using an average angle of incidence for which measurements are not sensitive to its value (294). The convergence to a 50-μm spot has been neglected (295) and a 21-μm region has been examined at perpendicular incidence (296).

Except for the double-reflection comparison ellipsometer discussed in Section 3.4.5, for which a 2-μm resolution has been obtained with a modified design (283), the ellipsometric imaging of surfaces has been accomplished by scanning on the specimen or in the image. An illuminated spot of 50 μm diameter has been scanned by moving the specimen with stepping motors (297). Photometric measurements with photoacoustic retardation modulation on this system have required several seconds for each position.

Regions of 10 μm diameter on the specimen have been isolated for measurement in enlarged images by use of a diaphragm (298) or a pinhole (299). In the latter case, the image plane was inclined to the optic axis according to the Scheimpflug principle in order to keep parts of the (inclined) specimen at different distances in focus.

4. INTERPRETATION

4.1 Optical Models

Most physical properties of surfaces and thin films must be derived from ellipsometer measurements by the use of optical models. Optical models are often based on a knowledge of what can reasonably be expected, and they may represent only the principal features of real systems (162). A successful optical model is able to reproduce all experimental measurements.

4.1.1 Surface Parameters

A bare, smooth metal surface is described by the real and imaginary parts of its complex refractive index, or two parameters; and a single, homogeneous, isotropic, smooth film is described by its thickness and its real or complex refractive index, or another two to three parameters.

Real physical systems are usually more complex, however. A rough surface requires at least two more parameters for its characterization, such as the thickness and volume fraction of an equivalent layer in the simplest model. Anisotropic substrate or film materials are described by at least two refractive indices, both of which may be complex. A porous or composite film requires a knowledge of the volume fraction of constituents. Surface coverage needs to be specified for a discontinuous (island) film, and multiple or inhomogeneous films require still further parameters for their description.

4.1.2 Measured Parameters

Conventional ellipsometry provides only two measured parameters, but additional information is usually available that can be used to derive more than two surface parameters from the measurements. Additional optical information can be obtained by the measurement of reflectance, and of ellipsometry at different angles of incidence (170) or in different immersion media (295). For measurements during film growth, it has long been recognized that requirements of continuity can be used to exclude discontinuous interpretations, particularly if films are known not to change optical properties during growth (300). Restrictions on the range of acceptable values for unknown parameters can also be very useful.

Spectroscopic ellipsometry is a very effective way to derive additional film parameters, apart from its use for determining spectral properties of materials. Wavelength-independent film parameters, such as thickness, porosity, composition, or number of layers, are particularly suited for derivation by this approach, in which one considers ellipsometer measurements at different wavelengths as independent measurements (102,163).

For electrochemical film formation with known current efficiency, additional film parameters can be obtained on the basis of charge passed. Thus, for anodic film growth, a continuous mass and charge balance has been used to determine the total amount of products formed and their distribution between different parts of the interface under consideration of diffusion, ionic migration, and convection (213). In vacuum deposition, rate monitors can provide information on amount of material.

4.1.3 Optimization of Models

The simultaneous determination of several surface parameters from a set of measurements generally requires the use of multidimensional optimization routines (least-squares regression analysis) to find a combination of physical parameters for which the difference (sum-of-squares error) between measurements and model predictions is a minimum (91,101,300,301). The sum-of-squares error S for N Δ, ψ pairs measured (M) and calculated (C) can be defined as

$$S_{\psi,\Delta} = \sum_{i=1}^{N} \left[\Delta_{M,i} - \Delta_{C,i}\right]^2 + \sum_{i=1}^{N} \left[\psi_{M,i} - \psi_{C,i}\right]^2 \quad . \tag{92}$$

Statistically defined model variance, parameter variance, and parameter confidence intervals can be determined by this process as measures of the validity of an interpretation (94,101,163,301). An excessive number of adjustable model parameters can improve agreement with experimental results but result in unacceptable correlation coefficients and confidence intervals (162).

Eight models of increasing complexity, illustrated in Fig. 4.1, have been investigated, and up to seven film parameters have been determined by use of mass and charge balances to account for monochromatic ellipsometer measurements of the anodic oxidation of silver and other metals (91,213). Two anodic Ag(I) oxide layers have also been reported by other authors (302,303).

Models considered for the spectroscopic ellipsometry of cathodic metal deposition are shown in Fig. 4.2 (102). The most realistic three-layer model (multilayer film) requires six parameters for its description and results in unacceptable parameter variances. The topmost dendritic island film, although it contained a large fraction of the deposited metal, was determined by an optical analysis to have a negligible optical effect. The optimization could therefore be conducted for a two-layer model with three unknown parameters (two thicknesses and one porosity). Results for three deposit thicknesses are given in Table 4.1 (102).

The uniqueness of optimized solutions is not easily determined. Optimization routines may select a local minimum in place of a deeper global minimum or miss sharply defined minima. Measures used to guard against misleading results include the use of different optical models, different optimization procedures, or variations in the proscribed parameter space, the initial guess, and the step size of the optimization.

A theoretical analysis of the sensitivity of ellipsometry for the analysis of two-layer films has concluded that both thicknesses can be found independently by least-squares analysis (304). The sensitivity of ellipsometer measurements to surface and single-film parameters was investigated earlier by the use of partial derivatives (305). The use of a complex bilinear transformation has recently been shown to provide faster, more accurate convergence than the Newton-Raphson method (306). For a single transparent film on an absorbing substrate, refractive index and thickness have been determined without the use of an initial guess, and an optimum angle of incidence has been determined in the process (307).

4.2 Combination and Comparison with Other Techniques

One of the attractive features of ellipsometry is that it can be combined with many other experimental techniques. Such combinations have been used to provide additional information or to compare interpretations.

4.2.1 Vacuum Techniques

A combination of low-energy electron diffraction (LEED) and ellipsometry (199) for studies of physical adsorption on silver from ultrahigh vacuum has shown that below 100 K contamination from residual gases was appreciable (308,309). LEED patterns were found to be insensitive to the presence of adsorbed material; a disordered nature of the layers and patchwise coverage were derived from these observations. Changes in LEED patterns have also been difficult to detect for oxygen on tungsten (310).

Ellipsometry has been used to calibrate Auger electron spectroscopy (AES) for oxygen adsorption on silicon. The Auger peak height was found to be proportional to coverage up to 1.5 monolayers (311). An absolute coverage calibration for oxygen on Cu(110) has been obtained by the combination of LEED with ellipsometry and AES (98). The cleaning and ordering of a ruthenium surface has been monitored by AES, LEED, and ellipsometry in preparation for measuring optical constants (312).

The average composition of passivating films on chromium has been determined by AES to be Cr_2O_3, with the thickness found by ellipsometry to increase linearly with anodic potential (313). The removal of material by ion bombardment for the determination of composition depth profiles may not occur uniformly over a surface; on lead films a formation of pits has been found by ellipsometry and confirmed by scanning electron microscopy (314).

The use of ion etching of lead films to determine composition profiles by AES has shown that after removal of a very thin oxide layer, submicroscopic pits form in the lead (Fig. 4.3). These pits reach the copper substrate before all the lead is removed, resulting in the wrong interpretation of a gradual change in composition at the bottom of the film. In the ellipsometer measurements, an island-film model with coherent superposition (Section 2.3.4) has been used (314).

4.2.2 Radiotracer Techniques

In an early comparison of ellipsometric and radiotracer methods for the study of adsorption from solutions and vapors on different metals, the optical film thickness was found to be a good measure of surface concentration ranging from fractional monolayers to several monolayers (97). Oxygen-isotope and

nuclear microanalysis have since been used for passive layers on iron (315).

4.2.3 Other Techniques

The thickness of anodic oxide layers (15–180 nm thick) formed on tantalum in sulfuric acid, as determined by ellipsometry, has shown excellent agreement with thicknesses derived from interference spectra (316). Good agreement has also been obtained for the thickness of two metal and two oxide layers (30–130 nm thick) determined by ellipsometry and six other techniques: step height measured with stylus profilometer and interference microscope, interference spectroscopy, x-ray electron microprobe, microbalance, and chemical analysis (317).

For vapor adsorption on Ge and Si, film thicknesses determined on surfaces compared well with volumetric measurements on powders (318).

A comparison of x-ray fluorescence and stylus step-height measurements with ellipsometry for 2.5-14 nm thick silicon films has shown a good relative correlation, but ellipsometry was found to be far more accurate (319).

5. APPLICATIONS

The literature on applications of ellipsometry is growing rapidly. The following section is intended to illustrate questions investigated about processes and materials of electrochemical interest and point out some of the results obtained by the use of the technique.

5.1 Anodic Oxidation

The study of anodic film-formation is among the most prominent applications of ellipsometry, because changes on surfaces can be observed with great sensitivity while the surfaces are immersed in liquids, typically aqueous solutions. Anodic films, which are mostly of oxidic composition, are formed under well-controlled conditions and are therefore well suited to investigate questions on the mechanism of film formation and to serve as models for spontaneous film-formation processes. Anodic films are finding an increasing number of practical applications (320).

5.1.1 Valve Metals

The rectifying and dielectric properties of certain anodic oxides have a long history of practical use and study that more recently has included ellipsometer measurements.

The anodic oxide on tantalum formed in phosphoric acid has been shown to consist of two layers, with the lower refractive index of the outer layer caused by phosphate incorporation (321). Oxides formed in sulfuric or citric acids are, however, uniform, nonabsorbing, and isotropic at zero field (322), except for a recently found absorbing layer of constant 2-nm thickness at the metal surface (316). Anodic oxides on Ta-Al (323) and Ta-Nb (324) alloys consist of homogeneous mixtures of oxides in the same ratio as that of the metal. The anodic oxidation of niobium is in many ways similar to that of tantalum.

The anodic oxidation of aluminum in phosphoric acid results in a growing porous layer on top of a pore-free barrier layer of fixed thickness (325), and a similar model, but with a smooth transition between both layers, accounts for measurements in alkaline solutions (326). In boric and tartaric acid uniform barrier-type layers are found (327–329).

A dual-layer structure has also been found for the anodic oxide on titanium formed in KOH, with both layers increasing in thickness during formation (330). For oxides formed in sulfuric acid, a single-film model has provided a satisfactory interpretation of spectroscopic ellipsometer measurements of film formation (331), but no clear picture could be derived for potential cycling (332).

Anodic oxide growth on zirconium in carbonate solution has been found to be similar to that on other valve metals, except that the oxide is optically slightly absorbing and its properties are not affected by changes in the electric field (333).

Electrostriction (change in thickness with electric field) has been observed for anodic oxides of tantalum, niobium, tungsten, and molybdenum (127–130,334). A field-dependent birefringence has been found for oxides of tantalum, niobium, and tungsten (129,130,334,335). This birefringence can be described by an elastic dielectric model (336).

5.1.2 Nickel, Iron, and Manganese

The growth of oxide layers on nickel in alkaline solutions (337) involves a change in optical constants (338,339) that has been related to a change in electrocatalytic activity for oxygen evolution (340). The change in composition during potential cycling has also been observed optically (341). Very thin, transparent oxide or hydroxide layers on rough nickel surfaces can appear absorbing (154,155).

The anodic oxidation of iron in neutral borate and acidic sulfate solutions has been interpreted by a two-layer model (342–344). In alkaline solution, passivation occurs in two stages (345), and during cycling the low-density outer layer grows on top of the compact, thin inner layer.

The anodic deposition of iron and manganese oxides from their ions in solution has also been investigated (209,346). Manganese dioxide forms an island film below thicknesses of 50 nm.

Passivating films on nickel and iron are discussed in Section 5.3.

5.1.3 Platinum and Gold

The anodic oxide on platinum is so thin that the determination of its thickness and optical constants is difficult (347) and requires the simultaneous measurement of changes in reflectance (166,167). The

films are strongly absorbing (167) and change properties during potential cycling, with only a part of the film being reduced cathodically (348,349). The presence of a thin, optically absorbing outer α–oxide layer has been proposed (350,351). Films appear to form in patches (167); double-layer effects have also been considered (352). A high-field ionic-conduction mechanism has been found to hold for film growth, similar to oxide growth on Ta or Fe (347,349). The catalytic activity of platinum depends on the oxide film thickness (353).

Anodic oxides on gold have also been found to show a residual portion and to result in a restructuring of the metal surface (348) by a place-exchange mechanism (169). The successive formation of three oxide layers has been proposed (354,355). The determination of optical constants of gold is difficult because optical properties are strongly affected by interaction with solution species (electroreflectance) (167). Double-layer effects require different corrections for bare or oxide-covered surfaces (352). Electroreflectance effects have been taken into account for bipyridyl adsorption on gold (356).

5.1.4 Other Metals

The galvanostatic oxidation of copper in sodium carbonate solution has been shown to result in an inner, compact, monovalent layer and an outer divalent layer (357). The film grows by a dissolution-precipitation mechanism in KOH, and the inner layer is a light-sensitive semiconductor (358). During electropolishing of copper in phosphoric acid, the formation of a thin solid film and a viscous layer has been determined (359).

The early stages of anodic Ag_2O formation on Ag(111) have been interpreted by a dual-layer optical model that contains a nonporous underlayer and a porous island overlayer (representing crystallites), shown in Fig. 5.1. A large decrease in the number density of crystallites during their growth has been found (360).

Sulfate layers on lead represent an anodic film of nonoxidic composition. A gradient in refractive index across the film has been found and attributed to a gradient in porosity (361).

5.1.5 Semiconductors

The spectroscopic ellipsometry of anodic oxides on GaAs has indicated the presence of a very thin As-depleted region at the outer film surface (362). The oxide thickness had been found earlier to follow a linear relation with voltage, similar to that of the valve-metal oxides (363). Monochromatic ellipsometry has been combined with impedance measurements (364).

Anodic oxides on CdTe have been found by spectroscopic ellipsometry to be uniform, with sharp interfaces. Hg-containing substrates have been shown to produce a residual Te layer (365), which is also found as a result of chemical oxidation (366).

A connective layer has been identified by ellipsometry during growth and etch back of anodic oxides on Si (90). The successive anodization of monolayers in layered semiconductors has also been investigated (367).

5.2 Gas-Phase Oxidation

The optical properties of monolayers of oxygen on different crystal faces of copper have been found by spectroscopic ellipsometry to be different from those of bulk Cu_2O, but have been approximated by the Bruggeman effective-medium model (368).

The optical constants and thicknesses of air-formed oxides on zircaloy have been determined by multiple-angle ellipsometry at wavelengths of 0.3–3.4 μm (369).

The thermal oxidation of Si has been found to result in a layer of graded composition (90), and a complex mechanism for the oxidation reaction has been derived from earlier measurements (370).

The reaction of oxygen with magnesium has been investigated by spectroscopic ellipsometry. The surface layer has been determined to be a mixture of oxide and metal by use of the Bruggeman effective-medium model (371).

The chemisorption of oxygen on silver has been found to result in a 0.3-nm-thick surface layer (372). Oxide grown on Ta (373), Mo (374), and Pu (375) has also been investigated.

5.3 Corrosion

Ellipsometry is also well suited for corrosion studies, where properties, formation, and removal of surface layers is of central concern, as had been pointed out in previous reviews (9,376).

5.3.1 Passivation

The chemical passivation of iron by immersion in chromate, nitrate or nitrite solutions was an early subject of study by ellipsometry (377), and more recently, mixtures of different hydroxides have been identified in the passivation layers (378). Multiple-layer phosphate films have been identified after immersion of iron in aerated orthophosphate solutions (379).

The anodic passivation of iron in borate buffer has been determined to result in a simple FeIII layer by spectroscopic ellipsometer and change-in-reflectance measurements (168). However, anodic-passivation measurements in acidic sulfate have been interpreted by a two-layer model (344,380). A previous study had derived a two-layer structure resulting from the use of neutral or alkaline solutions, but a single layer from acidic solutions (381). The dual-layer model has also been found more recently for alkaline solutions (345,382,383).

The passivating film on nickel in acidic sulfate has been found to be much thinner than that on iron, with its properties depending on pH and potential (384).

The anodic passivation of chromium in aqueous sulfate has been found to result from the simultaneous dissolution and formation of a monolayer oxide film (385). In phosphate and borate solutions, the film thickness increased linearly with potential, and a uniform film composition of Cr_2O_3 was derived from the refractive index and confirmed by Auger analysis (313).

Micro-ellipsometry of 10-μm regions was used for passive and transpassive layers on individual grains in stainless steel (298).

Film growth during repassivation after abrasive film removal (tribo-ellipsometry) has been found for a titanium alloy in chloride and nitrate solutions to occur by an oxide-patch nucleation-and-growth mechanism (386). The same technique has been used to determine the optical constants of bare stainless

steel in sulfate solution (298).

5.3.2 Corrosion Layers

Corrosion layers on copper in water of different oxygen content have been shown to form at different rates on different crystal faces and to change composition from cuprous to cupric oxide during growth (387,388). With low O_2 concentrations, illumination promotes dissolution and results in lower film-formation rates (389). Cuprous oxide is formed in the corrosion of copper and brass in aqueous ammonia (390).

For corrosion under organic coatings, roughening and film growth have been separated, and anodic and cathodic sites have been identified (391,392).

Oxide layers of 0.7–4.0 nm thickness were found to form on evaporated aluminum in distilled water (393).

Ellipsometer measurements of corrosion layers on lithium in $LiClO_4$- PC solutions have been better represented by a linear refractive index profile in the film than by a constant or parabolic profile, shown in Fig. 5.2 (394). A small extinction coefficient, determined for layers formed on Li with water vapor, had earlier been attributed to embedded metal clusters or color centers (395).

5.3.3 Corrosion Inhibitors

Aliphatic acids adsorbed on iron have been found to affect the optical properties of corrosion layers (396). Corrosion layers formed on copper in the presence of benzotriazole, which are more protective, have been found to be less porous than those formed with benzimidazole (397). The optical properties of anodic oxides on gold are affected by adsorbed alcohols (398).

5.4 Cathodic Metal Deposition

5.4.1 Underpotential Deposits

For the underpotential layer of lead on gold, a change from an ionic to a metallic state of the layer with increasing cathodic potential was derived from ellipsometer and reflectance measurements by use of a

single-film model (399).

Different optical models have been investigated for the interpretation of measurements of underpotential film formation of Pb on Cu(111) and Ag(111) (94). An island model with coherent superposition of polarization states, described in Section 2.3.4, has provided good interpretation of measurements (Fig. 5.3). At complete coverage, the film thickness was that expected for a monolayer, with optical constants close to those for metallic lead, and fractional monolayer coverages derived from ellipsometer measurements agreed with those based on Faradaic charge passed (94).

5.4.2 Nucleation and Growth

The nucleation of three-dimensional Pb deposits, following formation of the underpotential layer, has been found to result in layers with dielectric-like optical properties. These properties result from the porosity of the layers and can be accounted for by an effective-medium model (101).

The optical constants of black nickel deposits have been determined by the use of a single-layer film model and have provided good agreement between computed and measured reflectivities (400).

5.4.3 Effect of Inhibitors

Rhodamine-B has been found to act as an inhibitor (leveling agent) for lead deposition. The presence of the material on the surface has been determined by spectroscopic ellipsometry and has been found to eliminate the microporosity otherwise found in the initial deposit (102). Measured ellipsometer data for Δ are shown in Fig. 5.4, together with predictions based on a two-layer model that employs optimized parameters given in Table 4.1.

5.5 Reduction of Oxides

5.5.1 Potential Cycling

The study of anodic films often includes their behavior under cathodic polarization or multiple anodic-cathodic cycles. Complex optical behavior with progressive irreversible changes has been found with PbO_2 (401); with MnO_2 partial reversible discharge has been separated optically from total

irreversible discharge (209). The reduction of anodic copper oxide films has been found to occur in three stages and is not a solid-state process, with repeated cycling resulting in an inhomogeneous structure (357).

5.5.2 Electrochromism

The cathodic conversion of transparent anodic oxides on molybdenum and vanadium results in the formation of an absorbing material. The conversion proceeds from the film-electrolyte interface toward the metal (402,403). In contrast, the electrochromic conversion of tungsten oxide has been found to occur uniformly throughout the layer (404). A dual-layer film structure had been proposed earlier for film formation (405). Electrochromism and electrostriction have been reviewed recently (406).

5.6 Adsorption Processes

5.6.1 Double Layers

The direct observation of electrolytic double layers is one of the more difficult applications of ellipsometry, because the free-electron contribution to the optical constants of the metal surface is affected by the adsorption of ions (352,407). This effect can be represented by a transition layer between bulk metal and bulk solution (408), and it forms the basis for electroreflectance measurements. An empirical correction for double-layer effects in formation and reduction of oxides on Au and Pt has been used (352). Measurements of the potential-dependent adsorption of sulfate, chloride, bromide, and iodide ions on platinum have been reported, with the adsorption of perchlorate and fluoride being undetectable (409).

5.6.2 Physical Adsorption

The physical adsorption of inert species changes the electronic structure of the substrate only minimally. The adsorption of different gases on Ge and Si (410) and of organic vapors on Si (411) has therefore been well represented by macroscopic optical theory, and molecular orientation could be determined for benzene on Si. The macroscopic optical theory has also been used for the low-temperature adsorption of different gases on Ag (308,309,412), for which heats of adsorption were derived from film thicknesses. For xenon on graphite, no difference was found according to interpretations based on macroscopic or microscopic optical models (413–415).

5.6.3 Chemisorption

Measurements of potential-controlled chemisorption of oxygen on platinum (416), Ni, Co, and Ag (417) have been interpreted by use of the (macroscopic) Drude equations. A chemisorbed hydrogen species on Pt, which is not detected in reflectance transients, has been observed by ellipsometry (169).

The optical principles of ellipsometry of chemisorption from the vapor phase have been discussed recently (23), and optical theories have been reviewed (99). In early work with oxygen on silicon, similar interpretations were obtained by the use of macroscopic and microscopic optical theories (418). In later studies on the adsorption of many gases on Si and Ge, the existence of an absorbing transition layer on clean substrates, representing dangling bonds, was proposed. This layer is either removed or made less absorbing by chemisorption (99,419,420). Changes in optical properties of Si have been found to primarily affect ψ, while Δ was a measure of coverage (318). A removal of surface states has also been observed for chemisorption on GaP (421).

Changes in optical constants of niobium during thermal oxidation have been attributed to oxygen dissolution in the metal (422). Surface states induced on silver by chemisorption of oxygen have been determined by ellipsometry and reflectance measurements (372).

The reaction of low-pressure chlorine with oxide-free aluminum has been found to result in physically and chemically adsorbed layers (423).

5.6.4 Oriented Layers

Langmuir-Blodgett films, up to 140 monomolecular layers thick, have been well represented by uniaxially birefringent film models with the optic axis oriented normal to the surface (137,424). An apparent extinction coefficient for such transparent layers is derived from the measurements by use of an (incorrect) isotropic-film model (139). A uniaxially anisotropic film model was also used to derive molecular orientation of Rhodamine B adsorbed on Pt, Ag, and Cu (102,135).

An edge-on molecular orientation of bipyridyl adsorbed on gold has been derived with an isotropic-film model (356). Molecular layers of carboxylic acids and an alcohol have been measured on a free water

surface (425).

Measurements of the adsorption of quinolines on mercury have been interpreted in terms of three molecular orientations, resulting in anisotropic layers (134), as did the adsorption of DNA (136). Adsorbed and reacted layers of different barbituates were found to be transparent, with some being anisotropic, some isotropic (426).

5.7 Mass-Transfer Boundary Layers

Electrochemical reactions proceeding at appreciable rates result in the formation of a region of solution adjacent to the electrode in which the concentration of reactants or products differs from that in the bulk solution. Optically, mass-transfer boundary layers are inhomogeneous films with the refractive index continuously varying as a function of distance from the electrode. The effect of such layers on the ellipsometry of surfaces has been accounted for by the deflection (refraction) of incident and reflected beams in the layer and the resulting change in the angle of incidence on the electrode (Fig. 5.5). Thus, ellipsometry has been used as a new technique to determine the interfacial concentration of a binary electrolyte ($CuSO_4$) and of a supporting electrolyte (H_2SO_4) at the limiting current (190,427).

5.8 Electronic Materials

Ellipsometry, particularly spectroscopic ellipsometry, is widely used in the study of thin films and interfaces of solid-state electronic materials (14,162). The dielectric function and thickness of films on known substrates can be determined unambiguously (428). Anodic oxides on semiconductors and metals have been discussed in Section 5.1.

5.8.1 Surface Cleaning

Chemical etching and cleaning procedures for different semiconductors have been investigated by spectroscopic ellipsometry (429). Both the thickness and the optical constants of damaged surface layers have been determined, as have changes in microtopography resulting from ion bombardment of Si (149,430,431,432). Layers responsible for the etch stop in heavily doped Si have been identified (433).

The removal of adsorbed layers on Ag (111) by ion bombardment and annealing has been studied (432), as has the removal of polishing layers from vitreous silica (434).

5.8.2 Ion Implantation

Complex refractive-index profiles of phosphorous-implanted silicon have been determined by multiple-angle ellipsometry and represented by optically homogeneous films (435).

Changes in complex refractive index with depth, caused by ion implantation in GaAs, have been determined by chemical stripping (436). Multilayer film growth in chemical vapor deposition and plasma processing of semiconductors has been followed by spectroscopic ellipsometry with variable angle of incidence (437).

Dielectric functions and depths of amorphized layers on ion-bombarded and annealed Ge surfaces have been determined (438). Layers showing radiation damage caused by ion implantation in GaP were determined earlier (439).

5.8.3 Vapor-Phase Metal Deposition

Ellipsometer measurements have been conducted during vacuum deposition of silver films (440,441), and axial ratios of ellipsoidal particles have been determined for an optical model with size-dependent optical constants and dipole-dipole interaction between particles.

5.8.4 Other Films

The thickness and refractive index of PMMA photoresist layers were determined on InP by the use of different angles of incidence (442) and on Si with a psi meter (443).

Ellipsometer studies of many other solid-state electronic materials have been reported. Among them are silicon nitride on gallium arsenide (444), silicon nitride and silicon dioxide on silicon (445,446), gallium arsenic oxide on gallium arsenide (445), and indium oxide on indium phosphide (447).

5.9 Optical Constants

Optical constants (refractive index and extinction coefficient) are needed in all optical models of surfaces and thin films. For opaque materials, optical constants are derived from reflection measurements by the numerical inversion of the Fresnel equations. Ellipsometry, often in combination with reflectance measurements, is primarily used for this purpose.

The optical constants of metals and semiconductors are among the less-established physical properties of materials, with uncertainties of many tens of percent being quite common. Many factors affect the determination of optical constants. Among them are surface contamination, surface topography, electronic surface states, and bulk microstructure. Many determinations still in use have been made before atomically clean surfaces could be prepared (448,449). Consistent data have been collected recently for 37 materials over a wide spectral range (450), but critically evaluated data over large ranges of wavelengths and temperatures are still largely lacking. Si and SiO_2 have been measured from 295 to 1333 K (451). For ellipsometer studies of surface layers, it is often necessary to determine the optical constants of the bare substrate immediately before film formation.

For very thin films, the accuracy with which complex optical constants can be derived from ellipsometer measurements is very low if the optical constants of both substrate and film are similar (452).

5.9.1 Contamination

The presence of only two to three monolayers of oxide on aluminum has been shown to cause large errors in the derived values of n and k (453). Similarly, neglecting an initial oxide layer on Ta has been shown to result in incorrect optical constants for the substrate in anodic film growth (322).

Optical constants of single crystals of Ru (312) and Ta (454) have been determined by ellipsometry after cleaning in ultrahigh vacuum. Differences between the results for Ta and literature values on polycrystalline or evaporated specimens have been attributed to greater cleanliness in the vacuum (454). Ion-beam processing of Mo has been shown to introduce significant surface roughness (152).

The effect of polishing layers and oxide layers has been considered in determining optical constants of zirconium alloys by use of multiple-angle, multiple-wavelength ellipsometry (369).

Immersion of oxide-covered aluminum (455) and silicon (295) specimens in liquids of matching refractive index has been used to eliminate the optical effect of oxide layers.

5.9.2 Roughness

An early study, in which surface roughness was represented by different inhomogeneous films, predicted large errors in optical constants for very small (5 nm) roughness (114). An attempt to avoid the effect of surface roughness and contamination has been made by use of internal reflection on thick metal films evaporated on glass substrates (455,456). In this approach, it is assumed that the glass surface before deposition is clean and that it does not react with the metal.

5.9.3 Microstructure

Optical constants are often different for the same metal as a polished, clean bulk specimen or as a vapor-deposited optically opaque film. Optical properties of metal films have been discussed recently (457). The particulate nature of evaporated metals has long been recognized. The selective optical absorption of granular tin films has been explained by an extended Maxwell Garnett effective-medium theory (113), and an abnormal absorption band in evaporated lithium has been ascribed to a two-dimensional distribution of grains on a continuous metal base (458). Differences in reported optical constants of gold have been explained by grain-size effects with a large volume fraction of imperfections (459). The effect of deposition conditions for Al on optical constants has been attributed to reaction with residual gases during deposition (460).

5.9.4 Anisotropy

The optical constants of GaAs have been determined by ellipsometry on planes parallel and perpendicular to the optic axis or cleavage plane (461). For bismuth tellurium sulfide, the optical constants normal to the cleavage plane are difficult to determine (462).

Although cubic crystals are isotropic in the interior, the (110) face of Cu has been found to be optically anisotropic because of a lack of fourfold symmetry (368).

5.10 Liquid Surfaces

Liquid metal surfaces of Hg, Cd, Pb, Bi, and Bi-amalgam have been measured in vacuum after cleaning by glow discharge. Measurements on Hg over the visible spectrum have also been made on Hg-glass and Hg-quartz interfaces (463). The optical constants of liquid Na have been determined by ellipsometry from 0.3 to 2 μm (464). More recently, the optical constants of liquid surfaces of Na, Sn, and Hg, and of Hg-quartz interfaces have been measured and compared to measurements on solid Na and Li (465).

For the anodic formation of calomel on Hg, a dissolution-precipitation mechanism has been supported by off-null ellipsometer transient photometric measurements (466).

The ellipsometry of liquid-vapor and liquid-solid interfaces has been reviewed recently (467). The existence of transition layers on the surface of several highly purified liquids had been derived previously from reflection measurements at Brewster's angle (468). From similar measurements, thicknesses of 0.5–4.0 nm have been derived for transition layers on water, carbon tetrachloride, and methylnaphthalene (271). Phase transitions on the surface of binary solutions have also been investigated (469).

The thickness of industrial oil coatings has also been determined by ellipsometry (224).

5.11 Other Studies

The photolytic decomposition of lead chloride has been determined to proceed as a surface reaction under formation of lead oxychloride latent-image centers in the presence of oxygen, but under formation of lead nuclei in the absence of oxygen (470).

Refractive indices of polymer layers resulting from the plasma polymerization of styrene and epichlorohydrin on Al have been measured (471), as have the initial stages of the electropolymerization of acrylonitrile on nickel (472), and of phenolic compounds on platinum (473).

6. OUTLOOK

6.1 Optical Theory

A continued improvement in understanding the optical properties of real surfaces can be expected and will be of great interest to users of ellipsometry. This understanding primarily concerns the effects of surface roughness, discontinuous films, and surface electronic states. The theory of composite and particulate media is also likely to be expanded into regions where present effective-medium models do not apply, e.g., large or nonspherical particles. An improved theory of off-specular reflection can be expected to lead to new types of measurements.

6.2 Instrumentation

Since spectroscopic ellipsometry has become more widely available in recent years, it can be expected to be used more generally. An improvement in the speed of most spectroscopic instruments will then become desirable. Such improvements can be achieved by adapting one of the present very-high-speed monochromatic techniques.

Introducing an imaging ellipsometric technique with microscopic resolution is another desirable direction for future development. A scanning ellipsometer microprobe could serve that purpose and would preferably have spectroscopic capabilities, thus generating an enormous amount of data. The simultaneous observation of extended surfaces could also be accomplished by holographic ellipsometry (8).

The analysis of scattered light in off-specular directions can be expected, following the development of suitable optical theory, to provide information on surface microtopography. Such measurements will probably have to include the degree of polarization.

The use of variable lateral coherence in the incident beam offers another approach to obtain information on the homogeneity of surfaces on the light-wavelength scale (8). The difference between coherent and incoherent illumination of a heterogeneous surface is shown schematically in Fig. 6.1.

Ellipsometer measurements outside the visible spectral range can be expected to attract greater interest in the future. The past use of infrared radiation to identify chemical species on electrode surfaces

(285) and to measure dopant layers in semiconductors (288) may be expanded. The remote determination of conductivity by microwave ellipsometry (292) may also find wider interest. Ellipsometry in the soft x-ray regime does not seem to have been investigated yet. The increased availability of tuneable, polarized x rays from free-electron devices and the recent development of optical components offer new possibilities for this approach.

6.3 Interpretation

With the continued increase in the computational capabilities of microcomputers, the numerical optimization of optical film and surface models can be expected to be used more widely for the interpretation of measurements. Computer programs can be expected to be more efficient and to consider many parameters in addition to spectroscopic ellipsometer measurements. These parameters could include specular reflectance, off-specular elastic and inelastic scattering, or nonoptical measurements such as mass or charge data as a function of time. A choice between different optical models may also be automated.

6.4 Applications

Ellipsometry will continue to be used for measurements on surfaces, particularly solid-liquid and solid-gas interfaces, for which its capabilities are unique. It will provide real-time, *in situ* information on the formation, breakdown, and removal of surface layers or on the cleaning, etching, and annealing of solids. The spectroscopic properties of bulk solids and surfaces will be determined more readily to derive chemical composition, ordering, electronic structure, and the distribution of materials in composite and inhomogenous systems.

The combination of ellipsometer measurements with other techniques will be of continued interest for the detailed study of surfaces and thin films.

Acknowledgment: This work was supported by the Director, Office of Energy Research, Office of Basic Energy Sciences, Materials Sciences Division of the U.S. Department of Energy under Contract No. DE-AC03-76SF00098.

TABLE 3.1
Derivation of relative amplitude parameter ψ and relative phase parameter Δ from ellipsometer azimuths of polarizer *p*, quarter-wave plate *q*, and analyzer *a*, at compensation (all angles in degrees) (8).
($\psi = 0°$ to $90°$, $\Delta = 0°$ to $360°$)

Zone	Range of polarizer transmission azimuth p	Compensator fast-axis azimuth q	Range of analyzer transmission azimuth a	Values of ellipsometer parameters	
				ψ	Δ
A-1	0 to 45	45	90 to 180	180 – a	90 – 2p
A-2	45 to 90	135	90 to 180	180 – a	2p – 90
A-3	90 to 135	45	0 to 90	a	270 – 2p
A-4	135 to 180	135	0 to 90	a	2p – 270
B-1	0 to 45	135	0 to 90	a	90 + 2p
B-2	45 to 90	45	0 to 90	a	270 – 2p
B-3	90 to 135	135	90 to 180	180 – a	2p – 90
B-4	135 to 180	45	90 to 180	180 – a	450 – 2p
C-1	0 to 45	45	0 to 90	a	270 – 2p
C-2	45 to 90	135	0 to 90	a	90 + 2p
C-3	90 to 135	45	90 to 180	180 – a	450 – 2p
C-4	135 to 180	135	90 to 180	180 – a	2p – 90
D-1	0 to 45	135	90 to 180	180 – a	270 + 2p
D-2	45 to 90	45	90 to 180	180 – a	450 – 2p
D-3	90 to 135	135	0 to 90	a	90 + 2p
D-4	135 to 180	45	0 to 90	a	630 – 2p

TABLE 4.1
Optimization of two-layer model for spectroscopic ellipsometry of Pb deposits on Cu. Model parameters given with 95% confidence limits (after 102).

Thickness (nm)[a] derived from charge passed	Derived from ellipsometric measurements		
	Thickness of porous layer (nm)	Volume fraction Pb in porous layer	Thickness of compact (UPD) layer (nm)
30	31 ± 4	0.59 ± 0.14	0.48 ± 0.11
60	50 ± 16	0.78 ± 0.17	0.48 ± 0.11
110	87 ± 266	0.97 ± 0.27	0.48 ± 0.11

[a]Equivalent compact deposit.

REFERENCES

1. A.C. Hall, "A Century of Ellipsometry," Surf. Sci., *16*, 1–13 (1969).

2. A. Rothen, "The Ellipsometer, an Apparatus to Measure Thicknesses of Thin Surface Films," Rev. Sci. Instrum., *16*, 26–30 (1945).

3. A. Rothen, "Measurements of the Thickness of Thin Films by Optical Means, From Rayleigh and Drude to Langmuir, and the Development of the Present Ellipsometer," in E. Passaglia, R.R. Stromberg, and J. Kruger, Eds., *Ellipsometry in the Measurement of Surfaces and Thin Films*, Nat. Bur. Stand. Misc. Pub. 256, Washington, D.C., 1964, pp. 7–21.

4. A. Vašíček, "A New Method for Investigating the Refractive Index and Thickness of Thin Interference Films on Glass," Phys. Rev., *57*, 925–931 (1940).

5. A. Vašíček, "Polarimetric Methods for the Determination of the Refractive Index and the Thickness of Thin Films on Glass," J. Opt. Soc. Am., *37*, 145–153 (1947).

6. K.H. Zaininger and A.G. Revesz, "Ellipsometry — A Valuable Tool in Surface Research," RCA Review, pp. 85–115 (March 1964).

7. J.M. Weingart and A.R. Johnston, "Electronic Polarimeter Techniques," in E. Passaglia, R.R. Stromberg, and J. Kruger, Eds., *Ellipsometry in the Measurement of Surfaces and Thin Films*, Nat. Bur. Stand. Misc. Pub. 256, Washington, D.C., 1964, pp. 113–117.

8. R.H. Muller, "Principles of Ellipsometry," in R.H. Muller, Ed., *Advances in Electrochemistry and Electrochemical Engineering, Vol. 9: Optical Techniques in Electrochemistry*, series edited by P. Delahay and C.W. Tobias, Wiley-Interscience, New York, 1973, pp. 167–226.

9. J. Kruger, "Application of Ellipsometry to Electrochemistry," in R.H. Muller, Ed., *Advances in Electrochemistry and Electrochemical Engineering, Vol. 9: Optical Techniques in Electrochemistry*, series edited by P. Delahay and C.W. Tobias, Wiley-Interscience, New York, 1973, pp. 227–280.

10. K. Kinosita and M. Yamamoto, "Recent Developments in Ellipsometry that are Useful for Thin Film

Studies," Thin Solid Films, *34*, 283–290 (1976).

11. W.E.J. Neal, "Optical Examination and Monitoring of Surfaces," Appl. Surf. Sci., *2*, 445–501 (1979).

12. W. Paik, "Ellipsometric Optics with Special Reference to Electrochemical Systems," in J. O'M. Bockris, Ed., *Electrochemistry*, Vol. 6 in the series *MTP International Review of Science*, Butterworths, London, 1973, pp. 239–285.

13. D.E. Aspnes, "Spectroscopic Ellipsometry of Solids," in B.O. Seraphin, Ed., *Optical Properties of Solids: New Developments*, North-Holland, Amsterdam, 1976, pp. 800–846.

14. D.E. Aspnes, "Interface Ellipsometry; An Overview," Surf. Sci., *101*, 84–98 (1980).

15. D.E. Aspnes, "Optical Characterization by Ellipsometry — A Prospective," J. Phys. (Paris), *44*, C10-3 to C10-12 (1983).

16. R.H. Muller, "Present Status of Automatic Ellipsometers," Surf. Sci., *56*, 19–36 (1976).

17. P.S. Hauge, "Recent Developments in Instrumentation in Ellipsometry," Surf. Sci., *96*, 108–140 (1980).

18. W. Haller, "Ellipsometrie — Eine Methode zur Charakterisierung dünner Filme," Ber. Bunsenges. Phys. Chem., *85*, 847–851 (1981).

19. R.J. Kutko, "Ellipsometry for Semiconductor Process Control," Solid State Technol., Feb. 1978, pp. 43–44, 47.

20. N.M. Bashara and R.M.A. Azzam, "Ellipsometry: Technique for Characterization of Surfaces and Interfaces in Light-transmitting Ambients," J. Vac. Sci. Technol., *12*, 887–890 (1975).

21. N.M. Bashara, A.C. Hall, and A.B. Buckman, "Ellipsometry," in A. Weissberger and B.W. Rossiter, Eds., *Physical Methods of Chemistry*, Part IIIC, Polarimetry, Wiley-Interscience, New York, 1972, pp. 453–504.

22. B.E. Conway, "Special Techniques in the Study of Electrode Processes and Electrochemical Adsorption," in E. Yeager and A.J. Salkind, Eds., *Techniques of Electrochemistry*, Vol. 1, Wiley-Interscience,

New York, 1972, pp. 393–439.

23. G.A. Bootsma, L.J. Hanekamp, and O.L.J. Gijzeman, "Chemisorption Investigated by Ellipsometry," in R. Vanselow and R. Howe, Eds., *Chemistry and Physics of Solid Surfaces IV*, Springer Series in Chemical Physics, Vol. 20, Springer, Berlin, 1982, pp. 77–105.

24. R. Greef, "Ellipsometry," in R.E. White, J. O'M. Bockris, B.E. Conway, and E. Yeager, Eds., *Comprehensive Treatise of Electrochemistry*, Vol. 8, Plenum, New York, 1984, pp. 339–371.

25. R.M.A. Azzam and N.M. Bashara, *Ellipsometry and Polarized Light*, North-Holland, Amsterdam, 1977.

26. W.E.J. Neal, *Ellipsometry: Theory and Applications*, Plenum, New York, 1982.

27. R.J. Archer, *Manual on Ellipsometry*, Gaertner, Chicago, 1968.

28. F. Abelès, Ed., "Ellipsometry and Other Optical Methods for Surface and Thin Film Analysis," J. Phys. (Paris), *44*, Colloque C10 (1983).

29. N.M. Bashara, A.B. Buckman, and A.C. Hall, Eds., *Proceedings of the Symposium on Recent Developments in Ellipsometry*, North-Holland, Amsterdam, 1969; Surf. Sci., *16* (1969).

30. N.M. Bashara and R.M.A. Azzam, Eds., *Ellipsometry, Proceedings of the Third International Conference on Ellipsometry*, North-Holland, Amsterdam, 1976; Surf. Sci. *56* (1976).

31. R.H. Muller, R.M.A. Azzam, and D.E. Aspnes, Eds., *Ellipsometry, Proceedings of the Fourth International Conference on Ellipsometry*, North-Holland, Amsterdam, 1980; Surf. Sci. *96* (1980).

32. E. Passaglia, R.R. Stromberg, and J. Kruger, Eds., *Ellipsometry in the Measurement of Surfaces and Thin Films*, National Bureau of Standards Misc. Pub. 256, Washington, D.C., 1964.

33. R.H. Muller, "Definitions and Conventions in Ellipsometry," Surf. Sci., *16*, 14–33 (1969).

34. J.A. Faucher, G.M. McManus, and H. Trurnit, "Simplified Treatment of Ellipsometry," J. Opt. Soc. Am., *48*, 51–54 (1958).

35. R.M.A. Azzam, "Mapping of Fresnel's Interface Reflection Coefficients Between Normal and

Oblique Incidence: Results for the Parallel and Perpendicular Polarizations at Several Angles of Incidence," Appl. Opt., *19*, 3361–3369 (1980).

36. R.W. Ditchburn, *Light*, Wiley-Interscience, New York, 1964.

37. P. Drude, "Über Oberflächenschichten. II. Theil," Ann. Phys. & Chem. N.F., *36*, 865–897 (1889).

38. A. Vašíček, *Optics of Thin Films*, North-Holland, Amsterdam, 1960.

39. M. Born and E. Wolf, *Principles of Optics: Electromagnetic Theory of Propagation, Interference, and Diffraction of Light*, 2nd Ed., MacMillan, New York, 1964.

40. H. Mayer, *Physik dünner Schichten*, Wissenschaftliche Verlagsgesellschaft, Stuttgart, 1950.

41. G. Szivessy, "Polarisation," in H. Geiger and K. Scheel, Eds., *Handbuch der Physik, Vol. 20, Licht als Wellenbewegung*, Springer, Berlin, 1928, pp. 83–120.

42. H. Poincaré, *Théorie mathématique de la lumière, Vol. II, Nouvelles études sur la diffraction — Théorie de la dispersion de Helmholtz*, Gauthier-Villars, Paris, 1892.

43. G.N. Ramachandran and S. Ramaseshan, "Crystal Optics. A. Polarisation of Light," in S. Flügge, Ed., *Encyclopedia of Physics*, Vol. XXV/1, Springer, Berlin, 1961, pp. 1–54.

44. J.R. Partington, *An Advanced Treatise on Physical Chemistry, Vol. 4: Physico-Chemical Optics*, Longmans, Green, London, 1953.

45. W.A. Shurcliff, *Polarized Light, Production and Use*, Harvard University Press, Cambridge, MA, 1962, pp. 109–123.

46. D. Clarke and J.F. Grainger, *Polarized Light and Optical Measurement*, Pergamon, New York, 1971.

47. M. Françon, "Interférences, diffraction et polarisation," in S. Flügge, Ed., *Encyclopedia of Physics*, Vol. 24, Springer, Berlin, 1956, pp. 171–460.

48. D.A. Holmes, "Exact Theory of Retardation Plates," J. Opt. Soc. Am., *54*, 1115-1120 (1964).

49. E. Spiller, "Totally Reflecting Thin-film Phase Retarders," Appl. Opt., *23*, 3544–3549 (1984).

50. J.M. Bennett and H.E. Bennett, "Polarization," in W.G. Driscoll, Ed., *Handbook of Optics*, McGraw-Hill, New York, 1978, pp. 10-1 to 10-164.

51. P.S. Hauge, R.H. Muller, and C.G. Smith, "Conventions and Formulas for Using the Mueller-Stokes Calculus in Ellipsometry," Surf. Sci., *96*, 81–107 (1980).

52. E. Spiller, "Phase Conventions in Thin Film Optics and Ellipsometry," Appl. Opt., *23*, 3036–3037 (1984).

53. A. Robert, "The Application of Poincaré's Sphere to Precision Ellipsometry," in E.R. Robertson and J.M. Harvey, Eds., *The Engineering Uses of Holography*, Cambridge University Press, Cambridge, England, 1970, pp. 225–236.

54. F.L. McCrackin, E. Passaglia, R.R. Stromberg, and H.L. Steinberg, "Measurement of the Thickness and Refractive Index of Very Thin Films and the Optical Properties of Surfaces by Ellipsometry," J. Res. Nat. Bur. Standards, *67A*, 363–377 (1963).

55. C.S. Barrett, "The Stereographic Projection," in *Structure of Metals*, Crystallographic Methods, Principles and Data, McGraw-Hill, New York, 1943, pp. 25–43.

56. P.S. Theocaris, "Elliptic Polarization Represented by the Carter and Smith Charts," Appl. Opt., *18*, 4017–4024 (1979).

57. F.E. Wright, "A Spherical Projection Chart for Use in the Study of Elliptically Polarized Light," J. Opt. Soc. Am., *20*, 529–564 (1930).

58. H.G. Jerrard, "Transmission of Light Through Birefringent and Optically Active Media: The Poincaré Sphere," J. Opt. Soc. Am., *44*, 634–640 (1954).

59. M. Johnson, "Poincaré Sphere Representation of Birefringent Networks," Appl. Opt., *20*, 2075–2080 (1981).

60. H. Kubo and R. Nagata, "Vector Representation of Behavior of Polarized Light in a Weakly Inhomogeneous Medium with Birefringence and Dichroism. II. Evolution of Polarization States," J. Opt. Soc.

Am. A, 2, 30–34 (1985).

61. F. El-Hosseiny, "Methods for Determining the Optical Parameters of Elliptic Retarders," J. Opt. Soc. Am., *65*, 1279–1282 (1975).

62. F. Holtz, "Zur Messgenauigkeit der Ellipsometrie," Z. angew. Phys., *30*, 196–200 (1970).

63. R.M.A. Azzam and N.M. Bashara, "Polarization Transfer Function of an Optical System as a Bilinear Transformation," J. Opt. Soc. Am., *62*, 222–229 (1972).

64. R.M.A. Azzam and N.M. Bashara, "Equi-Azimuth and Equi-Ellipticity Contour Charts for Ellipsometry," Surf. Sci., *30*, 101–108 (1972).

65. R. Greef and M.M. Wind, "Polar Representation of Ellipsometric Data," Appl. Opt., *25*, 1627–1629 (1986).

66. J. Cernosek, "Simple Geometrical Method for Analysis of Elliptical Polarization," J. Opt. Soc. Am., *61*, 324–327 (1971).

67. M. Richartz and H.-Y. Hsü, "Analysis of Elliptical Polarization," J. Opt. Soc. Am., *39*, 136–157 (1949).

68. W.H. McMaster, "Polarization and the Stokes Parameter," Am. J. Phys., *22*, 351–362 (1954).

69. M.J. Walker, "Matrix Calculus and the Stokes Parameters of Polarized Radiation," Am. J. Phys., *22*, 170–174 (1954).

70. H.G. Berry, G. Gabrielse, and A.E. Livingston, "Measurement of the Stokes Parameters of Light," Appl. Opt., *16*, 3200–3205 (1977).

71. G.R. Boyer, B.F. Lamouroux, and B.S. Prade, "Automatic Measurement of the Stokes Vector of Light," Appl. Opt., *18*, 1217–1219 (1979).

72. R.C. Thompson, J.R. Bottiger, and E.S. Fry, "Measurement of Polarized Light Interactions via the Mueller Matrix," Appl. Opt., *19*, 1323–1332 (1980).

73. A. Gerrard and J.M. Burch, *Introduction to Matrix Methods in Optics*, Wiley, New York, 1975.

74. P. Yeh, "Extended Jones Matrix Method," J. Opt. Soc. Am., *72*, 507–513 (1982).

75. M. Born, *Optik*, Springer, Berlin, 1965, 2nd edition.

76. B. Rossi, *Optics*, Addison-Wesley, Reading, MA, 1959.

77. J.M. Stone, *Radiation and Optics*, McGraw-Hill, New York, 1963.

78. M.E. Zaret, *Outline of Electromagnetic Theory*, Regents, New York, 1964.

79. J.R. Reitz, F.J. Milford, and R.W. Christy, *Foundations of Electromagnetic Theory*, Addison-Wesley, Reading, MA, 1960.

80. E.U. Condon, "Electromagnetic Waves," in E.U. Condon and H. Odishaw, Eds., *Handbook of Physics*, McGraw-Hill, New York, 1958, pp. 6-3 to 6-19.

81. J. Van Kranendank and J.E. Sipe, "Foundations of the Macroscopic Electromagnetic Theory of Dielectric Media," in E. Wolf, Ed., *Progress in Optics*, Vol. XV, North-Holland, Amsterdam, 1977, pp. 247–350.

82. M. von Laue, "Die Spiegelung und Brechung des Lichtes an der Grenze zweier isotroper Körper," in *Handbuch der Experimentalphysik*, Vol. 18, Akademische Verlagsgesellschaft, Leipzig, 1928, pp. 125–207.

83. P.H. Berning, "Theory and Calculations of Optical Thin Films," in G. Hass, Ed., *Physics of Thin Films*, Vol. 1, Academic Press, New York, 1963, pp. 69–121.

84. W.J. Plieth and K. Naegele, "Über die Bestimmung der optischen Konstanten dünnster Oberflächenschichten und das Problem der Schichtdicke," Surf. Sci., *64*, 484–496 (1977).

85. F. Partovi, "Theoretical Treatment of Ellipsometry," J. Opt. Soc. Am., *52*, 918–925 (1962).

86. F.L. McCrackin, *A Fortran Program for Analysis of Ellipsometer Measurements*, Nat. Bur. Stand. Tech. Note 479, 1969.

87. F.L. McCrackin and J.P. Colson, "Computational Techniques for the Use of the Exact Drude Equations in Reflection Problems," in E. Passaglia, R.R. Stromberg, and J. Kruger, Eds., *Ellipsometry in the*

Measurement of Surfaces and Thin Films, Nat. Bur. Stand. Misc. Pub. 256, Washington, D.C., 1964, pp. 61–82.

88. J.C. Charmet and P.G. de Gennes, "Ellipsometric Formulas for an Inhomogeneous Layer with Arbitrary Refractive-Index Profile," J. Opt. Soc. Am., *73*, 1777–1784 (1983).

89. K. Kinosita, M. Mishibori, M. Yamamoto, and H. Yokota, "Ellipsometry of a Transparent Film Overlaid on a Transparent Substrate Having a Surface Layer," Opt. Acta, *17*, 115–121 (1970).

90. D.E. Aspnes and J.B. Theeten, "Spectroscopic Analysis of the Interface Between Si and its Thermally Grown Oxide," J. Electrochem. Soc., *127*, 1359–1365 (1980).

91. C.G. Smith and R.H. Muller, "Interpretation of Ellipsometer Observations of Anodic Films," Proc. SPIE, *112*, 104–109 (1977).

92. R.H. Muller and C.G. Smith, "Ellipsometry of Mass-Transport Boundary Layers," Surf. Sci., *56*, 440–448 (1976).

93. T. Yamaguchi and H. Hasunuma, "A Quick Response Recording Ellipsometer," Sci. Light, *16*, 64–71 (1967).

94. R.H. Muller and J.C. Farmer, "Macroscopic Optical Model for the Ellipsometry of an Underpotential Deposit: Lead on Copper and Silver," Surf. Sci., *135*, 521–531 (1983).

95. T. Smith, "Ellipsometry for Measurements at and Below Monolayer Coverage," J. Opt. Soc. Am., *58*, 1069–1079 (1968).

96. T. Smith, "Ellipsometry of an Absorbing Film Below Monolayer Coverage: Cs/W," J. Opt. Soc. Am., *62*, 291–292 (1972).

97. J.R. Miller and J.E. Berger, "A Comparative Study of Adsorption by Ellipsometric and Radiotracer Methods," J. Phys. Chem., *70*, 3070–3075 (1966).

98. F.H.P.M. Habraken, E.Ph. Kieffer, and G.A. Bootsma, "A Study of the Kinetics of the Interactions of O_2 and N_2O with a Cu(111) Surface and of the Reaction of CO with Adsorbed Oxygen using AES, LEED,

and Ellipsometry," Surf. Sci., *85*, 45–59 (1979).

99. F.H.P.M. Habraken, O.L.J. Gijzeman, and G.A. Bootsma, "Ellipsometry of Clean Surfaces, Submonolayer and Monolayer Films," Surf. Sci., *96*, 482–507 (1980).

100. H.E. Bennett, D.K. Burge, R.L. Peck, and J.M. Bennett, "Validity of Ellipsometry for Determining the Average Thickness of Thin, Discontinuous, Absorbing Films," J. Opt. Soc. Am., *59*, 675–681 (1969).

101. J.C. Farmer and R.H. Muller, "Nucleation of Pb Electrodeposits on Ag and Cu," J. Electrochem. Soc., *132*, 39–45 (1985).

102. J.C. Farmer and R.H. Muller, "Effect of Rhodamine-B on the Electrodeposition of Lead on Copper," J. Electrochem. Soc., *132*, 313–319 (1985).

103. E.F.I. Roberts-Sengier, M.A. Hamilton, and R. Hunt, "Polyphase Substrate Ellipsometry — A Kinetic Investigation," J. Phys. (Paris), *44*, C10-199 to C10-203 (1983).

104. D.E. Aspnes, "Optical Properties of Thin Films," Thin Solid Films, *89*, 249–262 (1982).

105. D.E. Aspnes, "Local-Field Effects and Effective-Medium Theory: A Microscopic Perspective," Am. J. Phys., *50*, 704–709 (1982).

106. H.A. Lorentz, *Theory of Electrons*, Teubner, Leipzig, 1916, Chapter 4, 2nd ed., Dover, New York, 1952.

107. L. Lorenz, "Über die Refractionsconstante," Ann. Phys. Chem. (Leipzig), *11*, 70–103 (1880).

108. J.C. Maxwell Garnett, "Colours in Metal Glasses and in Metallic Films," Phil. Trans. Roy. Soc. London *203*, 385–420 (1904); *205*, 237–288 (1906).

109. D.A.G. Bruggeman, "Berechnung verschiedener physikalischer Konstanten von heterogenen Substanzen. I. Dielektrizitäts Konstanten und Leitfähigkeiten der Mischkörper aus isotropen Substanzen," Ann. Phys. (Leipzig), *24*, 636–679 (1935).

110. C.G. Granqvist and O. Hunderi, "Conductivity of Inhomogeneous Materials: Effective-medium Theory with Dipole-dipole Interaction," Phys. Rev. B, *18*, 1554–1561 (1978).

111. D.E. Aspnes, "Characterization of Materials and Interfaces by Visible-Near uv Spectrophotometry and Ellipsometry," J. Mater. Ed., *7*, 849–901 (1985).

112. J.-M. Thériault and P. Boivin, "Maxwell-Garnett Theory Extended for Cu-PbI_2 Cermets," Appl. Opt., *23*, 4494–4498 (1984).

113. V.V. Truong, F.E. Girouard, and G. Bosi, "Optical Properties of Granular Tin Films from 0.22 to 1.0 μm," Appl. Opt., *21*, 2508–2511 (1982).

114. C.A. Fenstermaker and F.L. McCrackin, "Errors Arising from Surface Roughness in Ellipsometric Measurement of the Refractive Index of a Surface," Surf. Sci., *16*, 85–96 (1969).

115. A. Heller, D.E. Aspnes, J.D. Porter, T.T. Sheng, and R.G. Vadimsky, "Transparent Metals: Preparation and Characterization of Light-Transmitting Platinum Films," J. Phys. Chem. *89*, 4444–4452 (1985).

116. J.D. Porter, A. Heller, and D.E. Aspnes, "Experiment and Theory of 'Transparent' Metal Films," Nature, *313*, 664–666 (1985).

117. D.A. Holmes, *Optics of a Birefringent Plate with Applications to Ellipsometry*, Thesis, Department of Electrical Engineering, Carnegie Institute of Technology, Pittsburgh, PA, 1965.

118. H. Schopper, "Zur Optik dünner doppelbrechender und dichroitischer Schichten," Z. Physik, *132*, 146–170 (1952).

119. D.J. De Smet, "Application of Generalized Ellipsometry to Anisotropic Crystals," J. Opt. Soc. Am., *65*, 461 (1975).

120. D.J. De Smet, "Ellipsometry of Anisotropic Surfaces," J. Opt. Soc. Am., *63*, 958–964 (1973).

121. D.J. De Smet, "Ellipsometry of Anisotropic Thin Films," J. Opt. Soc. Am., *64*, 631–638 (1974).

122. D.J. De Smet, "Ellipsometry of a Biaxial Surface," J. Opt. Soc. Am., *65*, 542–547 (1975).

123. R.M.A. Azzam, "Determination of the Optic Axis and Optical Properties of Absorbing Uniaxial Crystals by Reflection Perpendicular-Incidence Ellipsometry on Wedge Samples," Appl. Opt., *19*, 3092–3095 (1980).

124. R.M.A. Azzam and N.M. Bashara, "Simplified Approach to the Propagation of Polarized Light in Anisotropic Media — Application to Liquid Crystals," J. Opt. Soc. Am., *62*, 1252–1257 (1972).

125. R.M.A. Azzam and N.M. Bashara, "Application of Generalized Ellipsometry to Anisotropic Crystals," J. Opt. Soc. Am., *64*, 128–133 (1974).

126. D.A. Holmes and D.L. Feucht, "Electromagnetic Wave Propagation in Birefringent Multilayers," J. Opt. Soc. Am., *56*, 1763–1769 (1966).

127. D.J. De Smet and J.L. Ord, "Optical Anisotropy and Electrostriction in the Anodic Oxide of Molybdenum," J. Electrochem, Soc., *130*, 280–284 (1983).

128. C.G. Matthews, J.L. Ord, and W.P. Wang, "Optical Anisotropy and Electrostriction in the Anodic Oxide of Niobium," J. Electrochem. Soc., *130*, 285–290 (1983).

129. J.L. Ord and W.P. Wang, "Optical Anisotropy and Electrostriction in the Anodic Oxide of Tantalum," J. Electrochem. Soc., *130*, 1809–1814 (1983).

130. K.K. Yee and L. Young, "Ellipsometric Investigation of Quadratic Electrooptic and Electrostrictive Effects with Anodic Niobium Pentoxide Films," Appl. Opt., *14*, 1316–1321 (1975).

131. M.E. Pedinoff, M. Braunstein, and D.M. Stafsudd, "Strain Induced Anisotropy in As_2S_3, As_2Se_3, and ZnSe Films on KCl Substrates via 10.6-μm and 0.6328-μm Ellipsometer Measurements and 0.6328-μm Reflector Measurements," Appl. Opt., *18*, 201–211 (1979).

132. T. Yamaguchi, S. Yoshida, and A. Kinbara, "Effects of Optical Anisotropy of Aggregated Silver Films on Ellipsometric Determination of n, k, and d," J. Opt. Soc. Am., *62*, 634–638 (1972).

133. M.A.B. Gültepe, "Some Considerations on the Determination of Optical Properties of Adsorbed Films," Surf. Sci., *56*, 76–86 (1976).

134. M.W. Humphreys and R. Parsons, "Ellipsometric Studies of the Adsorption of Quinolines at the Mercury Electrode," J. Electroanal. Chem., *82*, 369–390 (1977).

135. J.C. Farmer and R.H. Muller, "Spectroscopic Ellipsometry of Rhodamine-B Adsorbed on Platinum,

Silver, and Copper," in *Int. Soc. Electrochem. 35th Meeting, August 5–10, 1984*, Ext. Abs. A8-8.

136. M.W. Humphreys and R. Parsons, "Ellipsometry of DNA Adsorbed at Mercury Electrodes, A Preliminary Study," J. Electroanal. Chem., *75*, 427–436 (1977).

137. D. Den Engelsen, "Ellipsometry of Anisotropic Films," J. Opt. Soc. Am., *61*, 1460–1466 (1971).

138. M.J. Dignam and M. Moskovits, "Azimuthal Misalignment and Surface Anisotropy as Sources of Error in Ellipsometry," Appl. Opt., *9*, 1868–1873 (1970).

139. M.J. Dignam, M. Moskovits, and R.W. Stobie, "Specular Reflectance and Ellipsometric Spectroscopy of Oriented Molecular Layers," Trans. Faraday Soc., *67*, 3306–3317 (1971).

140. P.J. Lin-Chung and S. Teitler, "4 X 4 Matrix Formalisms for Optics in Stratified Anisotropic Media," J. Opt. Soc. Am. A, *1*, 703–705 (1984).

141. P. Beckmann and A. Spizzichino, *The Scattering of Electromagnetic Waves from Rough Surfaces*, Pergamon, New York, 1963.

142. P. Beckmann, "Scattering of Light by Rough Surfaces," in E. Wolf, Ed., *Progress in Optics, Vol. VI*, North-Holland, Amsterdam, 1967, pp. 53–69.

143. I. Ohlídal, K. Navrátil, and F. Lukeš, "Optical Studies of Rough Surfaces and Systems Substrate — Thin Film with Rough Boundaries," Universita J.E. Purkyně v Brně — přírodovědecká fakulta. Folia, *XV*(3), 1–113 (1974).

144. O. Hunderi, "Optics of Rough Surfaces, Discontinuous Films and Heterogeneous Materials," Surf. Sci., *96*, 1–31 (1980).

145. K. Brudzewski, "Ellipsometric Investigations of a Substrate–Thin Film System with Rough Boundaries Using the Equivalent Film Theory," Thin Solid Films, *61*, 183–191 (1979).

146. E.C. Chan and J. P. Marton, "Generalized Maxwell Garnett Equations for Rough Surfaces," J. Appl. Phys., *45*, 5004–5007 (1974).

147. I. Ohlídal, F. Lukeš, and K. Navrátil, "The Problem of Surface Roughness in Ellipsometry and

Reflectometry," J. Phys. (Paris), *38*, C5-77 to C5-88 (1977).

148. D.E. Aspnes and J.B. Theeten, "Investigation of Effective-Medium Models of Microscopic Surface Roughness by Spectroscopic Ellipsometry," Phys. Rev. B, *20*, 3292–3302 (1979).

149. D.E. Aspnes, "Surface Transition Regions and Visible-Near UV Optical Properties of Some Semiconductors," Physica, *117B & 118B*, 359–361 (1983).

150. J.P. Marton and E.C. Chan, "Surface Roughness Interpretation of Ellipsometer Measurements Using the Generalized Maxwell Garnett Theory," J. Appl. Phys., *45*, 5008–5014 (1974).

151. R.M.A. Azzam and N.M. Bashara, "Polarization Characteristics of Scattered Radiation from a Diffraction Grating by Ellipsometry with Application to Surface Roughness," Phys. Rev. B, *5*, 4721–4729 (1972).

152. G.H. Bu-Abbud, D.L. Mathine, P. Snyder, J.A. Woollam, D. Poker, J. Bennett, D. Ingram, and P. Pronko, "Roughness Studies of Ion Beam Processed Molybdenum Surfaces," J. Appl. Phys., *59*, 257–262 (1986).

153. K. Brudzewski, "Effect of Surface Roughness on Change of the Polarization State of Light Reflected from Silicon and Germanium," Appl. Opt., *15*, 115–119 (1976).

154. T. Smith and G. Lindberg, "Interpretation of Ellipsometric Data for Transparent Films on Rough Metal Surfaces," Surf. Technol., *8*, 1–35 (1979).

155. T. Smith, P. Smith, and F. Mansfeld, "Ellipsometry Interpretation for Electrochemistry," J. Electrochem. Soc., *126*, 799–803 (1979).

156. I. Ohlídal and F. Lukeš, "Ellipsometric Parameters of Rough Surfaces and a System Substrate — Thin Film with Rough Boundaries," Opt. Acta, *19*, 817–843 (1972).

157. T.V. Vorburger and K.C. Ludema, "Ellipsometry of Rough Surfaces," Appl. Opt., *19*, 561–573 (1980).

158. M.D. Williams and D.E. Aspnes, "Polarimetry of Specular and Non–Multiple-Scattered

Electromagnetic Radiation from Selectively Roughened Si Surfaces," Phys. Rev. Lett., *41*, 1667–1670 (1978).

159. T. Smith, "Effect of Surface Roughness on Ellipsometry of Aluminum," Surf. Sci., *56*, 252–271 (1976).

160. T. Smith, "Measurement of the Growth of Sub-Microscopic Fatigue Cracks by Ellipsometry," Surf. Sci., *45*, 117–127 (1974).

161. D.E. Aspnes, "The Characterization of Materials by Spectroscopic Ellipsometry," Proc. SPIE, *452*, 60 (1983).

162. D.E. Aspnes, "Recent Progress in the Nondestructive Analysis of Surfaces, Thin Films, and Interfaces by Spectroellipsometry," Appl. Surf. Sci., *22/23*, 792–803 (1985).

163. R.H. Muller and J.C. Farmer, "Fast, Self-Nulling Spectroscopic Ellipsometer: Instrumentation and Application," J. Phys. (Paris), *44*, C10-57–C10-61 (1983).

164. B.D. Cahan, "Implications of Three Parameter Solutions to the Three-Layer Model," Surf. Sci., *56*, 354–372 (1976).

165. B.D. Cahan, J. Horkans, and E. Yeager, "Modulation Ellipsometry and its Application to the Study of the Electrode-Electrolyte Interface," Surf. Sci., *37*, 559–567 (1973).

166. S.H. Kim, W.-K. Paik, and J.O'M. Bockris, "Reflectance and Ellipsometric Study of Anodic Film on Platinum Electrode," Surf. Sci., *33*, 617–623 (1972).

167. J. Horkans, B.D. Cahan, and E. Yeager, "Electrode Potential Scanning Ellipsometric Spectroscopy: Study of the Formation of the Anodic Oxide Film on Noble Metals," Surf. Sci., *46*, 1–23 (1974).

168. C.-T. Chen and B.D. Cahan, "The Nature of the Passive Film on Iron. I. Automatic Ellipsometric Spectroscopy Studies," J. Electrochem. Soc., *129*, 17–26 (1982).

169. S. Gottesfeld, M. Babai, and B. Reichman, "The Analysis of Surface Processes on Solid Electrodes by Combined Modulated Ellipsometric and Reflectometric Experiments," Surf. Sci. *57*, 251–265 (1976).

170. O. Hunderi, "On the Problems of Multiple Overlayers in Ellipsometry and a New Look at Mutiple Angle of Incidence Ellipsometry," Surf. Sci., *61*, 515–520 (1976).

171. J. Humlíček, "Sensitivity Extrema in Multiple-Angle Ellipsometry," J. Opt. Soc. Am. A, *2*, 713–722 (1985).

172. Y. Gaillyová, E. Schmidt, and J. Humlíček, "Multiple-Angle Ellipsometry of Si-SiO_2 Polycrystalline Si System," J. Opt. Soc. Am. A, *2*, 723–726 (1985).

173. G.H. Bu-Abbud and N.M. Bashara, "Parameter Correlation and Precision in Multiple-Angle Ellipsometry," Appl. Opt., *20*, 3020–3026 (1981).

174. M. Delfino and R.R. Razouk, "Optical Constants of Arsenic and Boron Implants in Silicon Determined by a Four-Phase Complex Refractive Index Model," J. Electrochem. Soc., *129*, 606–609 (1982).

175. R.M.A. Azzam, "Theory, Implementation, and Applications of AIDER," J. Phys. (Paris), *44*, C10-71 to C10-74 (1983).

176. R.H.W. Graves, "Ellipsometry Using Imperfect Polarizers," Appl. Opt., *10*, 2679–2684 (1971).

177. A.R.M. Zaghloul and R.M.A. Azzam, "Single-Element Rotating-Polarizer Ellipsometer for Film-Substrate Systems," J. Opt. Soc. Am., *67*, 1286–1287 (1977).

178. R.M.A. Azzam, M. Elshazly-Zaghloul, and N.M. Bashara, "Combined Reflection and Transmission Thin-Film Ellipsometry: A Unified Linear Analysis," Appl. Opt., *14*, 1652–1663 (1975).

179. I. Ohlídal and F. Lukeš, "Optical Analysis of Thin Gold Films by Combined Reflection and Transmission Ellipsometry," Thin Solid Films, *85*, 181–190 (1981).

180. I. Ohlídal and F. Lukeš, "Optical Analysis of Absorbing Double Layers by Combined Reflection and Transmission Ellipsometry," Thin Solid Films, *115*, 269–282 (1984).

181. M. Yamamoto, K. Ichiji, Y. Wada, K. Takeuchi, and K. Kinosita, "Immersion-Type Transmission Ellipsometry of Very Thin Metal Films," J. Phys. (Paris), *44*, C10-383 to C10-386 (1983).

182. G.A. Candela and D. Chandler-Horowitz, "An Ellipsometry System for High Accuracy Metrology of

Thin Films," Proc. SPIE, *480*, 2–8 (1984).

183. D.E. Aspnes, "Precision Bounds in Ellipsometer Systems," Appl. Opt., *14*, 1131–1136 (1975).

184. J.A. Johnson and N.M. Bashara, "General Equations of Symmetrical Ellipsometer Arrangements," J. Opt. Soc. Am., *60*, 221–224 (1970).

185. P.H. Smith, "A Theoretical and Experimental Analysis of the Ellipsometer," Surf. Sci., *16*, 34–66 (1969).

186. M.P. Kothiyal, "Ellipsometer Nulling: Coupling and Setting Uncertainty," Appl. Opt., *18*, 1019–1024 (1979).

187. R.M.A. Azzam and N.M. Bashara, "Ellipsometry with Imperfect Components Including Incoherent Effects," J. Opt. Soc. Am., *61*, 1380–1391 (1971).

188. R.M.A. Azzam and N.M. Bashara, "Unified Analysis of Ellipsometry Errors Due to Imperfect Components, Cell-Window Birefringence, and Incorrect Azimuth Angles," J. Opt. Soc. Am., *61*, 600–607 (1971).

189. D.E. Aspnes, "Measurement and Correction of First-Order Errors in Ellipsometry," J. Opt. Soc. Am., *61*, 1077–1085 (1971).

190. R.H. Muller, "Ellipsometry of Electrochemical Surface Layers," Proc. SPIE, *112*, 68–73 (1977).

191. B.R. Grunstra and H.B. Perkins, "A Method for the Measurement of Optical Retardation Angles Near 90 Degrees," Appl. Opt., *5*, 585–587 (1966).

192. M.R. Steel, "Method for Azimuthal Alignment in Ellipsometry," Appl. Opt., *10*, 2370–2371 (1971).

193. J.H.P. Castelijns, "Improved Method for Azimuthal Alignment in Ellipsometry," Appl. Opt., *14*, 806–807 (1975).

194. J.R. Zeidler, R.B. Kohles, and N.M. Bashara, "High Precision Alignment Procedure for an Ellipsometer," Appl. Opt., *13*, 1115–1120 (1974).

195. R.M.A. Azzam and N.M. Bashara, "Calibration of Ellipsometer Divided Circles," J. Opt. Soc. Am.,

61, 1118 (1971).

196. D.E. Aspnes and A.A. Studna, "Geometrically Exact Ellipsometer Alignment," Appl. Opt., *10*, 1024–1030 (1971).

197. A.P. Lenham, "Alignment of Both Polarizers, Relative to the Specimen, in Ellipsometry," J. Opt. Soc. Am., *63*, 1175–1176 (1973).

198. J.R. Adams and N.M. Bashara, "In Process Ellipsometer Azimuth Angle Calibration," Appl. Opt., *15*, 3179–3184 (1976).

199. R.H. Muller, "Ellipsometer for Use with LEED Chamber," Rev. Sci. Instrum., *39*, 1593–1594 (1968).

200. W.R. Hunter, "Effects of Component Imperfections on Ellipsometer Calibration," J. Opt. Soc. Am., *63*, 951–957 (1973).

201. W.R. Hunter, D.H. Eaton, and C.T. Sah, "The Effects of Polarizer Ellipticity on Ellipsometry Measurements," Surf. Sci., *20*, 355–376 (1970).

202. G. Forgács, "A Modified Method for Calibrating the Analyser and the Polarizer in an Ellipsometer," J. Phys. D., *3*, 1513–1516 (1970).

203. J.R. Zeidler, R.B. Kohles, and N.M. Bashara, "Sensitivity of the Ellipsometric Parameters to Angle-of-Incidence Variations," Appl. Opt., *13*, 1591–1594 (1974).

204. J.R. Zeidler, R.B. Kohles, and N.M. Bashara, "Beam Deviation Errors in Ellipsometric Measurements; an Analysis," App. Opt., *13*, 1938–1945 (1974).

205. J.L. Ord, "An Ellipsometer for Following Film Growth," Surf. Sci., *16*, 155–165 (1969).

206. J.L. Ord and B.L. Wills, "A Computer-Operated Following Ellipsometer," Appl. Opt., *6*, 1673–1677 (1967).

207. R.J. King and M.J. Downs, "Ellipsometry Applied to Films on Dielectric Substrates," Surf. Sci., *16*, 288–302 (1969).

208. C.C. Matheson, J.G. Wright, R. Gundermann, and H. Norris, "A High Precision, Polychromatic, Automatic Ellipsometer," Surf. Sci., *56*, 196–211 (1976).

209. J.L. Ord and Z.Q. Huang, "An Optical Study of the Deposition, Discharge, and Recharge of Manganese Dioxide Films," J. Electrochem. Soc., *132*, 1183–1186 (1985).

210. C.K. Dyer and J.S.L. Leach, "Reversible Optical Changes within Anodic Oxide Films on Titanium and Niobium," J. Electrochem. Soc., *125*, 23–29 (1978).

211. H.P. Layer, "Circuit Design for An Electronic Self-Nulling Ellipsometer," Surf. Sci., *16*, 177–192 (1969).

212. H.J. Mathieu, D.E. McClure, and R.H. Muller, "Fast Self-Compensating Ellipsometer," Rev. Sci. Instrum., *45*, 798–802 (1974).

213. R.H. Muller and C.G. Smith, "Use of Film-Formation Models for the Interpretation of Ellipsometer Observations," Surf. Sci., *96*, 375–400 (1980).

214. A.B. Winterbottom, "Increased Scope of Ellipsometric Studies of Surface Film Formation," in E. Passaglia, R.F. Stromberg, and J. Kruger, Eds., *Ellipsometry In The Measurement of Surfaces on Thin Films*, Nat. Bur. Stand. Misc. Pub. 256, 1964, pp. 97–112.

215. H.G. Jerrard, "A High-Precision Photoelectric Ellipsometer," Surf. Sci., *16*, 137–146 (1969).

216. R.H. Muller and H.J. Mathieu, "Performance Tests for Automatic Ellipsometers," Appl. Opt., *13*, 2222–2227 (1974).

217. R.H. Muller and J.C. Farmer, "Fast, Self-Compensating Spectral-Scanning Ellipsometer," Rev. Sci. Instrum., *55*, 371–374 (1984).

218. D.N. Henty and H.G. Jerrard, "A Universal Ellipsometer," Surf. Sci., *56*, 170–181 (1976).

219. A.C. Lowe, "Practical Limitations to Accuracy in a Nulling Automatic Wavelength-Scanning Ellipsometer," Surf. Sci., *56*, 134–147 (1976).

220. R.M. Duffy and R.P. Netterfield, "Design of Faraday Rotators and Modulators," Rev. Sci. Instrum.,

55, 743–746 (1984).

221. P.H. Lissberger, I.W. Salter, M. Fitzpatrick, and P.L. Taylor, "Automatic Ellipsometry Without a Phase Plate," J. Phys. E., *10*, 635–641 (1977).

222. M. Billardon, "Méthode polarimétrique de précision dans le visible et l'ultra-violet, Applications à des problèmes de dispersion rotatoire," Ann. de Phys., *7*, 233–267 (1962).

223. H. Takasaki, "Photoelectric Measurement of Polarized Light by Means of an ADP Polarization Modulator. I. Photoelectric Polarimeter," J. Opt. Soc. Am., *51*, 462–463 (1961); "Photoelectric Measurement of Polarized Light by Means of an ADP Polarization Modulator. II. Photoelectric Elliptic Polarimeter," J. Opt. Soc. Am., *51*, 463 (1961).

224. T. Kasai, "High-Speed Automatic Ellipsometer for Industrial Uses," Rev. Sci. Instrum., *47*, 1044–1048 (1976).

225. D.A. Jackson, A.D. Kersey, P. Akhavan Leilabady, and J.D.C. Jones, "High Frequency Non-Mechanical Optical Linear Polarisation State Rotator," J. Phys. E., *19*, 146–148 (1986).

226. B.D. Zak, B. Chang, and T. Hadeishi, "Current-Controlled Phase Retardation Plate," Appl. Opt., *14*, 1217–1219 (1975).

227. H. Takasaki, "Automated Ellipsometer. Automatic Polarimetry by Means of an ADP Polarization Modulator III," Appl. Opt., *5*, 759–764 (1966).

228. I. Wilmanns, "A Double-Modulation Photoelectric Ellipsometer," Surf. Sci., *16*, 147–154 (1969).

229. J.H. Apfel, "Graphical Method to Design Internal Reflection Phase Retarders," Appl. Opt., *23*, 1178–1183 (1984).

230. J.M. Bennett, "A Critical Evaluation of Rhomb-Type Quarterwave Retarders," Appl. Opt., *9*, 2123–2129 (1970).

231. B.D. Cahan and R.F. Spanier, "A High Speed Precision Automatic Ellipsometer," Surf. Sci., *16*, 166–176 (1969).

232. P.S. Hauge and F.H. Dill, "Design and Operation of ETA, an Automated Ellipsometer," IBM J. Res. Develop., *17*, 472–489 (1973).

233. R. Greef, "An Automatic Ellipsometer for Use in Electrochemical Investigations," Rev. Sci. Instrum., *41*, 532–538 (1970).

234. R.W. Stobie, B. Rao, and M.J. Dignam, "Analysis of a Novel Ellipsometric Technique with Special Advantages for Infrared Spectroscopy," J. Opt. Soc. Am., *65*, 25–28 (1975).

235. D.E. Aspnes, "Fourier Transform Detection System for Rotating-Analyzer Ellipsometers," Opt. Commun., *8*, 222–225 (1973).

236. D.E. Aspnes and A.A. Studna, "High-Precision Scanning Ellipsometer," Appl. Opt., *14*, 220–228 (1975).

237. R. Kirsch, "Ein Fourier-Stokes-Analysatorsystem für polarisiertes Licht," Exp. Techn. Phys., *23*, 583–592 (1975).

238. D.E. Aspnes, "Optimizing Precision of Rotating-Analyzer Ellipsometers," J. Opt. Soc. Am., *64*, 639–646 (1974).

239. W.R. Hunter, "Effects of Detector Nonlinearity on Calibration and Data Reduction of Rotating-Analyzer Ellipsometers," J. Opt. Soc. Am., *66*, 94–97 (1976).

240. R.C. O'Handley, "Modified Jones Calculus for the Analysis of Errors in Polarization-Modulation Ellipsometry," J. Opt. Soc. Am., *63*, 523–528 (1973).

241. R.M.A. Azzam and N.M. Bashara, "Analysis of Systematic Errors in Rotating-Analyzer Ellipsometers," J. Opt. Soc. Am., *64*, 1459–1469 (1974).

242. S. Kawabata, "Improved Measurement Method in Rotating-Analyzer Ellipsometry," J. Opt. Soc. Am. A, *1*, 706–710 (1984).

243. R.M.A. Azzam, "Oscillating-Analyzer Ellipsometer," Rev. Sci. Instrum., *47*, 624–628 (1976).

244. N. Umeda and H.Takasaki, "New Ellipsometry Realized by the Use of a Stabilized Two-Frequency

Laser," Surf. Sci., *96*, 141–148 (1980).

245. R.M.A. Azzam, "Mueller-Matrix Measurement Using the Four-Detector Photopolarimeter," Opt. Lett., *11*, 270–272 (1986).

246. P.S. Hauge, "Automated Mueller Matrix Ellipsometry," Opt. Commun., *17*, 74–76 (1976).

247. P.S. Hauge, "Generalized Rotating-Compensator Ellipsometry," Surf. Sci., *56*, 148–160 (1976).

248. P.S. Hauge and F.H. Dill, "A Rotating-Compensator Fourier Ellipsometer," Opt. Commun., *14*, 431–437 (1975).

249. D.E. Aspnes, "Photometric Ellipsometer for Measuring Partially Polarized Light," J. Opt. Soc. Am., *65*, 1274–1278 (1975).

250. R.M.A. Azzam, "Simulation of Mechanical Rotation by Optical Rotation: Application to the Design of a New Fourier Photopolarimeter," J. Opt. Soc. Am., *68*, 518–521 (1978).

251. R.M.A. Azzam, "Photopolarimetric Measurement of the Mueller Matrix by Fourier Analysis of a Single Detected Signal," Opt. Lett., *2*, 148–150 (1978).

252. O. Hunderi, "Rotating Depolarizer Ellipsometry," Appl. Opt., *16*, 3012–3015 (1977).

253. S.N. Jasperson, D.K. Burge, and R.C. O'Handley, "A Modulated Ellipsometer for Studying Thin Film Optical Properties and Surface Dynamics," Surf. Sci., *37*, 548–558 (1973).

254. S.N. Jasperson and S.E. Schnatterly, "An Improved Method for High Reflectivity Ellipsometry Based on a New Polarization Modulation Technique," Rev. Sci. Instrum., *40*, 761–767 (1969); Erratum, *41*, 152 (1970).

255. S.V. Pihlajamäki and J.J. Kankare, "A Microprocessor Controlled Spectroellipsometer for Study of Electrochemical Systems," J. Phys. (Paris), *44*, C10-53 to C10-56 (1983).

256. J.J. Treu, A.B. Callender, and S.E. Schnatterly, "Use of a Stable Polarization Modulator in a Scanning Spectrophotometer and Ellipsometer," Rev. Sci. Instrum., *44*, 793–797 (1973).

257. J. Shamir and A. Klein, "Ellipsometry with Rotating Plane-Polarized Light," Appl. Opt., *25*,

1476–1480 (1986).

258. M.E. Pedinoff, M. Braunstein, and D.M. Stafsudd, "Refractive Indices of ir Materials: 10.6-μm Ellipsometer Measurements," Appl. Opt., *16*, 2849–2857 (1977).

259. G.J. Sprokel, "Photoelastic Modulated Ellipsometry on Magnetooptic Multilayer Films," Appl. Opt., *25*, 4017–4022 (1986).

260. A. Moritani, Y. Okuda, H. Kubo, and J. Nakai, "High-Speed Retardation Modulation Ellipsometer," Appl. Opt., *22*, 2429–2436 (1983).

261. A. Moritani, Y. Okuda, H. Kubo, and J. Nakai, "High-Speed Retardation Modulation Ellipsometer: Erratum," Appl. Opt., *23*, 11 (1984).

262. A. Moritani, Y. Okuda, and J. Nakai, "A Retardation Modulation Ellipsometer for Studying Fast Surface Transients," J. Phys. (Paris), *44*, C10-63 to C10-66 (1983).

263. V.M. Bermudez and V.H. Ritz, "Wavelength-Scanning Polarization-Modulation Ellipsometry: Some Practical Considerations," Appl. Opt., *17*, 542–552 (1978).

264. A. Moritani, Y. Okuda, and J. Nakai, "Use of an ADP Four-Crystal Electrooptic Modulator in Ellipsometry," Appl. Opt., *22*, 1329–1336 (1983).

265. F.A. Modine, G.E. Jellison, Jr., and G.R. Gruzalski, "Errors in Ellipsometry Measurements Made with a Photoelastic Modulator," J. Opt. Soc. Am., *73*, 892–900 (1983).

266. T. Smith, "An Automated Scanning Ellipsometer," Surf. Sci., *56*, 212–220 (1976).

267. R.M.A. Azzam, "Integrated Polarimeters Based on Anisotropic Photodetectors," Opt. Lett., *12*, 555–557 (1987).

268. M. Yamamoto, "A New Type of Precision Ellipsometer Without Employing a Compensator," Opt. Commun., *10*, 200–202 (1974).

269. T. Yamaguchi and H. Takahashi, "Autocollimation-Type Ellipsometer for Monitoring Film Growth Through a Single Window," Appl. Opt., *15*, 677–680 (1976).

270. R.M.A. Azzam, "Return-Path Ellipsometry and a Novel Normal-Incidence Null Ellipsometer (NINE)," Opt. Acta., *24*, 1039–1049 (1977).

271. K. Kinosita and M. Yamamoto, "Principal Angle-of-Incidence Ellipsometry," Surf. Sci., *56*, 64–75 (1976).

272. E.G. Lluesma, C.A. Pela, and I. Wilmanns, "A New Automatic Ellipsometer," Surf. Sci., *56*, 189–195 (1976).

273. A.B. Marchant and J.J. Wrobel, "Simple Ellipsometer Design," Appl. Opt., *20*, 2040–2041 (1981).

274. R.M.A. Azzam and A.R.M. Zaghloul, "Principal Angle, Principal Azimuth, and Principal-Angle Ellipsometry of Film-Substrate Systems," J. Opt. Soc. Am., *67*, 1058–1065 (1977).

275. D. Chandler-Horowitz and G.A. Candela, "Principal Angle Spectroscopic Ellipsometry Utilizing a Rotating Analyzer," Appl. Opt., *21*, 2972–2977 (1982).

276. A.R.M. Zaghloul and R.M.A. Azzam, "Single-Element Rotating-Polarizer Ellipsometer: Psi Meter," Surf. Sci., *96*, 168–173 (1980).

277. T. Yoshino and K. Kurosawa, "All-Fiber Ellipsometry," Appl. Opt., *23*, 1100–1102 (1984).

278. H.F. Hazebroek and A.A. Holscher, "Interferometric Ellipsometry," J. Phys. E., *6*, 822–826 (1973).

279. D.H. Auston and C.V. Shank, "Picosecond Ellipsometry of Transient Electron-Hole Plasmas in Germanium," Phys. Rev. Lett., *32*, 1120–1123 (1974).

280. G.E. Jellison, Jr., and D.H. Lowndes, "Time-Resolved Ellipsometry," Appl. Opt., *24*, 2948–2955 (1985).

281. E. Collett, "Determination of the Ellipsometric Characteristics of Optical Surfaces Using Nanosecond Laser Pulses," Surf. Sci., *96*, 156–167 (1980).

282. T. Sandström, "Differential Ellipsometry," J. Phys. (Paris), *44*, C10-75 to C10-78 (1983).

283. L. Stiblert and T. Sandström, "Geometrical Resolution in the Comparison Ellipsometer," J. Phys. (Paris), *44*, C10-79 to C10-82 (1983).

284. M.J. Dignam and J. Fedyk, "Infrared Ellipsometric Spectroscopy of Adsorbed Species," Appl. Spectrosc. Revs., *14*, 249–285 (1978).

285. J.D. Fedyk, P. Mahaffy, and M.J. Dignam, "Applications of IR Ellipsometric Spectroscopy to Surface Studies," Surf. Sci., *89*, 404–424 (1979).

286. M.J. Dignam, B. Rao, M. Moskovits, and R.W. Stobie, "Ellipsometric Determination of the Spectra of Adsorbed Molecules," Canad. J. Chem., *49*, 1115–1132 (1971).

287. R.W. Stobie, B. Rao, and M.J. Dignam, "Automatic Ellipsometer with High Sensitivity and Special Advantages for Infrared Spectroscopy of Adsorbed Species," Appl. Opt., *14*, 999–1003 (1975).

288. R.R. Schaefer, "Infrared Ellipsometry—A New Technique for Characterization of Dopant Parameters in Silicon," J. Phys. (Paris), *44*, C10-87 to C10-90 (1983).

289. T. Motooka, T. Warabisako, and T. Tokuyama, "Optical Measurement of Carrier Profiles in Silicon," J. Electrochem. Soc., *131*, 174–179 (1984).

290. R.O. DeNicola, M.A. Saifi, and R.E. Frazee, "Epitaxial Layer Thickness Measurement by Far Infrared Ellipsometry," Appl. Opt., *11*, 2534–2539 (1972).

291. T.F. Thonn and R.M.A. Azzam, "Three-Reflection Halfwave and Quarterwave Retarders Using Dielectric-Coated Metallic Mirrors," Appl. Opt., *23*, 2752–2759 (1984).

292. T. Sakurai, S. Mochizuki, and M. Ishigame, "Measurement of Electrical Conductivity of Oxides at High Temperature by Microwave Ellipsometry," High Temp.–High Press., *7*, 411–417 (1975).

293. R. Sardos, "Resolution of the Ambiguity of Measurement Between Rotation and Ellipticity in the Microwave Polarimetry of Nonstationary Plasmas," Rev. Sci. Instrum., *43*, 1726–1727 (1972).

294. K.K. Svitashev, A.I. Semenenko, L.V. Semenenko, and V.K. Sokolov, "Use of a Convergent Light Beam for Ellipsometric Measurements," Opt. Spectrosc. (USSR), *30*, 288–291 (1971).

295. J.-P. Moy, "Immersion Ellipsometry," Appl. Opt., *22*, 3821–3822 (1981).

296. D.W. Stevens, "A Perpendicular-Incidence Microellipsometer," Surf. Sci., *96*, 174–201 (1980).

297. D.J. Dunlavy, R.B. Hammond, and R.K. Ahrenkiel, "Scanning Microellipsometer for the Spatial Characterization of Thin Films," Proc. SPIE, *288*, 390–394 (1981).

298. K. Sugimoto and S. Matsuda, "Analysis of Passive Films on Austeno-Ferritic Stainless Steel by Microscopic Ellipsometry," J. Electrochem. Soc., *130*, 2323–2328 (1983).

299. F. Holtz, "Optische Untersuchungen von Mikrostrukturen in dünnen Oberflächenschichten," Z. Angew. Phys., *25*, 65–71 (1968).

300. J. Sarakinos and J. Spyridelis, "Ellipsometer Data Analysis of a Multilayer Film with a Suitable Computer Program," Thin Solid Films, *28*, 167–177 (1975).

301. D.H. Loescher, R.J. Detry, and M.J. Clauser, "Least-Squares Analysis of the Film-Substrate Problem in Ellipsometry," J. Opt. Soc. Am., *61*, 1230–1235 (1971).

302. J. Zerbino, M. Lopez Teijelo, J.R. Vilche, and A.J. Arvía, "Electrochemical and Ellipsometric Data Related to the Formation of Soluble Silver (I) During the Potentiodynamic Polarization of Polycrystalline Silver in Basic Solutions," Electrochim. Acta, *30*, 1521–1525 (1985).

303. M. Lopez Teijelo, J.O. Zerbino, J.R. Vilche, and A.J. Arvía, "Ellipsometry of Silver Electrodes in Base Solutions Under Different Potential Controlled Perturbation Conditions," Electrochim. Acta, *29*, 939–946 (1984).

304. S.A. Alterovitz, G.H. Bu-Abbud, and J.A. Woollam, "Analytic Solutions for Optimized Ellipsometric Measurements of Interfaces and Surface Layers in Thin Film Structures," Thin Solid Films, *123*, 183–195 (1985).

305. D.H. Loescher, "Formulas for the Derivatives of the Complex Index of Refraction with Respect to Δ, ψ, ϕ, and d," Appl. Opt., *10*, 1031–1033 (1971).

306. Y. Yoriume, "Method for Numerical Inversion of the Ellipsometry Equation for Transparent Films," J. Opt. Soc. Am., *73*, 888–891 (1983).

307. D. Charlot and A. Maruani, "Ellipsometric Data Processing: An Efficient Method and an Analysis

of the Relative Errors," Appl. Opt., *24*, 3368–3373 (1985).

308. R.F. Steiger, J.M. Morabito, Jr., G.A. Somorjai, and R.H. Muller, "A Study of the Optical Properties and of the Physical Adsorption of Gases on Silver Single Crystal Surfaces by Ion Energy Electron Diffraction and Ellipsometry," Surf. Sci., *14*, 279–304 (1969).

309. R.H. Muller, R.F. Steiger, G.A. Somorjai, and J.M. Morabito, "Gas Adsorption Studies by Ellipsometry in Combination with Low Energy Electron Diffraction and Mass Spectrometry," Surf. Sci., *16*, 234–250 (1969).

310. A.J. Melmed, H.P. Layer, and J. Kruger, "Ellipsometry, Low-Energy Electron Diffraction and Field Electron Microscopy Combined," Surf. Sci., *9*, 476–483 (1968).

311. J.J. Vrakking and F. Meyer, "Auger Electron Spectroscopy Made Quantitative by Ellipsometric Calibration," Appl. Phys. Lett., *18*, 226–228 (1971).

312. J.J. Carroll and A.J. Melmed, "Optical Constants of $(11\bar{2}0)$ Ruthenium in the Visible Region," J. Opt. Soc. Am., *66*, 1050–1051 (1976).

313. M. Seo, R. Saito, and N. Sato, "Ellipsometry and Auger Analysis of Chromium Surfaces Passivated in Acidic and Neutral Aqueous Solutions," J. Electrochem. Soc., *127*, 1909–1912 (1980).

314. M.J. Armstrong and R.H. Muller, "Effects of Ion Bombardment on the Morphology of Lead Films," in *Int. Soc. Electrochem. 36th Meeting, Sept. 23–28, 1985*, Ext. Abs. 0236, J. Appl. Phys. (in press).

315. B. Agius and J. Siejka, "Étude par ellipsométrie et microanalyse nucléaire de l'interface fer passive-solution," J. Phys. (Paris), *38*, C5-139 to C5-144 (1977).

316. D.J. Smith and L. Young, "Comparison of Spectrophotometric and Ellipsometric Method of Measuring the Thickness of Anodic Oxide Films on Tantalum," Thin Solid Films, *101*, 11–19 (1983).

317. A. Piegari and E. Masetti, "Thin Film Thickness Measurement: A Comparison of Various Techniques," Thin Solid Films, *124*, 249–257 (1985).

318. F. Meyer, "Ellipsometric Study of Adsorption Complexes on Silicon," Surf. Sci., *27*, 107–116

(1971).

319. P.J. Magill, "Ellipsometric Measurement of Thin Silicon Films on Evaporated Aluminum-Copper," J. Vac. Sci. Technol., *15*, 122–124 (1978).

320. R.H. Muller, "Anodic Films," in R. Alkire and D.T. Chin, Eds., *AIChE Symp. Ser.*, *79*, 211–217 (1983).

321. C.J. Dell'Oca and L. Young, "Ellipsometric Studies of Anodic Oxide Films Formed on Tantalum in Dilute Phosphoric Acid," J. Electrochem. Soc., *117*, 1545–1548 (1970).

322. S. Kumagai and L. Young, "Ellipsometric Investigation of the Optical Properties of Anodic Oxide Film on Tantalum," J. Electrochem. Soc., *111*, 1411–1416 (1964).

323. D.G. Muth and J.P. Sitarik, "Anodic Oxides of Ta-Al Alloy Films," J. Appl. Phys., *42*, 4941–4944 (1971).

324. L.N. Velikodnyi, V.A. Shepelin, É.V. Kasatkin, Yu. V. Zhikharev, and G.M. Pavlushina, "Ellipsometric Study of the Effect of Ta-Nb Alloy Components on Certain Anodic Oxide Properties," Sov. Electrochem., *16*, 628–631 (1980).

325. C. J. Dell'Oca and P.J. Fleming, "Initial Stages of Oxide Growth and Pore Initiation in the Porous Anodization of Aluminum," J. Electrochem. Soc., *123*, 1487–1493 (1976).

326. R. Greef and C.F.W. Norman, "Ellipsometry of the Growth and Dissolution of Anodic Oxide Films on Aluminum in Alkaline Solution," J. Electrochem. Soc., *132*, 2362–2369 (1985).

327. R.M. Goldstein and R.J. Lederich, "Ellipsometric Determination of the Ionic Current Efficiency of Anodic Alumina," Thin Solid Films, *5*, R11–R14 (1970).

328. R.M. Goldstein, R.J. Lederich, and F.W. Leonhard, "Determination of Optical Constants and Growth Rates of Anodic Alumina by Ellipsometry," J. Electrochem. Soc., *117*, 503–504 (1970).

329. C.J. Dell'Oca, "Properties and Anodization of Evaporated Aluminum Films Studied by Ellipsometry," Thin Solid Films, *26*, 371–380 (1975).

330. I.A. Krasil'nikova, É.V. Kasatkin, Z.A. Iofa, and V.A. Safonov, "Ellipsometric Study of Anodic Oxide Film Formation on Titanium in 5N KOH," Sov. Electrochem., *17*, 500–503 (1981).

331. J. Joseph and G. Gagnaire, "Ellipsometric Study of Anodic Oxide Growth: Application to Titanium Oxide Systems," Thin Solid Films, *103*, 257–265 (1983).

332. C.P. De Pauli, M.C. Giordano, and J.O. Zerbino, "Ellipsometric Response of Titanium Electrodes in Sulphate Acid Solutions Under Different Potential Perturbations," Electrochim. Acta, *28*, 1781–1788 (1983).

333. M.A. Hopper, J.A. Wright, and D.J. De Smet, "Anodic Oxidation of Zirconium: Evidence of Typical Valve Metal Behavior," J. Electrochem. Soc., *124*, 44–48 (1977).

334. J.L. Ord, J.C. Clayton, and K. Brudzewski, "The Effect of Electrostriction on the Anodic Oxidation of Tungsten," J. Electrochem. Soc., *125*, 908–914 (1978).

335. J.C. Clayton and D.J. De Smet, "The Optical Anisotropy of the Anodic Oxide of Vanadium," J. Electrochem. Soc., *123*, 1886–1889 (1976).

336. J.L. Ord and E.M. Lushiku, "Open-Circuit Transient Analysis of the Anodic Oxidation of Tungsten and Niobium," J. Electrochem. Soc., *126*, 1374–1380 (1979).

337. W. Paik and Z. Szklarska-Smialowska, "Reflectance and Ellipsometric Study of Anodic Passive Films Formed on Nickel in Sodium Hydroxide Solution," Surf. Sci., *96*, 401–412 (1980).

338. Yu. N. Chernykh and A.A. Yakovleva, "Anodic Behavior of a Nickel Oxide Electrode in Alkaline Solutions. III. Study of the Optical Properties of Oxide Films by an Ellipsometric Method," Sov. Electrochem., *7*, 513–516 (1971).

339. J.O'M. Bockris, A.K.N. Reddy, and B. Rao, "An Ellipsometric Determination of the Mechanism of Passivity of Nickel," J. Electrochem. Soc., *113*, 1133–1144 (1966).

340. P.W.T. Lu and S. Srinivasan, "Electrochemical-Ellipsometric Studies of Oxide Film Formed on Nickel During Oxygen Evolution," J. Electrochem. Soc., *125*, 1416–1422 (1978).

341. J.L. Ord, J.C. Clayton, and D.J. De Smet, "An Ellipsometric Study of the Anodic Oxidation of Nickel in Neutral Electrolyte," J. Electrochem. Soc., *124*, 1714–1719 (1977).

342. J.L. Ord and D.J. De Smet, "The Anodic Oxidation of Iron: Overpotential Analysis for a Two-Phase Film," J. Electrochem. Soc., *123*, 1876–1882 (1976).

343. F.C. Ho and J.L. Ord, "The Anodic Oxide of Iron: Its Component Layers and Their Properties," J. Electrochem. Soc., *119*, 139–145 (1972).

344. E.V. Lisovaya, A.M. Sukhotin, P.P. Konorov, and Yu. A. Tarantov, "Ellipsometric Study of the Passivating Film on Iron in Acidic Sulfate Solutions. The Effect of Potential and pH," Sov. Electrochem., *22*, 845–850 (1986).

345. T. Zakroczymski, C.-J. Fan, and Z. Szklarska-Smialowska, "Kinetics and Mechanism of Passive Film Formation on Iron in 0.05M NaOH," J. Electrochem. Soc., *132*, 2862–2867 (1985).

346. J.L. Ord and D.J. De Smet, "An Ellipsometric Study of the Anodic Deposition of Iron Oxide Films," J. Electrochem. Soc., *118*, 206–209 (1971).

347. J.L. Ord and F.C. Ho, "The Anodic Oxidation of Platinum: Evidence for a High-Field Ionic Conduction Mechanism," J. Electrochem. Soc., *118*, 46–51 (1971).

348. F. Chao, M. Costa, and A. Tadjeddine, "Application de l'ellipsométrie a l'étude des films formés sur les électrodes," Bull. Soc. Chim. (France), *7*, 2465–2474 (1971).

349. J.L. Ord, D.J. De Smet, and M.A. Hopper, "The Anodic Oxidation of Platinum: Determining the Dependence of Current Density on Potential," J. Electrochem. Soc., *123*, 1352–1358 (1976).

350. Yu. Ya. Vinnikov, V.A. Shepelin, and V.J. Veselovskii, "An Ellipsometric and Electrochemical Investigation of the Pt Electrode II. Formation and Properties of Oxide Films in the Oxygen Evolution Region," Sov. Electrochem., *9*, 624–626 (1973).

351. S.O. Martikyan, V.A. Shepelin, and É.V. Kasatkin, "Ellipsometric and Electrochemical Study of Perphosphate Formation at a Platinum Electrode II. Composition and Properties of Anodic Coatings in

Solutions Containing Phosphate Ions," Sov. Electrochem., *13*, 479–481 (1977).

352. B.E. Conway, H. Angerstein-Kozlowska, and L. Laliberté, "Reflectance Changes During Formation and Reduction of Oxide Films on Gold and Platinum: Correction for 'Double-Layer Effects,'" J. Electrochem. Soc., *121*, 1596–1603 (1974).

353. A. Damjanovic, A.T. Ward, and M. O'Jea, "Effect of the Thickness of Anodic Oxide Films on the Rate of the Oxygen Evolution Reaction at Pt in H_2SO_4 Solution," J. Electrochem. Soc., *121*, 1186–1190 (1974).

354. Yu. Ya. Vinnikov, V.A. Shepelin, and V.I. Veselovskii, "Ellipsometric and Electrochemical Investigation of the Au Electrode I. Qualitative Assessment of Optical and Coulometric Data," Sov. Electrochem., *8*, 1201–1204 (1972).

355. Yu. Ya. Vinnikov, V.A. Shepelin, and V.I. Veselovskii, "Ellipsometric and Electrochemical Study of the Au Electrode II. Assessment of the Thickness and the Optical Parameters of Coatings," Sov. Electrochem., *8*, 1352–1354 (1972).

356. D. Elliott, A. Hamnett, O.C. Lettington, H.A.O. Hill, and N.J. Walton, "The Determination, by Ellipsometry, of the Mode of Adsorption on Gold of Some Promoters of Redox-Protein Direct Electrochemistry," J. Electroanal. Chem., *202*, 303–314 (1986).

357. J.L. Ord, D.J. De Smet, and Z.Q. Huang, "An Ellipsometric Study of the Anodic Oxidation of Copper in pH 12 Sodium Carbonate," J. Electrochem. Soc., *134*, 826–832 (1987).

358. M. Yamashita, K. Omura, and D. Hirayama, "Passivating Behavior of Copper Anodes and its Illumination Effects in Alkaline Solutions," Surf. Sci., *96*, 443–460 (1980).

359. M. Novak, A.K.N. Reddy, and H. Wroblowa, "An Ellipsometric Study of Surface Films on Copper Electrodes Undergoing Electropolishing," J. Electrochem. Soc., *117*, 733–737 (1970).

360. S.T. Mayer and R.H. Muller, "Nucleation of Silver(I) Oxide Investigated by Spectroscopic Ellipsometry," in *Electrochem. Soc. Meeting, Oct. 19–24, 1986*, Vol. 86-2, Ext. Abstr. 506; J. Electrochem. Soc. *135*, 2133–2142 (1988).

361. N. Yu. Lyzlov, V.J. Pshenitsyn, and I.A. Aguf, "Ellipsometric Investigation of the Anodic Passivation of Lead in Sulfuric Acid Solution," Sov. Electrochem., *13*, 1201–1203 (1978).

362. D.E. Aspnes, G.P. Schwartz, G.J. Gualtieri, A.A. Studna, and B. Schwartz, "Optical Properties of GaAs and its Electrochemically Grown Anodic Oxide from 1.5 to 6.0 eV," J. Electrochem. Soc., *128*, 590–597 (1981).

363. C.J. Dell'Oca, G. Yan, and L. Young, "Ellipsometry of Anodic Oxide Films on GaAs," J. Electrochem. Soc., *118*, 89–91 (1971).

364. J. Joseph and A. Gagnaire, "Etude 'in situ' de la croissance d'oxyde anodique par ellipsométrie," J. Phys. (Paris), *44*, C10-183 to C10-186 (1983).

365. H. Arwin and D.E. Aspnes, "Nondestructive Analysis of $Hg_{1-x}Cd_xTe$ (x=0.00, 0.20, 0.29, and 1.00) by Spectroscopic Ellipsometry. II. Substrate, Oxide, and Interface Properties," J. Vac. Sci. Technol., *A2*, 1316–1323 (1984).

366. D.E. Aspnes and H. Arwin, "Nondestructive Analysis of $Hg_{1-x}Cd_xTe$ (x=0.00, 0.20, 0.29, and 1.00) by Spectroscopic Ellipsometry. I. Chemical Oxidation and Etching," J. Vac. Sci. Technol., *A2*, 1309–1315 (1984).

367. A. Moritani, H. Kubo, and J. Nakai, "In Situ Ellipsometric Study of Successive Anodization of Monolayers in Some Layered Semiconductors," Surf. Sci., *96*, 476–481 (1980).

368. L.J. Hanekamp, W. Lisowski, and G.A. Bootsma, "Spectroscopic Ellipsometric Investigation of Clean and Oxygen Covered Copper Single Crystal Surfaces," Surf. Sci., *118*, 1–18 (1982).

369. N.M. Bashara and Y.-K. Peng, "Optical Properties of Zircaloy and Zircaloy Oxide by Ellipsometry," Appl. Opt., *19*, 3245–3251 (1980).

370. Y.J. van der Meulen, "Kinetics of Thermal Growth of Ultra-Thin Layers of SiO_2 on Silicon," J. Electrochem. Soc., *119*, 530–534 (1972).

371. R. Kötz, B. Hayden, E. Schweizer, and A.M. Bradshaw, "The Application of Spectroscopic

Ellipsometry to the Oxidation of Magnesium," Surf. Sci., *112*, 229–240 (1981).

372. R.C. O'Handley and D.K. Burge, "Optical Studies of Chemisorption on Metals," Surf. Sci., *48*, 214–228 (1975).

373. R.M. Aguado-Bombin and W.E.J. Neal, "Ellipsometric Measurements on Tantalum and Tantalum Oxide Films and Variation of the Optical Constants with Structure," Thin Solid Films, *42*, 91–96 (1977).

374. R.J. Lederich, "Ellipsometric Data Analysis of the Oxidation of Thin Molybdenum Films," J. Opt. Soc. Am., *62*, 1524–1525 (1972).

375. D.T. Larson and D.L. Cash, "Ellipsometer Studies of Plutonium Oxidation," J. Phys. Chem., *73*, 2814–2820 (1969).

376. J. Kruger, "Use of Ellipsometry in the Study of Corrosion," Corrosion, *22*, 88–97 (1966).

377. J. Kruger, "Optical Studies of the Formation and Breakdown of Passive Films Formed on Iron Single Crystal Surfaces in Inorganic Inhibitor Solutions," J. Electrochem. Soc., *110*, 654–663 (1963).

378. Z. Szklarska-Smialowska and R.W. Staehle, "Ellipsometric Study of the Formation of Films on Iron in Chromate Solutions," J. Electrochem. Soc., *121*, 1146–1152 (1974).

379. Z. Szklarska-Smialowska and R.W. Staehle, "Ellipsometric Study of the Formation of Films on Iron in Orthophosphate Solutions," J. Electrochem. Soc., *121*, 1393–1401 (1974).

380. E.V. Lisovaya, A.M. Sukhotin, P.P. Konorov, and Yu. A. Tarantov, "Ellipsometric Studies of the Passivating Film on Iron in Acidic Sulfate Solutions. Measuring and Calculating Procedure," Sov. Electrochem., *22*, 792–795 (1986).

381. N. Sato, T. Noda, and K. Kudo, "Thickness and Structure of Passive Films on Iron in Acidic and Basic Solution," Electrochim. Acta, *19*, 471–475 (1974).

382. T.G. Stepina, Z.A. Iofa, É.V. Kasatkin, V.A. Shepelin, and V.A. Safonov, "Ellipsometric Study of Anodic Ferrous Oxide Films on Iron in Alkaline Solutions," Sov. Electrochem., *16*, 1548–1550 (1980).

383. T. Zakroczymski, C.-J. Fan, and S. Szklarska-Smialowska, "Passive Film Formation on Iron and

Film Breakdown in a Sodium Hydroxide Solution Containing Chloride Ions," J. Electrochem. Soc., *132*, 2868–2871 (1985).

384. T. Ohtsuka and K.E. Heusler, "Ellipso-Reflectometry Applied to the Study of Passivating Films on Nickel," J. Electroanal. Chem., *100*, 319–333 (1979).

385. M.A. Genshaw and R.S. Sirohi, "An Ellipsometric Study of Chromium Passivation," J. Electrochem. Soc., *118*, 1558–1563 (1971).

386. J.R. Ambrose and J. Kruger, "Tribo-Ellipsometric Study of the Repassivation Kinetics of a Ti 8Al-1Mo-1V Alloy," J. Electrochem. Soc., *121*, 599–604 (1974).

387. J. Kruger, "The Oxide Films Formed on Copper Single Crystal Surfaces in Pure Water. I. Nature of Films Formed at Room Temperature," J. Electrochem. Soc., *106*, 847–853 (1959).

388. J. Kruger, "The Oxide Films Formed on Copper Single Crystal Surfaces in Water. II. Rate of Growth at Room Temperature," J. Electrochem. Soc., *108*, 503–509 (1961).

389. J. Kruger and J.P. Calvert, "The Oxide Films Formed on Copper Single Crystal Surfaces in Water. III. Effect of Light," J. Electrochem. Soc., *111*, 1038–1041 (1964).

390. J.A.S. Green, H.D. Mengelberg, and H.T. Yolken, "Oxide Growth on Copper and Alpha-Brasses in Aqueous Ammonia," J. Electrochem. Soc., *117*, 433–437 (1970).

391. J.J. Ritter and J. Kruger, "A Qualitative Ellipsometric–Electrochemical Approach to the Study of Film Growth Under Organic Coatings," Surf. Sci., *96*, 364–374 (1980).

392. J.J. Ritter and T. Kruger, "Further Development of the Qualitative Ellipsometric Technique for the Study of Corrosion Processes Under Organic Coatings," J. Phys. (Paris), *44*, C10-225 to C10-228 (1983).

393. K.A. Phatak, S.S. Tamhankar, and K. Sathianandan, "Ellipsometric Study of the Corrosion of Evaporated Aluminum Films in Distilled Water at Various Temperatures," Thin Solid Films, *41*, 137–142 (1977).

394. F. Schwager, Y. Geronov, and R.H. Muller, "Ellipsometer Studies of Surface Layers on Lithium," J.

Electrochem Soc., *132*, 285–289 (1985).

395. O. Hunderi, "Ellipsometric Study of Lithium Hydroxide Overlayers on Lithium," Surf. Sci., *57*, 451–459 (1976).

396. G. Mrowczynski and Z. Szklarska-Smialowska, "Electrochemical and Ellipsometric Study of Iron Corrosion Inhibition in Sodium Sulphate Solutions Containing Aliphatic Acids," J. Appl. Electrochem., *9*, 201–207 (1979).

397. N.D. Hobbins and R.F. Roberts, "An Ellipsometric Study of Thin Films Formed on Copper by Aqueous Benzotriazole and Benzimidazole," Surf. Technol., *9*, 235–239 (1979).

398. S. Minc and A. Misiura, "Ellipsometric Study of the Adsorption of Certain Aliphatic Alcohols on the Gold Electrode," Sov. Electrochem., *15*, 123–126 (1979).

399. J. Horkans, B.D. Cahan, and E. Yeager, "An Ellipsometric Investigation of the Underpotential Deposition of Lead on Gold," J. Electrochem. Soc., *122*, 1585–1589 (1975).

400. E.M. Lushiku and K.R. O'Shea, "Ellipsometry in the Study of Selective Radiation-Absorbing Surfaces," Solar Energy, *19*, 271–276 (1977).

401. J.L. Ord, Z.Q. Huang, and D.J. De Smet, "An Ellipsometric Study of Electrodeposition and Electrochemical Conversion of Lead Dioxide Films," J. Electrochem. Soc., *132*, 2076–2081 (1985).

402. D.J. De Smet, "An Ellipsometric Investigation of the Anodic Oxide of Molybdenum," Electrochim. Acta, *21*, 1137–1142 (1976).

403. J.C. Clayton and D.J. De Smet, "A Study of the Anodic Oxide of Vanadium Under Anodic and Cathodic Conditions," J. Electrochem. Soc., *123*, 174–179 (1976).

404. J.L. Ord, "An Ellipsometric Study of Electrochromism in Tungsten Oxide," J. Electrochem. Soc., *129*, 767–771 (1982).

405. J. Sarakinos and J. Spyridelis, "Ellipsometry of Anodic Oxide Films on Tungsten," Thin Solid Films, *27*, 239–245 (1975).

406. J.L. Ord, "Application of Ellipsometry to Studies of Electrostriction and Electrochromism in Anodic Oxide Films," J. Phys. (Paris), *44*, C10-221 to C10-224 (1983).

407. J.D.E. McIntyre, "Specular Reflection Spectroscopy of the Electrode-Solution Interface," in R.H. Muller, Ed., *Advances in Electrochemistry and Electrochemical Engineering, Vol. 9: Optical Techniques in Electrochemistry*, series edited by P. Delahay and C.W. Tobias, Wiley-Interscience, New York, 1973, pp. 61–166.

408. W. Plieth, H. Bruckner, and H.J. Hensel, "Anisotropy of the Dielectric Properties of the Solid/Electrolyte Interface," Surf. Sci., *101*, 261–268 (1980).

409. Y.C. Chiu and M.A. Genshaw, "A Study of Anion Adsorption on Platinum by Ellipsometry," J. Phys. Chem., *73*, 3571–3577 (1969).

410. G.A. Bootsma and F. Meyer, "Ellipsometric Investigation of Physisorption at Low Temperatures,", Surf. Sci., *13*, 110–118 (1969).

411. B.H. Claussen, "An Ellipsometer Investigation of Vapor Adsorption on Etched Silicon," J. Electrochem. Soc., *111*, 646–652 (1964).

412. J.M. Morabito, Jr., R. Steiger, R. Muller, and G.A. Somorjai, "LEED and Ellipsometry Studies of Physical Adsorption on a (110) Silver Surface at Low Temperatures," in G.A. Somorjai, Ed., *The Structure and Chemistry of Solid Surfaces, Proc. Fourth Int. Matls. Symp.*, Wiley, New York, 1969, pp. 50-1 to 50-35.

413. G. Quentel and R. Kern, "Approche théorique par ellipsométrie des constantes optiques des couches monoatomiques physisorbées," Surf. Sci., *55*, 545–572 (1976).

414. G. Quentel and R. Kern, "Étude par ellipsométrie de films physisorbés sur graphite," J. Phys. (Paris), *38*, C5-109 to C5-113 (1977).

415. G. Quentel, J.M. Rickard, and R. Kern, "Étude de l'adsorption par ellipsométrie: Adsorption du Xe/(0001) graphite," Surf. Sci., *50*, 343–359 (1975).

416. Yu. Ya. Vinnikov, V.A. Shepelin, and V.I. Veselovskii, "Ellipsometric and Electrochemical Investigation of the Pt Electrode: I. Formation of a Monolayer of Oxygen-Containing Species," Sov. Electrochem., *9*, 534–536 (1973).

417. Z.I. Kudryavtseva, N.A. Shumilova, V.A. Openkin, N.A. Zhuchkova, and E.I. Krushcheva, "Ellipsometric Examination of Oxygen Adsorption and Oxide Layer Formation on Nickel, Cobalt, and Silver in Alkaline Solutions," Soc. Electrochem., *13*, 608–612 (1977).

418. R.J. Archer and G.W. Gobeli, "Measurement of Oxygen Adsorption on Silicon by Ellipsometry," J. Phys. Chem. Solids, *26*, 343–351 (1965).

419. G.A. Bootsma and F. Meyer, "Ellipsometry in the Sub-Monolayer Region," Surf. Sci., *14*, 52–76 (1969).

420. F. Meyer, E.E. De Kluizenaar, and G.A. Bootsma, "Ellipsometry and the Clean Surfaces of Silicon and Germanium," Surf. Sci., *27*, 88–106 (1971).

421. A.E. Morgan, "Ellipsometric Studies of Chemisorption on GaP(110) Single Crystals," Surf. Sci., *43*, 150–172 (1974).

422. R.J. Lederich and J.J. Bellina, Jr., "Interpretation of Ellipsometric Observations of Absorbed Oxygen in Niobium," J. Opt. Soc. Am., *60*, 1697–1698 (1970).

423. T. Smith, "Chlorine Adsorption on Clean Aluminum," Surf. Sci., *32*, 527–542 (1972).

424. M.S. Tomar and V.K. Srivastava, "Anisotropic Effects in the Ellipsometry of 'Built-Up' Films and Determination of Their Optical Constants," Thin Solid Films, *15*, 207–215 (1973).

425. S. Minc, "Ellipsometric Measurements of the Liquid-Air Interface in Presence of Surface Active Substances," J. Electroanal. Chem., *62*, 291–296 (1975).

426. K. Kunimatsu and R. Parsons, "Barbiturates at the Mercury/Solution Interface. An Ellipsometric Study," J. Electroanal. Chem., *100*, 335–363 (1979).

427. R.H. Muller, "Recent Advances in Some Optical Experimental Methods," Electrochim. Acta, *22*,

951–965 (1977).

428. H. Arwin and D.E. Aspnes, "Unambiguous Determination of Thickness and Dielectric Function of Thin Films by Spectroscopic Ellipsometry," Thin Solid Films, *113*, 101–113 (1984).

429. D.E. Aspnes and A.A. Studna, "Chemical Etching and Cleaning Procedures for Si, Ge, and Some III-V Compound Semiconductors," Appl. Phys. Lett., *39*, 316–318 (1981).

430. M.M. Ibrahim and N.M. Bashara, "Ellipsometric Study of Cleaning Silicon by Ion Bombardment and Heating in Vacuum," Surf. Sci., *30*, 680–686 (1972).

431. F. Ohira, "Ellipsometric Characterization of Si Surface Damage Induced by Sputter Etching," J. Electrochem. Soc., *130*, 1201–1206 (1983).

432. H. Albers, J.M.M. Droog, and G.A. Bootsma, "Ellipsometric Study of the Effect of Argon Ion Bombardment on the Structure and Reactivity of Ag(111)," Surf. Sci., *64*, 1–22 (1977).

433. E.D. Palik, V.M. Bermudez, and O.J. Glembocki, "Ellipsometric Study of the Etch-Stop Mechanism in Heavily Doped Silicon," J. Electrochem. Soc., *132*, 135–141 (1985).

434. K. Vedam and M. Malin, "Characterization of Real Surfaces of Vitreous Silica by Ellipsometry," Mat. Res. Bull., *9*, 1503–1510 (1974).

435. M. Delfino and R.R. Razouk, "A Four-Phase Complex Refractive Index Model of Ion-Implantation Damage: Optical Constants of Phosphorous Implants in Silicon," J. Appl. Phys., *52*, 386–392 (1981).

436. Q. Kim and Y.S. Park, "Ellipsometric Investigation of Ion-Implanted GaAs," Surf. Sci., *96*, 307–318 (1980).

437. J.B. Theeten, "Real-Time and Spectroscopic Ellipsometry of Film Growth: Application to Multilayer Systems in Plasma and CVD Processing of Semiconductors," Surf. Sci., *96*, 275–293 (1980).

438. D.E. Aspnes and A.A. Studna, "An Investigation of Ion-Bombarded and Annealed <111> Surfaces of Ge by Spectroscopic Ellipsometry," Surf. Sci., *96*, 294–306 (1980).

439. B.C. Dobbs, W.J. Anderson, and Y.S. Park, "Investigation of Ion-Implanted GaP Layers by

Ellipsometry," J. Appl. Phys., *48*, 5052–5056 (1977).

440. S. Yoshida, T. Yamaguchi, and A. Kinbara, "Optical Properties of Aggregated Silver Films," J. Opt. Soc. Am., *61*, 62–69 (1971).

441. S. Yoshida, T. Yamaguchi, and A. Kinbara, "Changes of the Optical Properties of Aggregated Silver Films After Deposition," J. Opt. Soc. Am., *61*, 463–469 (1971).

442. R. Scheps, "Film Thickness Determination of PMMA on InP by Ellipsometry," J. Electrochem. Soc., *131*, 540–543 (1984).

443. W.W. Flack, J.S. Papanu, D.W. Hess, D.S. Soong, and A.T. Bell, "*In Situ* Measurement of Resist Dissolution with a Psi-Meter," J. Electrochem. Soc., *131*, 2200–2201 (1984).

444. S.A. Alterovitz, G.H. Bu-Abbud, J.A. Woollam, and D.C. Liu, "An Enhanced Sensitivity Null Ellipsometry Technique for Studying Films on Substrates: Application to Silicon Nitride on Gallium Arsenide," J. Appl. Phys., *54*, 1559–1569 (1983).

445. J.B. Theeten and D.E. Aspnes, "The Determination of Interface Layers by Spectroscopic Ellipsometry," Thin Solid Films, *60*, 183–192 (1979).

446. L. Lundkvist, "Ellipsometry of Multilayered Dielectrics on Silicon, Applied to MNOS Structures," J. Electrochem. Soc., *120*, 1140–1142 (1973).

447. H.J. Lewerenz, D.E. Aspnes, B. Miller, D.L. Malm, and A. Heller, "Semiconductor Interface Characterization in Photoelectrochemical Solar Cells: The p-InP(111)A Face," J. Am. Chem. Soc., *104*, 3325–3329 (1982).

448. H. Schopper, "Optische Konstanten, Metalle und Legierungen," in *Landolt-Börnstein, Zahlenwerte und Funktionen*, Vol. 2, Part 8, 6th ed., Springer, Berlin, 1962, pp. 1-1 to 1-36.

449. G. Hass and L. Hadley, "Optical Properties of Metals," in D.E. Gray, Ed., *American Institute of Physics Handbook*, 3rd Ed., McGraw-Hill, New York, 1972, p. 6-118 to 6-160.

450. E.D. Palik, Ed., *Handbook of Optical Constants of Solids*, Academic Press, New York, 1985.

451. Y.J. van der Meulen and N.C. Hien, "Design and Operation of an Automated, High-Temperature Ellipsometer," J. Opt. Soc. Am., *64*, 804–811 (1974).

452. G. Vuye and T. López-Ríos, "Precision in the Ellipsometric Determination of the Optical Constants of Very Thin Films," Appl. Opt., *21*, 2968–2971 (1982).

453. T.H. Allen, "Study of Al with a Combined Auger Electron Spectrometer-Ellipsometer System," J. Vac. Sci. Technol., *13*, 112–115 (1976).

454. S.T. Ceyer, A.J. Melmed, J.J. Carroll, and W.R. Graham, "On the Atomic Structure and Optical Constants of (001) Tantalum," Surf. Sci., *144*, L444–L448 (1984).

455. A.C. Nyce and L.P. Skolnick, "Optical Constants of Bulk and Thin-Film Aluminum at 6328 Å," J. Opt. Soc. Am., *65*, 792–796 (1975).

456. E.C. Chan and J.P. Marton, "Internal Reflection Ellipsometry for Metal Deposits," J. Appl. Phys., *43*, 4027–4030 (1972).

457. P. Rouard and A. Meessen, "Optical Properties of Thin Metal Films," in E. Wolf, Ed., *Progress in Optics*, Vol. XV, North-Holland, Amsterdam, 1977, pp. 79–137.

458. M. Rasigni and G. Rasigni, "Anomalies of the Optical Properties of Thin Lithium Layers and Their Relation to Similar Anomalies Observed with Other Alkali Metals," J. Opt. Soc. Am., *63*, 775–785 (1973).

459. D.E. Aspnes, E. Kinsbron, and D.D. Bacon, "Optical Properties of Au: Sample Effects," Phys. Rev. B, *21*, 3290–3299 (1980).

460. J.H. Halford, F.K. Chin, and J.E. Norman, "Effects of Vacuum Deposition Conditions on Ellipsometric Parameters, Optical Constants, and Reflectance of Ultrapure Aluminum Films," J. Opt. Soc. Am., *63*, 786–792 (1973).

461. F. Meyer, E.E. De Kluizenaar, and D. den Engelsen, "Ellipsometric Determination of the Optical Anisotropy of Gallium Selenide," J. Opt. Soc. Am., *63*, 529–532 (1973).

462. M.L. Jones, H.H. Soonpaa, and B.S. Rao, "Optical Constants of Bismuth Tellurium Sulfide from

Ellipsometric Data," J. Opt. Soc. Am., *64*, 1591–1592 (1974).

463. T.E. Faber and N.V. Smith, "Optical Measurements on Liquid Metal Using a New Ellipsometer," J. Opt. Soc. Am., *58*, 102–108 (1968).

464. T. Inagaki, E.T. Arakawa, R.D. Birkhoff, and M.W. Williams, "Optical Properties of Liquid Na Between 0.6 and 3.8 eV," Phys. Rev. B, *13*, 5610–5612 (1976).

465. E.T. Arakawa, T. Inagaki, and M.W. Williams, "Optical Properties of Metals by Spectroscopic Ellipsometry," Surf. Sci., *96*, 248–274 (1980).

466. J. O'M. Bockris, M.A.V. Devanathan, and A.K.N. Reddy, "The Anodic Formation of Calomel Films on Mercury Electrodes—An Ellipsometric-Galvanostatic Study," Proc. Roy. Soc., A, *279*, 327–345 (1964).

467. D. Beaglehole, "Ellipsometry of Liquid Surfaces," J. Phys. (Paris), *44*, C10-147 to C10-154 (1983).

468. V.A. Kizel' and A.F. Stepanov, "Concerning the Existence of a Transition Layer on a Liquid Surface," Sov. Phys. JETP, *4*, 458–459 (1956).

469. J.W. Schmidt and M.R. Moldover, "Ellipsometry of Thin Films on Vapor-Liquid Interfaces," J. Phys. (Paris), *44*, C10-243 to C10-245 (1983).

470. J.-F. Reber and R. Steiger, "Ellipsometric Studies on the Photolysis of Lead Chloride Crystal Surfaces," Surf. Sci., *49*, 236–252 (1975).

471. P.J. Dynes and D.H. Kaelble, "Plasma Polymerization on Metals," J. Macromol. Sci.-Chem., *A10*, 535–557 (1976).

472. Y. Bouizem, F. Chao, M. Costa, and A. Tadjeddine, "Ellipsometric Study of Acrylonitrile Electropolymerisation on Nickel," J. Phys. (Paris), *44*, C10-509 to C10-512 (1983).

473. M. Babai and S. Gottesfeld, "Ellipsometric Study of the Polymeric Surface Films Formed on Platinum Electrodes by the Electrooxidation of Phenolic Compounds," Surf. Sci., *96*, 461–475 (1980).

Figure Captions

Fig. 2.1. Reflection of polarized light. The plane of incidence is defined by the incident and reflected beams (and the normal of the reflecting surface). The p and s components E_p and E_s of the electric field vectors parallel and normal to the plane of incidence are shown in incident (superscript i) and reflected (superscript r) waves (after 8).

Fig. 2.2. Definition of positive coordinate directions for p and s components (subscripts p and s) of electric field vectors in incident, reflected, and transmitted waves (superscripts i, r, and t, respectively). Propagation vectors k. Refractive indices of incident and reflecting media are n^i and n^t, respectively; angles of incidence and reflection $\phi^i = \phi^r$; angle of refraction ϕ^t.

Fig. 2.3. Intensity penetration depth for light at normal incidence on an absorbing medium with imaginary part of complex refractive index (extinction coefficient) k. Wavelength: 546.1 nm (after 8).

Fig. 2.4. Reflection from a film-covered substrate. Definition of symbols used in the Drude equation: angles of incidence ϕ^i and refraction ϕ^t; reflection coefficients for top interface $\hat{r}_1$ and for bottom interface $\hat{r}_2$; refractive indices of incident medium n^i, film $\hat{n}^t$, and substrate $\hat{n}^s$; film thickness L.

Fig. 2.5. Linear polarization E resulting from the superposition of two linear components E_s and E_p in phase. Vector addition of the two amplitudes $|E_s|$ and $|E_p|$ shown in the plane normal to the propagation direction k.

Fig. 2.6. Elliptic polarization E resulting from the superposition of two linear components E_s and E_p of different amplitude and phase. The resultant helix in space is projected as an ellipse on a plane normal to the propagation direction k. The physical parameters ψ and Δ of the elliptic polarization are shown at the top of the figure; the geometric parameters γ and θ are shown at the bottom (after 8).

Fig. 2.7. Ellipsometer parameters Δ (relative phase change) and ψ (relative amplitude change $\tan \psi$) for reflection from a bare surface of complex refractive index $n^t - ik^t$. Incident medium: dielectric of real refractive index n^i. Angle of incidence: 75°.

Fig. 2.8. Ellipsometer parameters Δ (relative phase change) and ψ (relative amplitude change tan ψ) as a function of angle of incidence ϕ^i for reflection from a bare dielectric surface (glass, solid line, n = 1.5) and an absorbing surface (tantalum, broken line, $\hat{n}$ = 3.3–2.3i). Wavelength: 546.1 nm.

Fig. 2.9. Representation of different states of polarization shown for selected points on the surface of the Poincaré sphere. Left and right circular poles L and R and horizontal plane of incidence H (p component) are marked on the sphere.

Fig. 2.10. Poincaré sphere (left) and its stereographic projection (right), as seen from the left-hand circular pole L. Reference point H denotes the (horizontal) plane of incidence. Top: grid for geometrical parameters, θ and γ; center: grid for physical parameters ψ and Δ; bottom: grid for retardation δ_c of a compensator with fast axis F (after 8).

Fig. 2.11. Poincaré sphere representation of amplitude EA′ of elliptic polarization E transmitted by analyzer A (extinction axis A′). The locus of polarization states of equal transmitted amplitude (square root of measured irradiance) is shown by the small circle I around A′ (after 16).

Fig. 2.12. Stokes parameters S_0, S_1, S_2, S_3, and geometric parameters θ, γ of elliptic polarization represented in the Poincaré sphere for elliptic polarization P.

Fig. 2.13. Nonlinear changes in ellipsometer parameters Δ and ψ ($\delta\Delta$, $\delta\psi$) as a function of coverage predicted by the Bruggeman effective-medium theory (solid lines) for an underpotential deposit (UPD) of Pb on Ag(111). Changes given in degrees. The observed linear dependence on coverage (determined from Faradaic charge) is shown by measured points. Wavelength: 515 nm; angle of incidence: 75°; optical constants of UPD derived from measurements at full coverage (94).

Fig. 2.14. Island-film model with coherent superposition of polarization states associated with reflection coefficients $\hat{r}^f$ and $\hat{r}^s$ for reflection from film-covered and bare surface elements, respectively.

Fig. 2.15. Refractive-index ellipsoid for biaxial (positive) anisotropic materials with principal refractive indices n_α, n_β, and n_γ and optic axes A1 and A2 normal to the circular cross sections of the ellipsoid. For a uniaxial material, $n_\alpha = n_\beta$ and the optic axis coincides with the n_γ direction.

Fig. 2.16. Representation of a rough surface (a) by a homogeneous (b) or inhomogeneous (c) transition layer.

Fig. 3.1. Components of compensating ellipsometer with elliptic polarization incident. P: polarizer with transmitted electric-field direction. The azimuth p at extinction is a measure of Δ. Q: fixed compensator (quarter-wave plate) of fixed azimuth (fast axis F at 45° to plane of incidence). E: elliptic state of polarization before reflection. S: reflecting specimen surface. A′: restored linear state of polarization after reflection. A: analyzer with transmitted electric-field direction. The azimuth a at extinction is a measure of ψ (after 8).

Fig. 3.2. Representation on the Poincaré sphere (stereographic projection) of the changes in the state of polarization in a compensating ellipsometer with elliptic polarization incident on the specimen. The linear polarization from polarizer P is converted to elliptic polarization E by the retardation δ_Q (90°) of the quarter-wave compensator of fast axis F. Reflection on the specimen introduces changes in relative phase Δ and relative amplitude (ψ). The resulting restored linear polarization A′ is extinguished by analyzer A (after 8).

Fig. 3.3. Arrangement of optical and electronic components in self-compensating ellipsometer with Faraday-cell modulation and compensation (after 190).

Fig. 3.4. Modulation of polarizer azimuth by use of a retardation modulator. (a) Sequence and relative azimuths of polarizer P (0°), modulator M (45°), and quarter-wave compensator Q (0°). (b) Azimuths of components and effect of modulation and compensation shown on the Poincaré sphere. (c) Stereographic projection of (b). The linear polarization P is transformed into a series of elliptic polarizations between states E_1 and E_2 by the retardation modulation with amplitude δ_M from the modulator with fast axis M. The quarter-wave compensator Q transforms the elliptic polarizations into linear polarizations with azimuth modulation amplitude dp (16).

Fig. 3.5. Three-reflection Fresnel rhomb for use as achromatic quarter-wave compensator, shown with light path.

Fig. 3.6. Components of photometric ellipsometer with rotating analyzer (shown without compensator). P: polarizer (shown in 45° azimuth); S: reflecting specimen surface; E: reflected elliptic polarization; A: rotating analyzer with rotation indicated by double arrow. The variable photodetector output provides the geometric parameters θ and γ.

Fig. 3.7. Analysis of elliptic polarization with a rotating analyzer. The axial ratio of the ellipse is derived from the ratio of intensity minima and maxima. The orientation θ of the major axis is determined from the azimuth of the intensity maximum (after 8).

Fig. 3.8. Transmitted amplitude with rotating analyzer represented in the Poincaré sphere by the lengths of chords between elliptic polarization E and extinction direction A′ of analyzer A. The rotation direction is indicated by the double arrow (16).

Fig. 3.9. Return-path ellipsometer without compensator. (a) Arrangement of components: L: collimated light source; B: beam splitter; P: polarizer; S: specimen; M: auxiliary (return) mirror; ϕ_p: principal angle of incidence; D: photodetector. (b) Poincaré sphere representation of states of polarization through the components: P: polarizer of azimuth p at compensation; Δ_1, Δ_2: changes in Δ (90°) upon first and second reflections; (ψ_1), (ψ_2): corresponding changes in ψ; $2p = 2\psi$ shown on sphere.

Fig. 3.10. Comparison ellipsometer. Specimen S and reference R have surface normals at right angles to each other; the angle of incidence is the same on both. The reflection from reference R (with continuously variable properties) is extinguished by a crossed analyzer and polarizer where properties of both surfaces are the same (after 282).

Fig. 4.1. Models of anodic films investigated for the interpretation of ellipsometer measurements of anodic oxide growth (after 213).

Fig. 4.2. Optical film models investigated for the interpretation of spectroscopic ellipsometer measurements of Pb deposition on Cu. Free parameters for compact film: 1; for porous (single) film: 2; for compact, single-layer island film: 2; for multilayer film with one compact film, one porous film, and dendrite islands: 6 (after 102).

Fig. 4.3. Formation of submicroscopic pits by the nonuniform removal of an oxide-covered thin lead film (a) by ion bombardment. After removal of the oxide layer, the island-film optical model has been used to represent the growth of pits (b) and the exposure of the substrate (c) (after 314).

Fig. 5.1. Nucleation and growth of crystalline oxide on top of a compact underlayer represented by a two-layer island-film model (360).

Fig. 5.2. Film models with schematic porosity profiles for corrosion layers on lithium. (a) Homogeneous film with uniform porosity; (b) inhomogeneous film with linear porosity profile; (c) inhomogeneous film with parabolic porosity profile (394).

Fig. 5.3. Changes in ellipsometer parameters ψ and Δ (deg.) predicted with an optimized island-film coherent-superposition model (solid lines) and measurements with coverage derived from charge (squares and circles) for underpotential deposition of Pb on Cu(111) (94,101).

Fig. 5.4. Spectroscopic ellipsometer measurements (solid curves) for Pb deposits on Cu. Compact thickness of 0, 30, 60, and 110 nm (based on charge passed) shown for curves. Circles show predictions resulting from a two-layer model with parameters given in Table 4.1 (102).

Fig. 5.5. Representation of a mass-transfer boundary layer by an optically inhomogeneous film with the refractive index decreasing toward the surface. The optical model consists of multiple homogeneous films with reflection and refraction taking place at each interface. The angle of incidence ϕ^b in the bulk solution is different from ϕ^i on the surface (427).

Fig. 6.1. Illumination of an inhomogeneous surface (shown as an island film) with light of different lateral coherence (indicated by the width of wavefronts). (a) Coherence larger than the surface inhomogeneities results in coherent superposition of polarization states for reflection from different surface elements. (b) Coherence smaller than the surface inhomogeneities results in incoherent superposition (after 8).

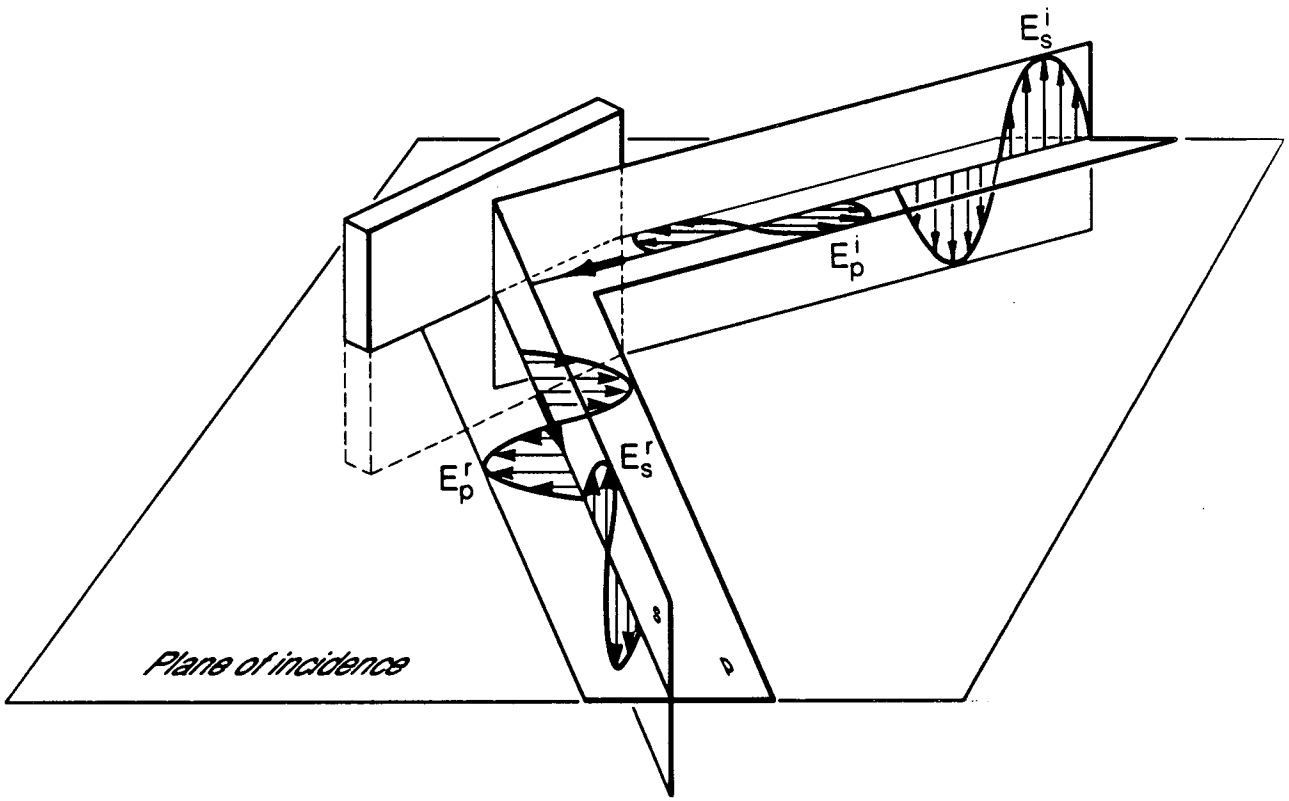

XBL 879-11158

Fig. 2.1

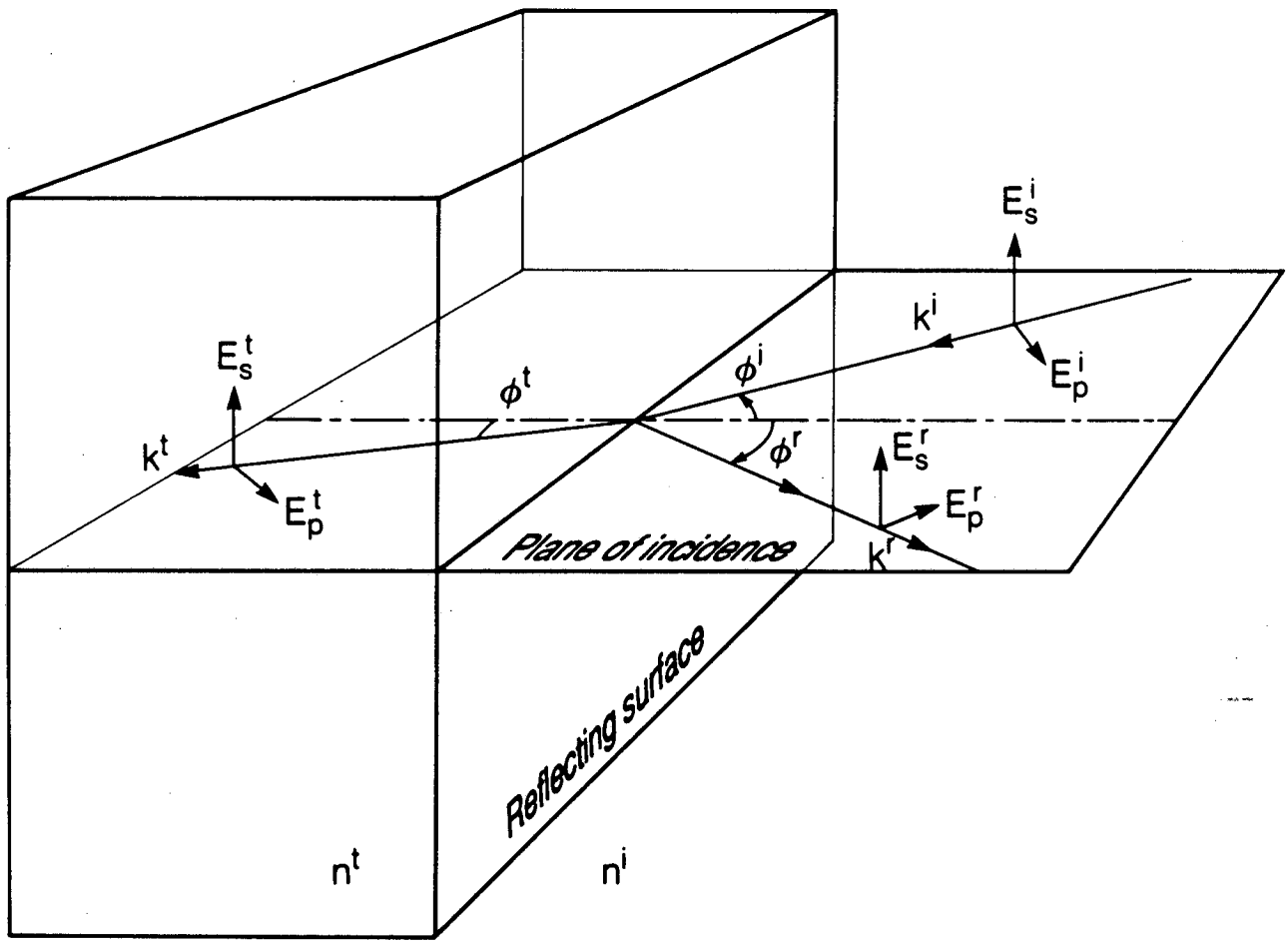

XBL 879-11152

Fig. 2.2.

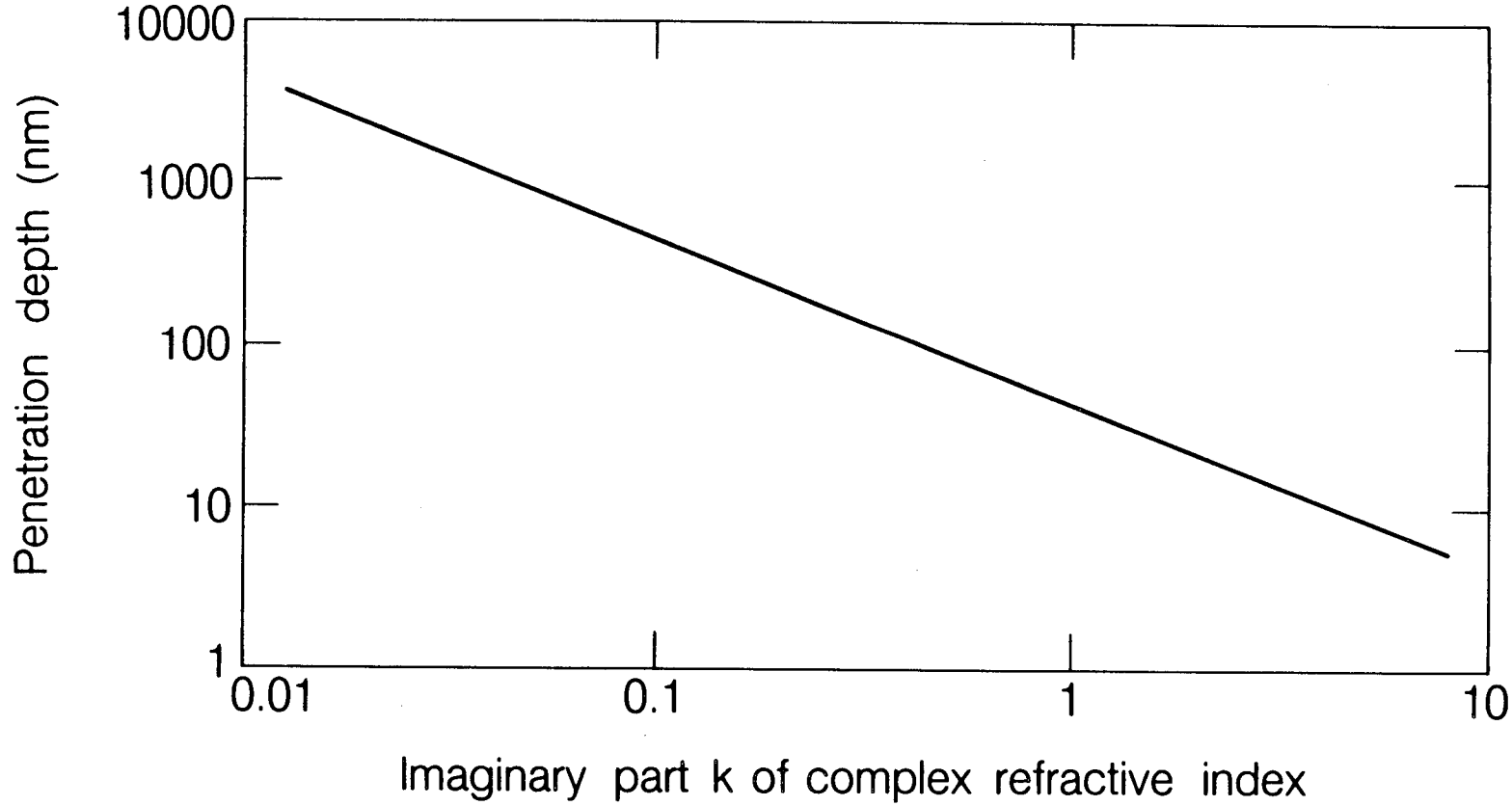

XBL 879-11149 B

Fig. 2.3

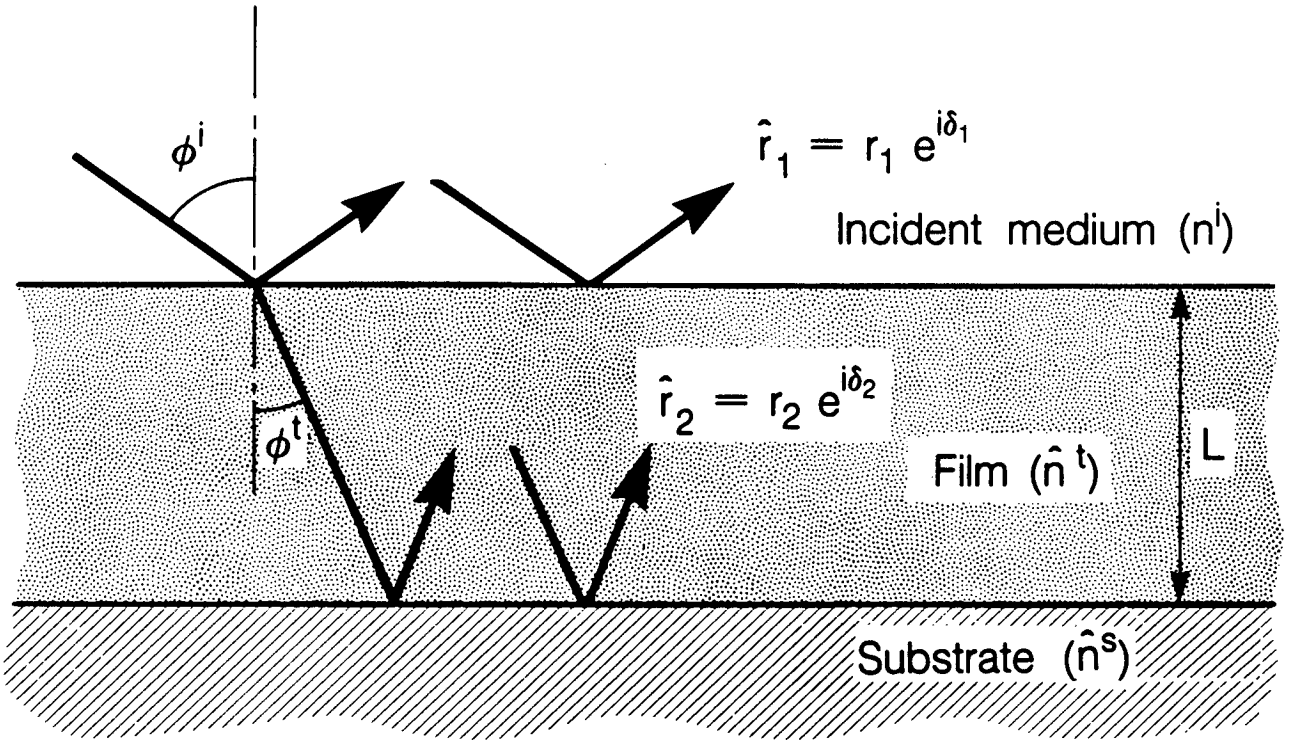

XBL 879-11159

Fig. 2.4

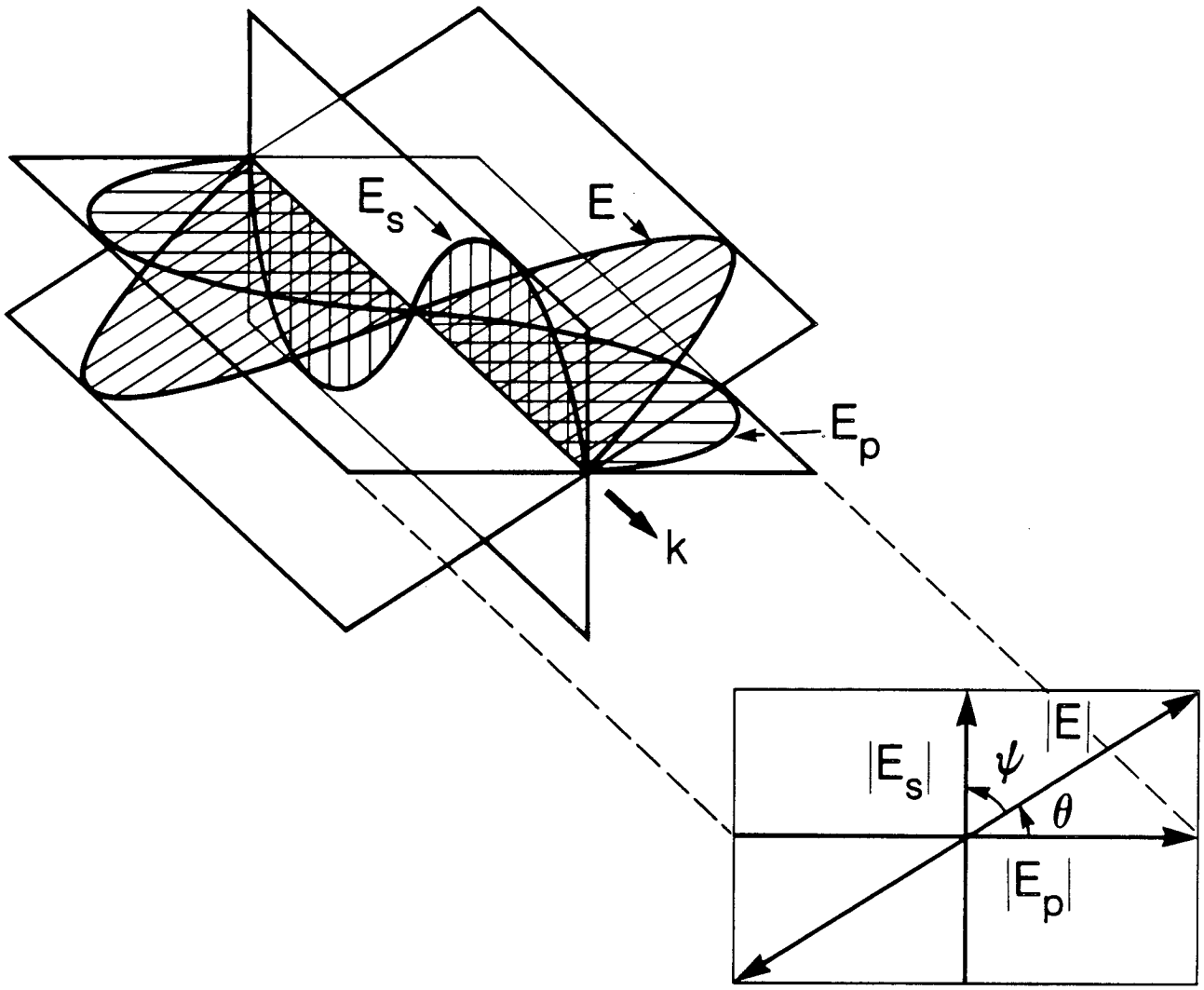

XBL 879-11153

Fig. 2.5

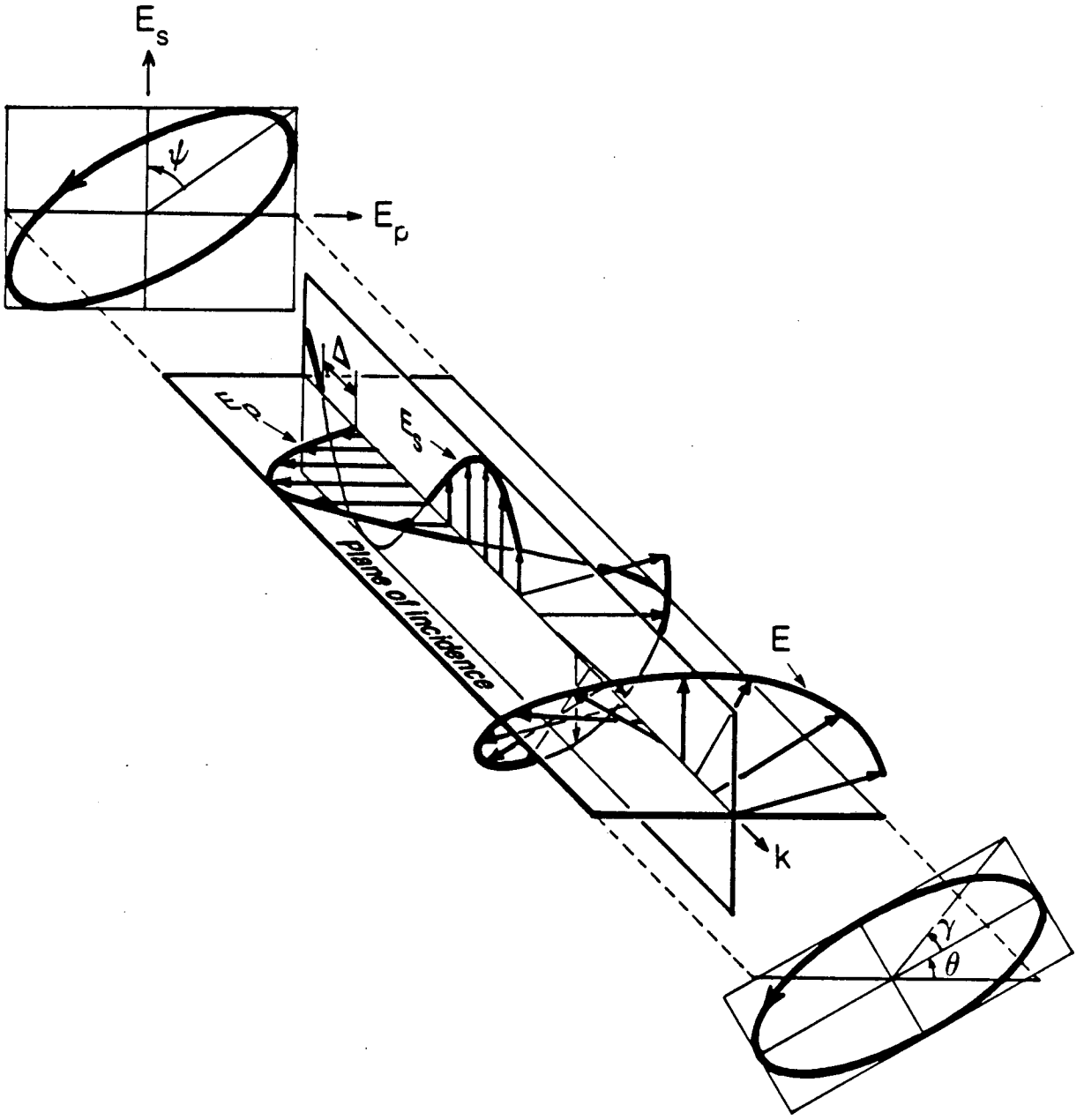

XBL 879-11164

Fig. 2.6

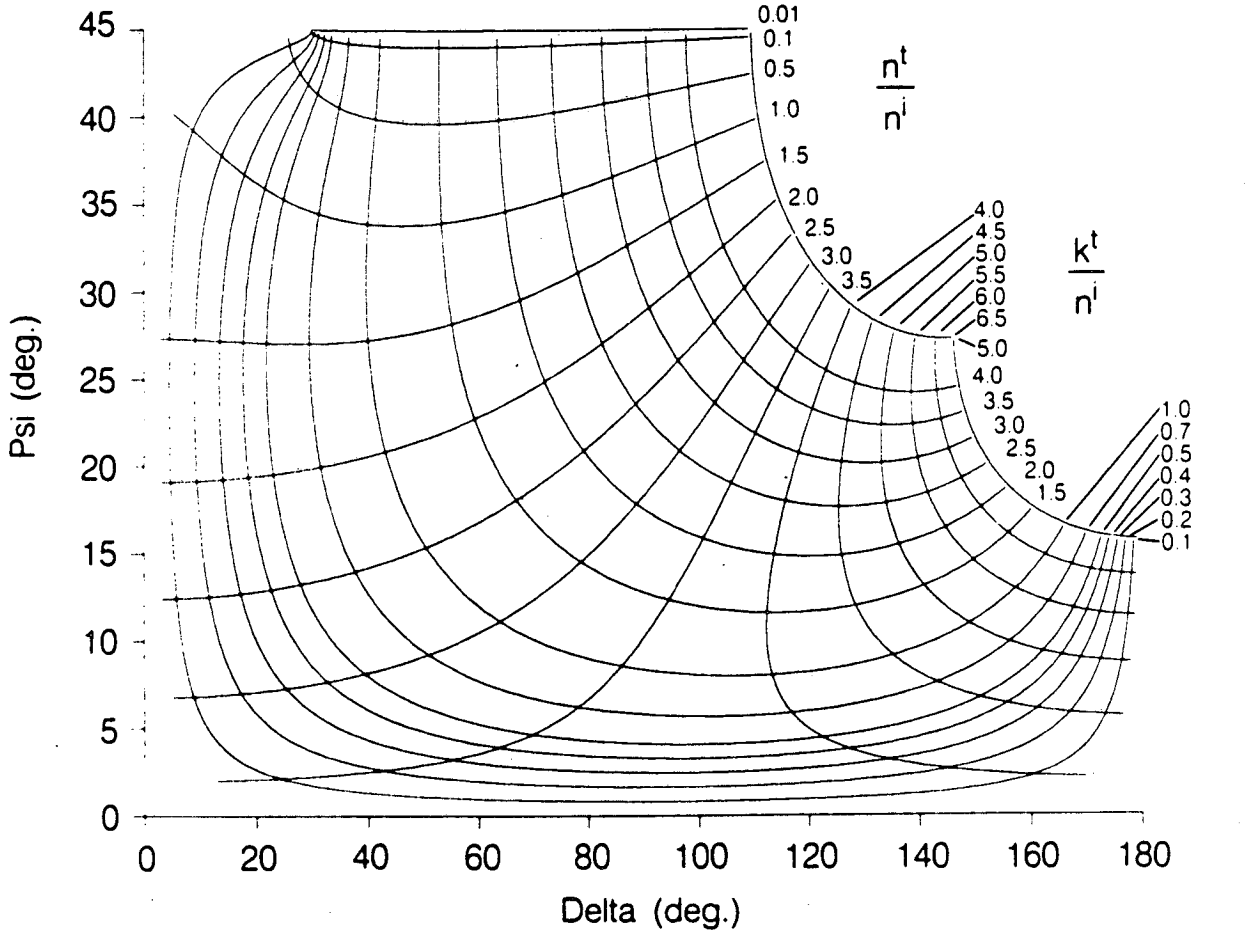

XBL 879-11169

Fig. 2.7

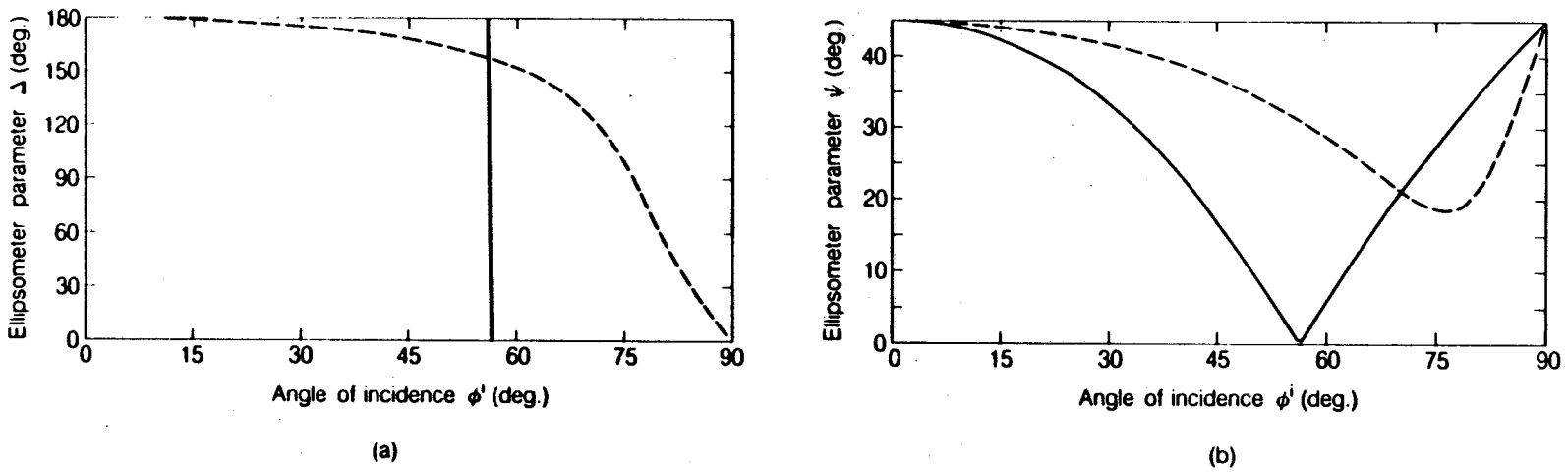

XBL 879-11155

Fig. 2.8

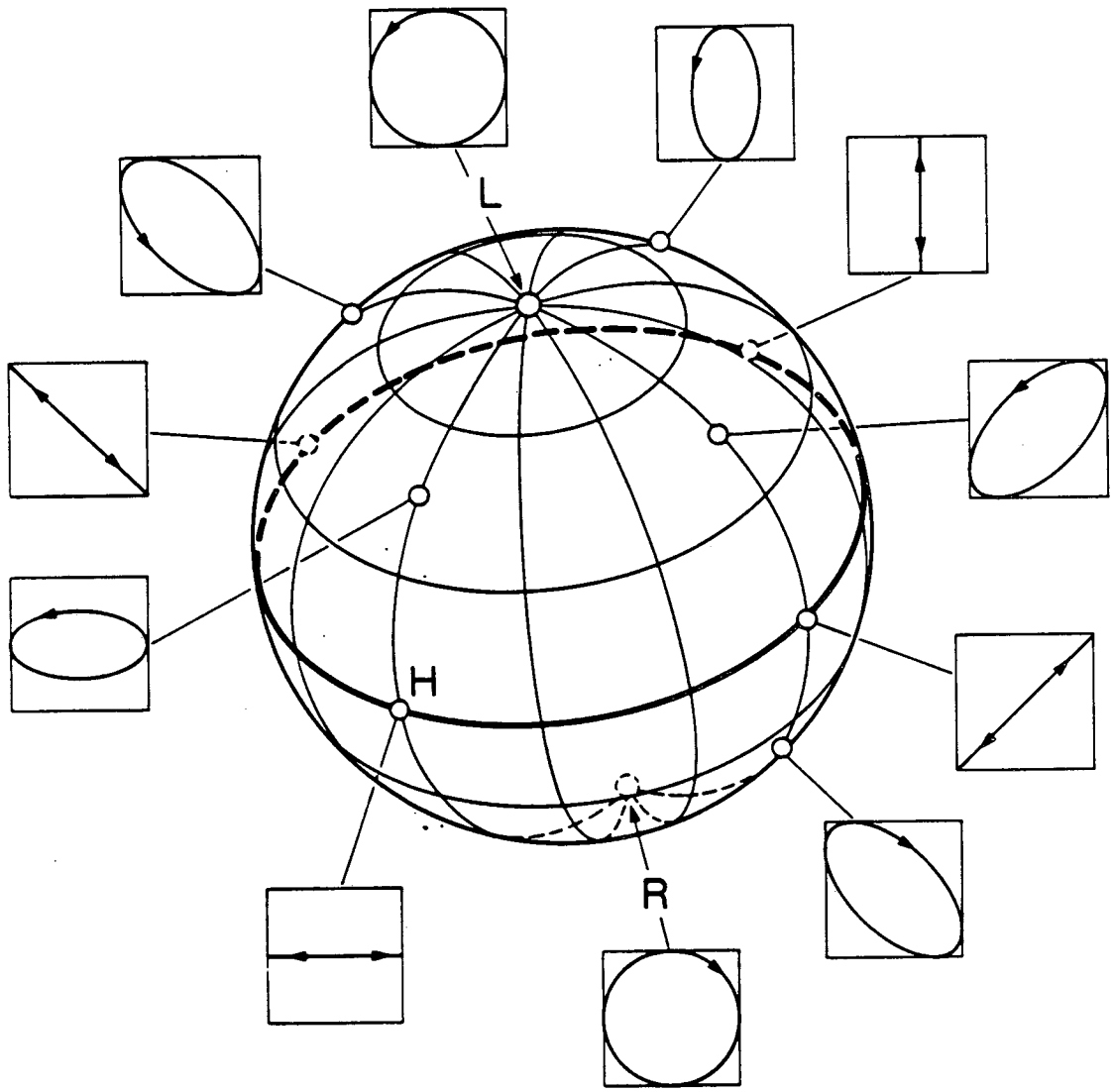

XBL 879-11147

Fig. 2.9

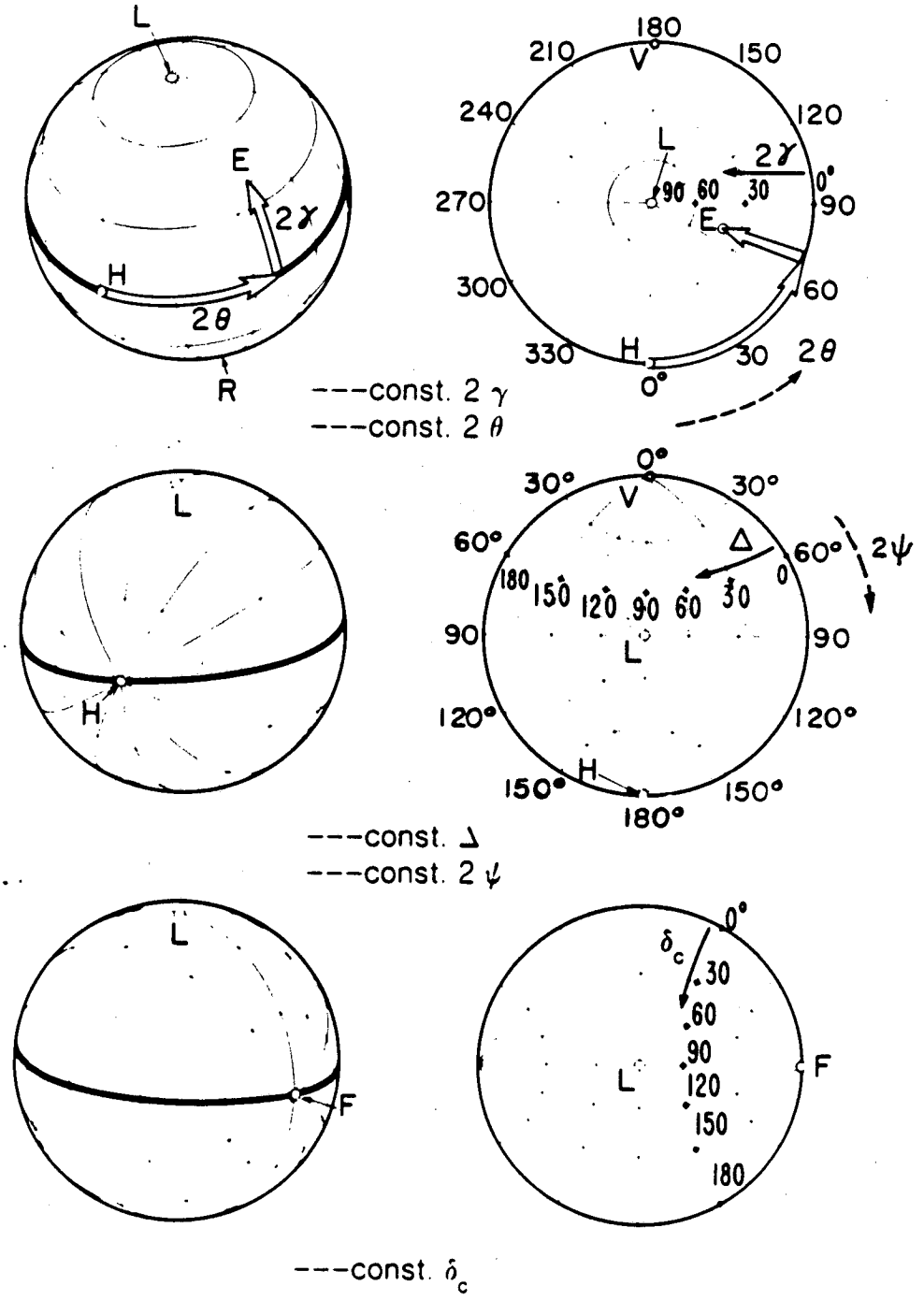

XBL 879-11160

Fig. 2.10

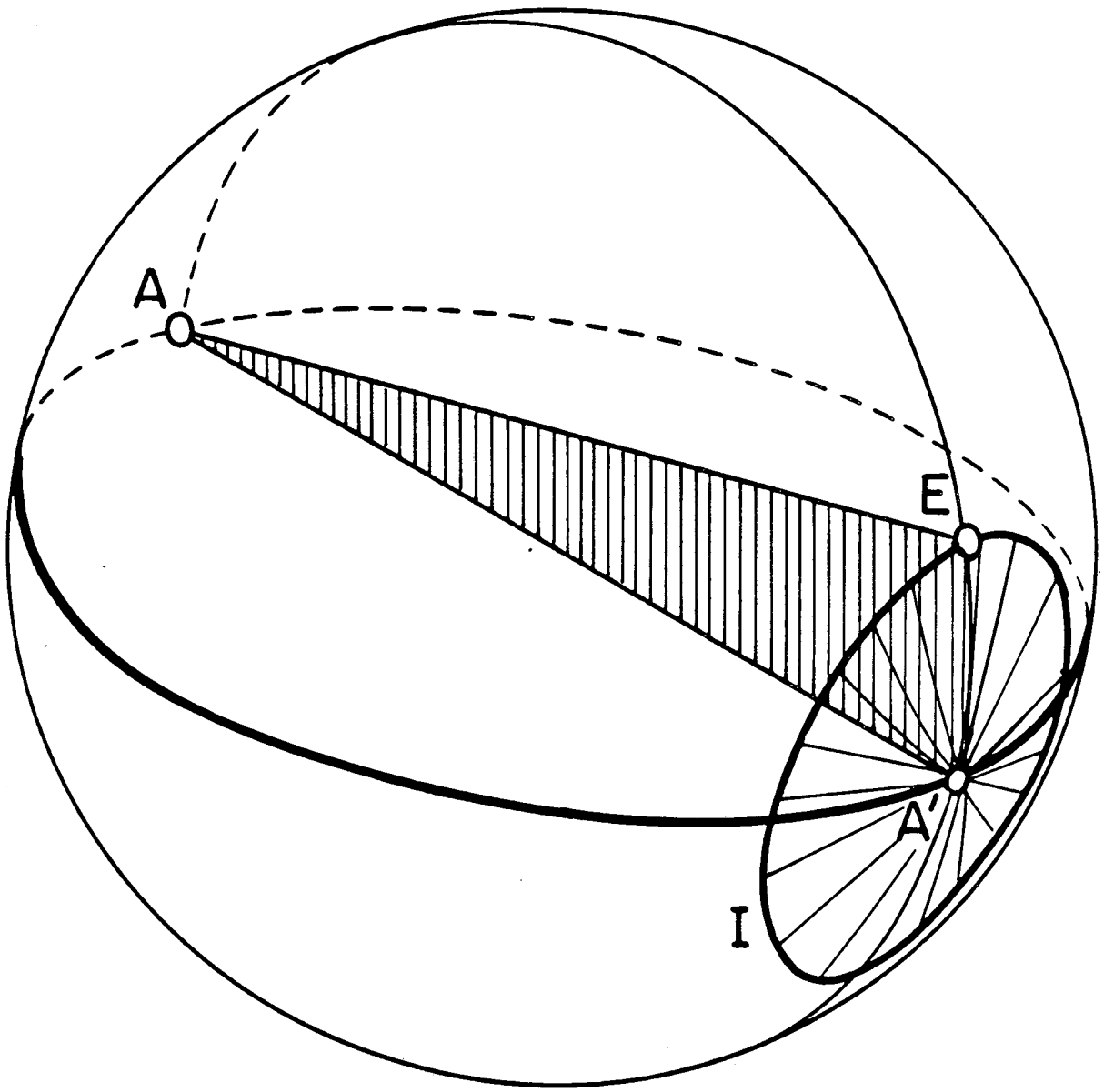

XBL 879-11163

Fig. 2.11

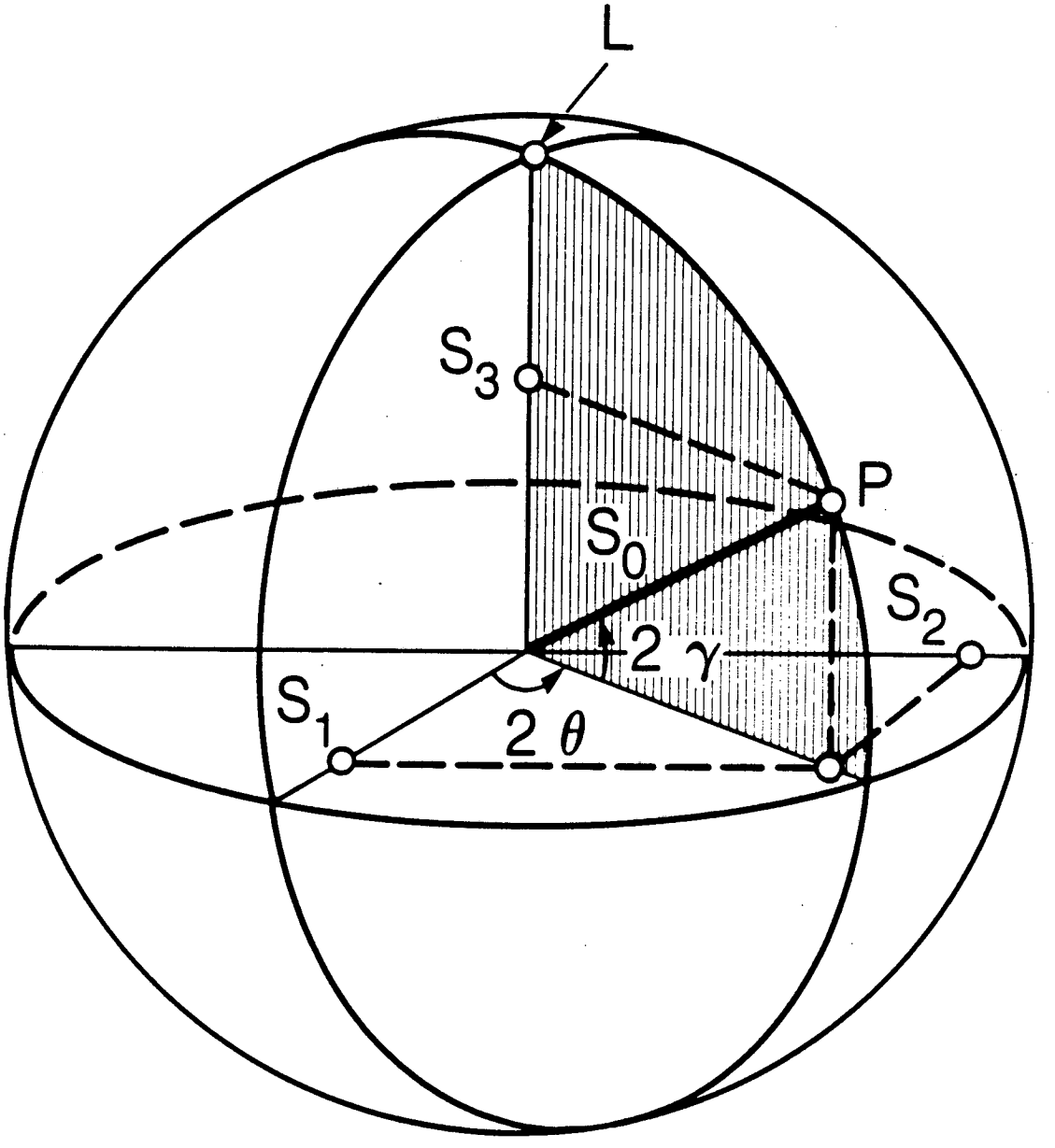

XBL 879-11151

Fig. 2.12

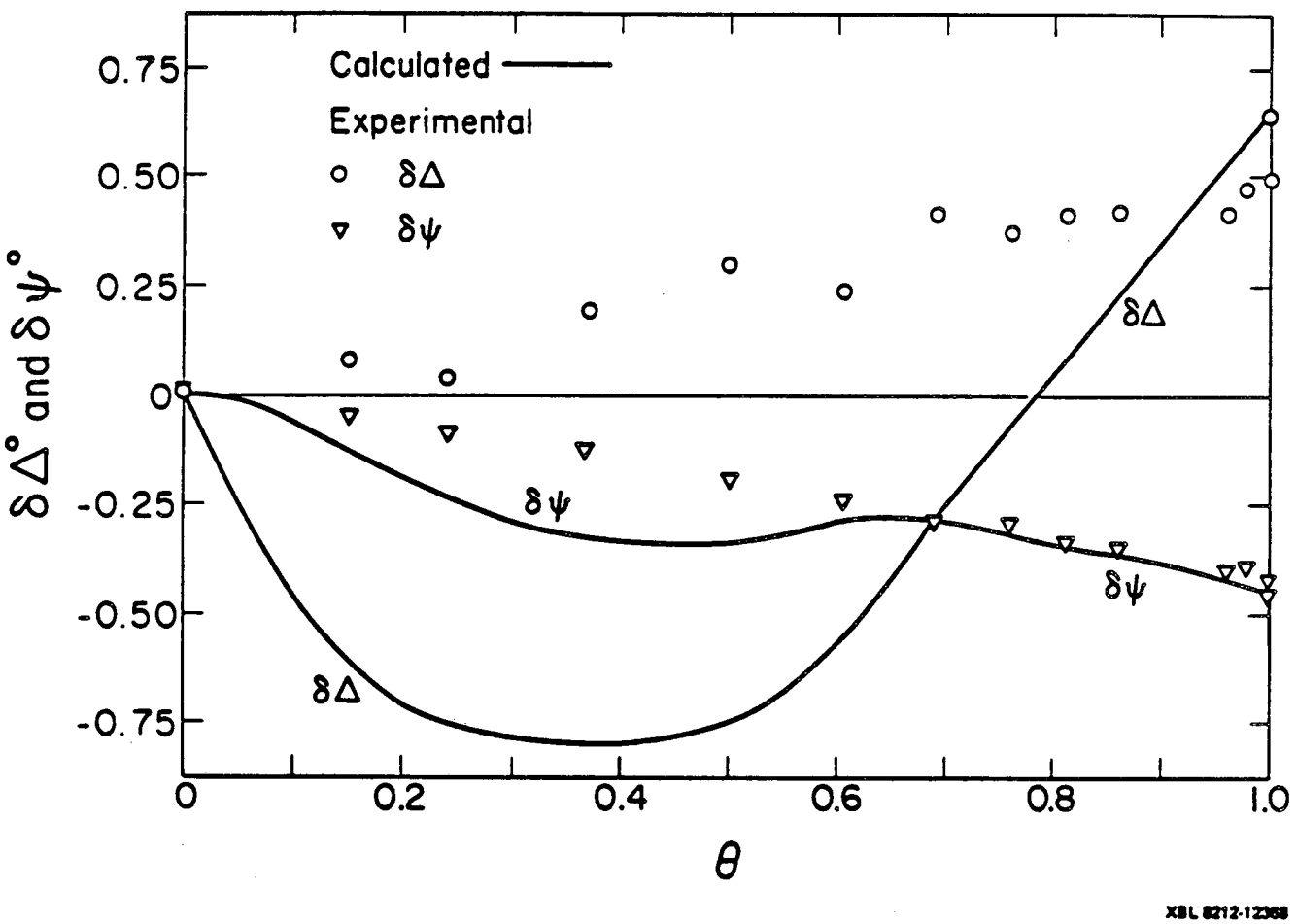
Calculated
Experimental
δΔ
δψ
0.75
0.50
0.25
0
-0.25
-0.50
-0.75
δΔ° and δψ°
δΔ
δψ
δψ
δΔ
0
0.2
0.4
0.6
0.8
1.0
θ
XBL 8212-12368

Fig. 2.13

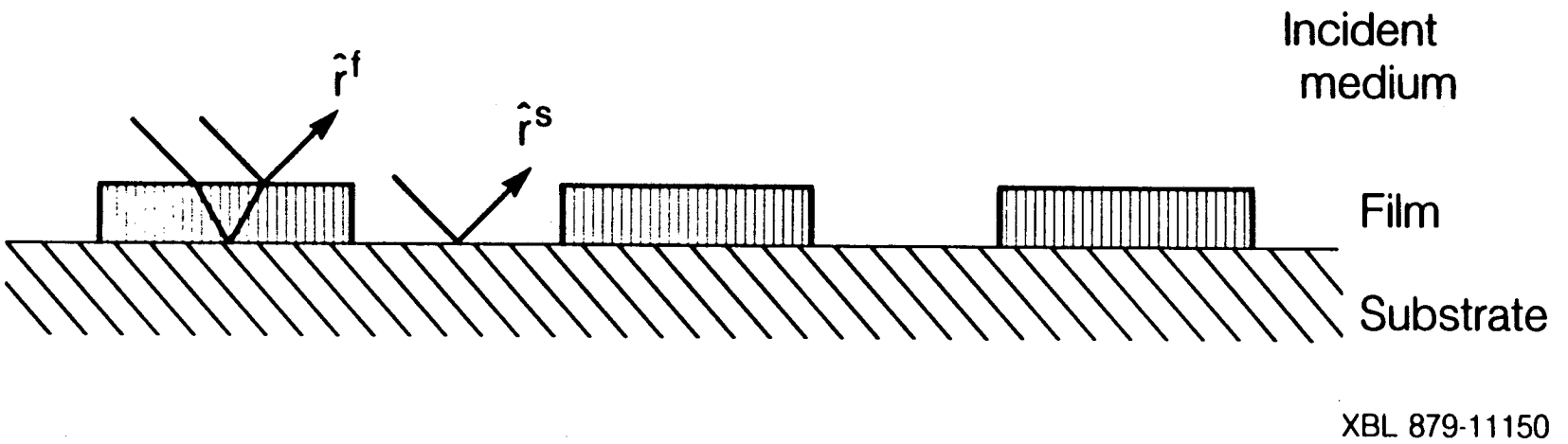

Fig. 2.14

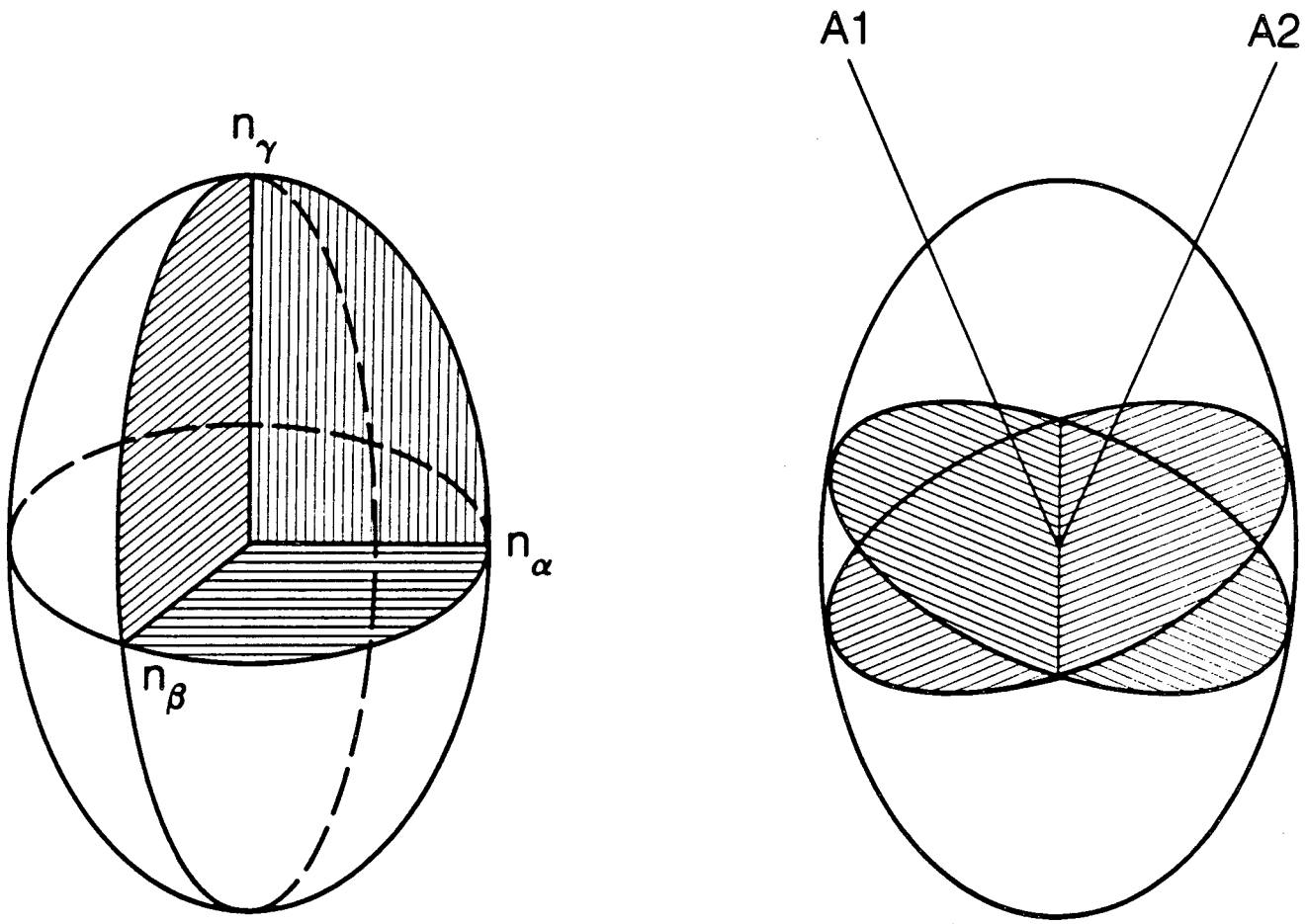

XBL 879-11144

Fig. 2.15

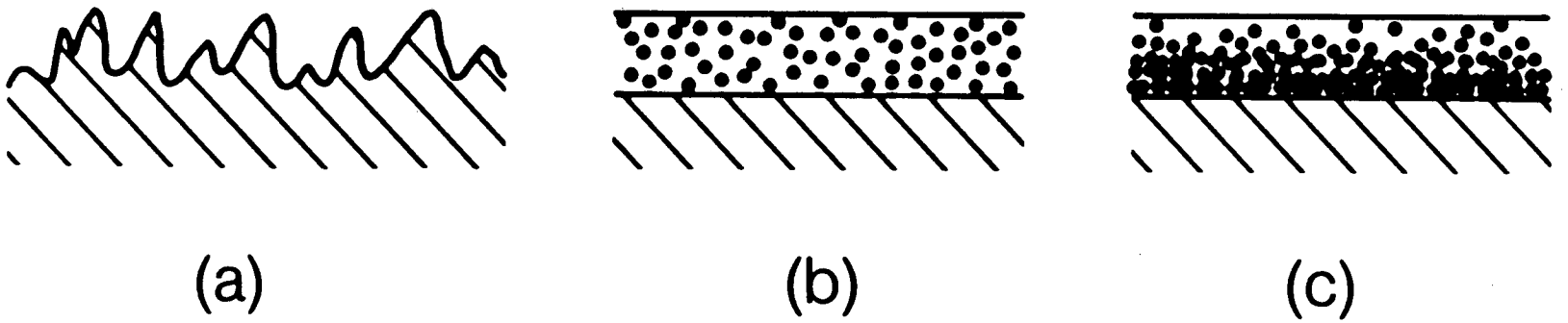

XBL 879-11148

Fig. 2.16

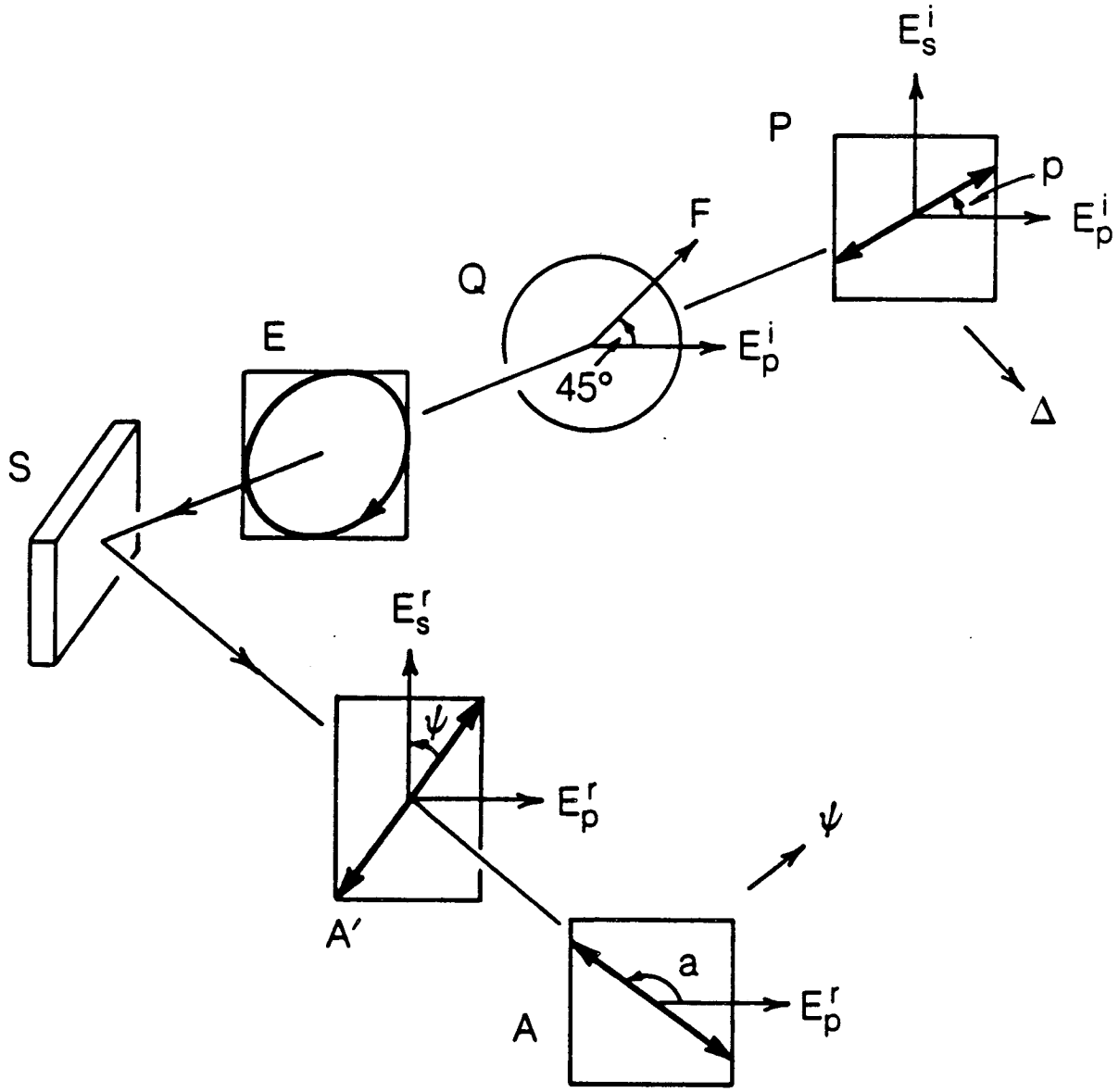

XBL 879-11156

Fig. 3.1

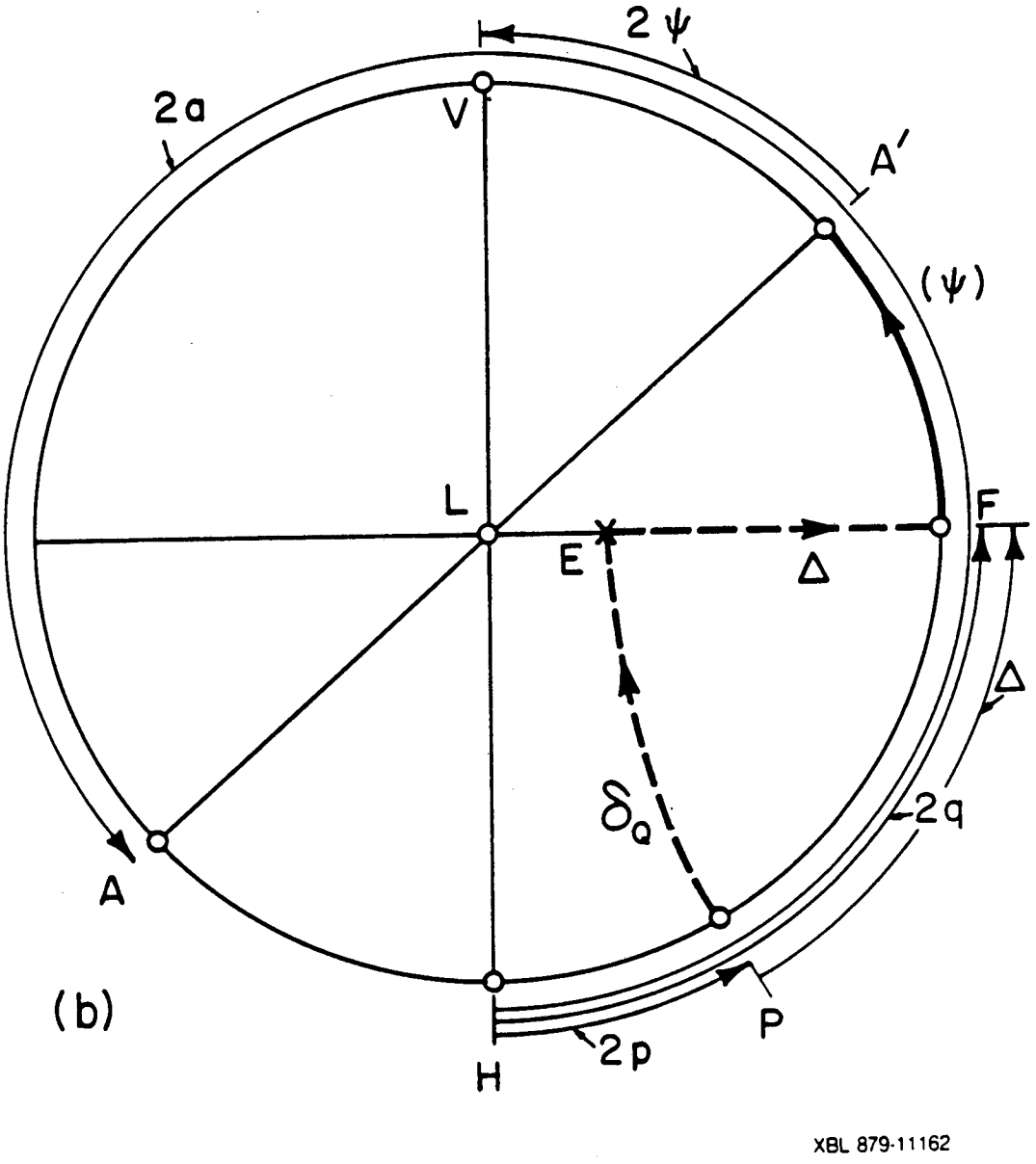

Fig. 3.2

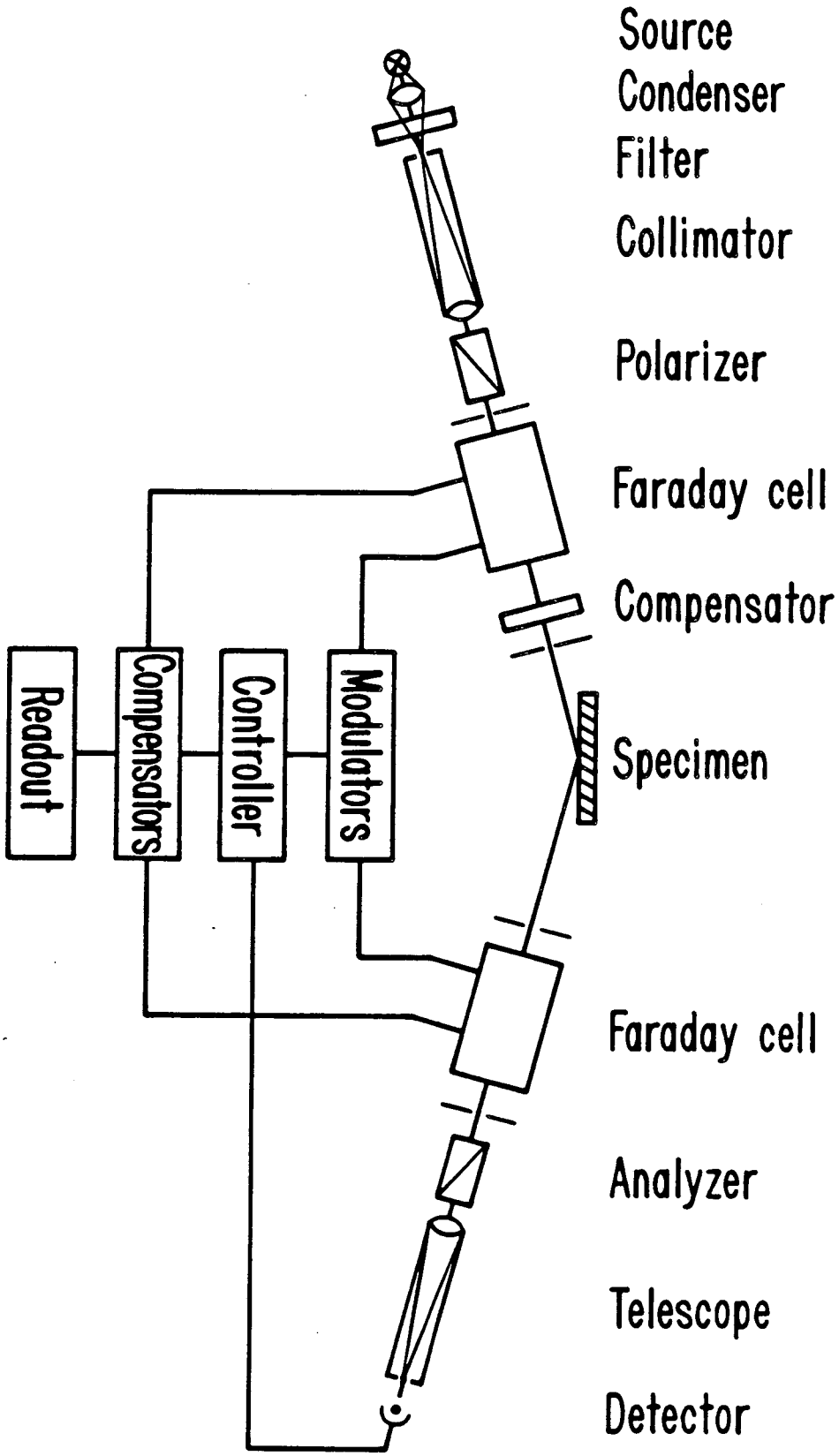

XBL 879-11161

Fig. 3.3

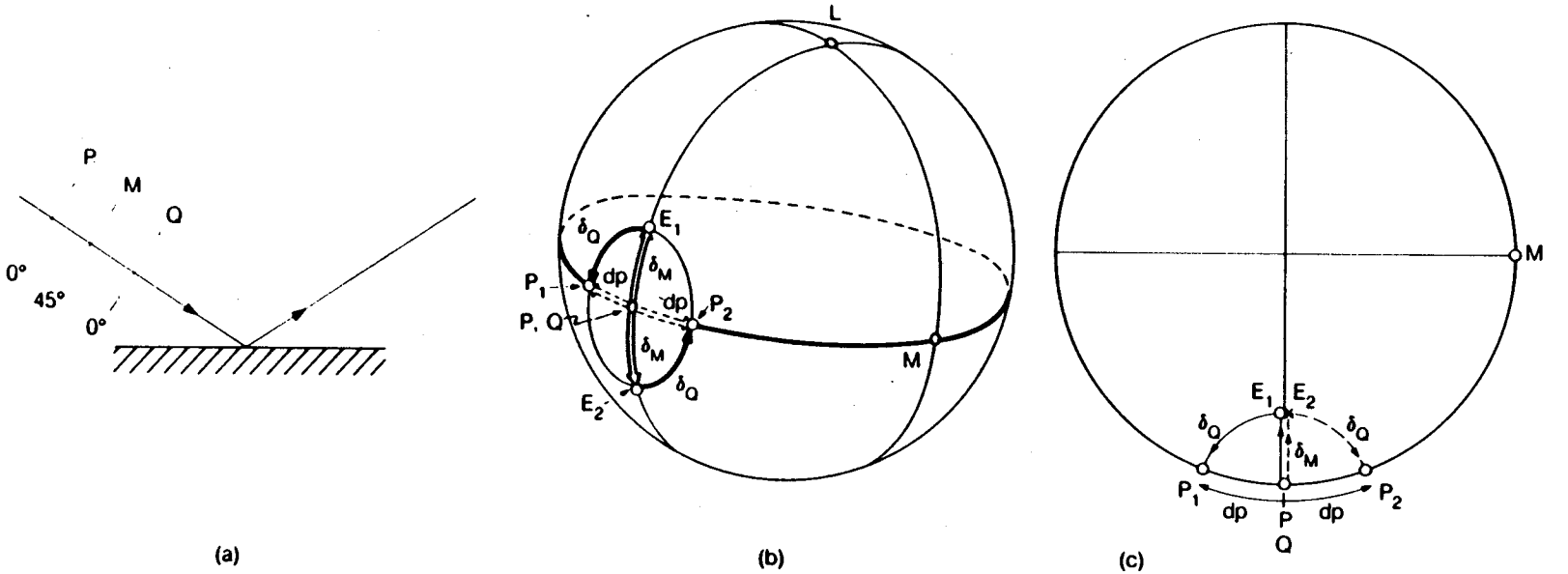
P
M
Q
0°
45°
0°
(a)
L
E1
δQ
δM
P1
dp
dp
P2
P, Q
δM
δQ
E2
M
(b)
M
E1
E2
δQ
δQ
δM
P1
dp
P
dp
P2
Q
(c)
XBL 879-11167

Fig. 3.4

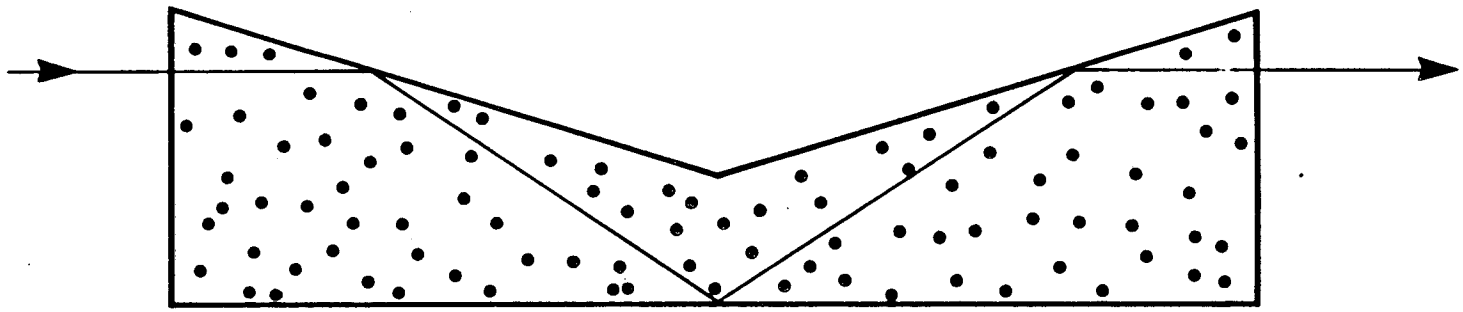

XBL 879-11146

Fig. 3.5

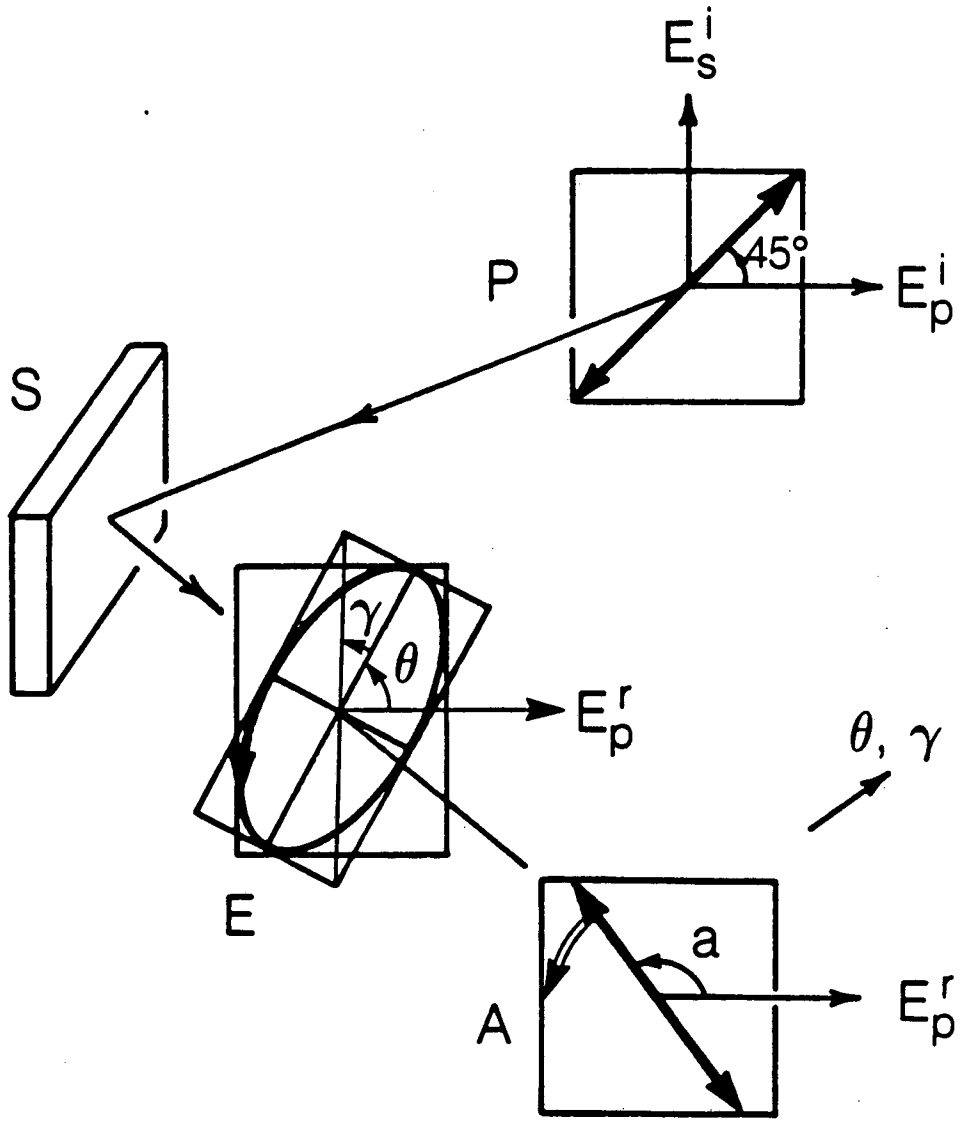

XBL 879-11157

Fig. 3.6

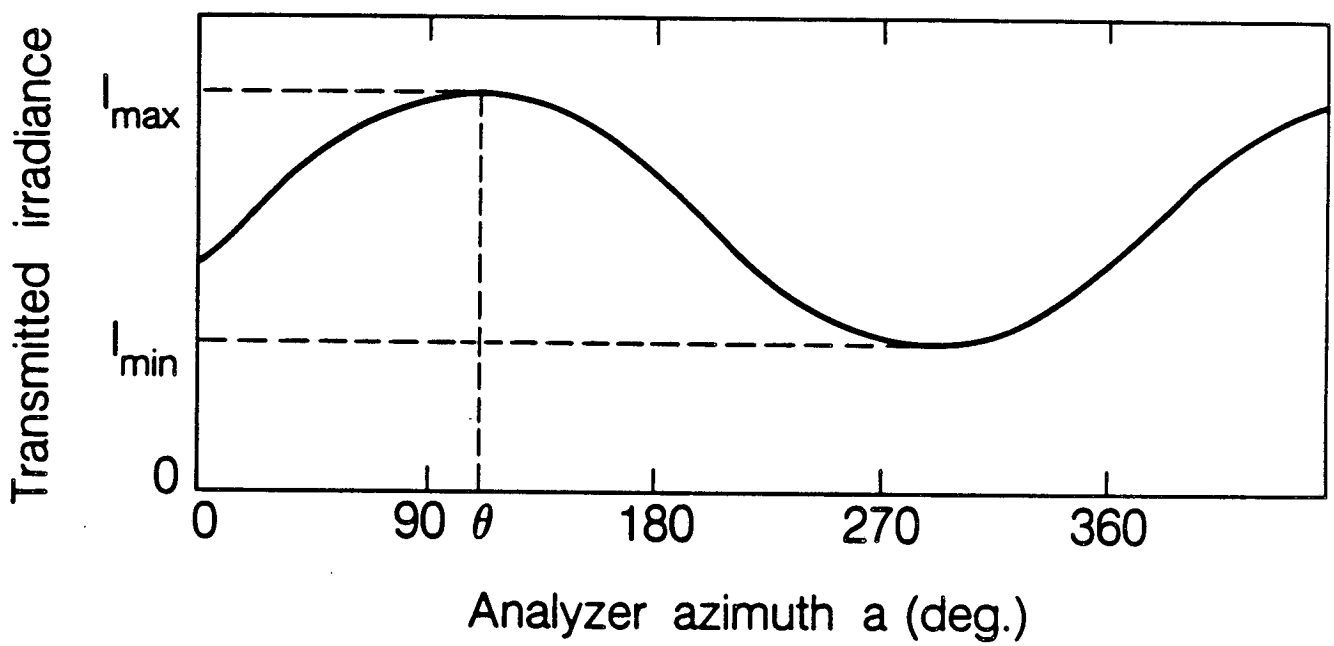

XBL 879-11143

Fig. 3.7

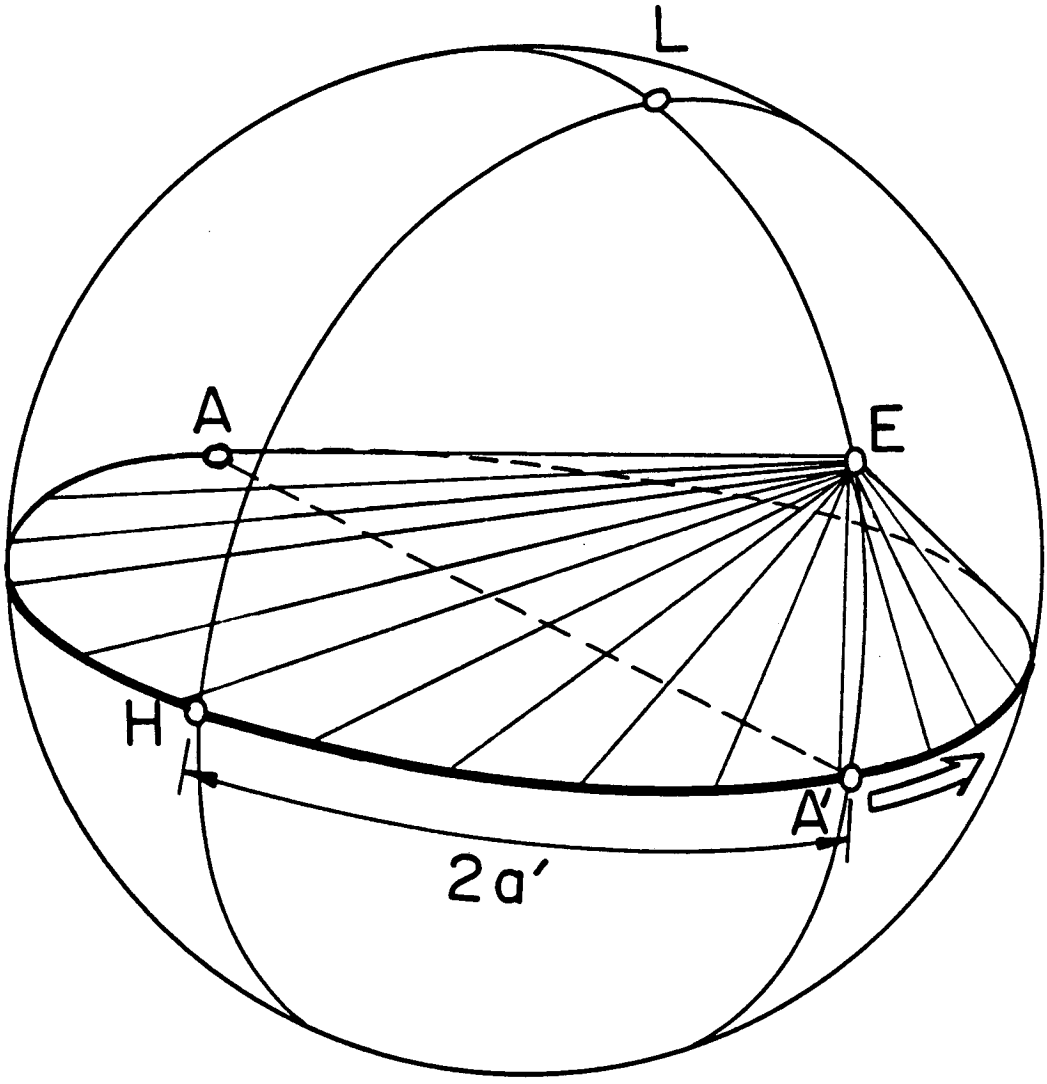

XBL 759-7247

Fig. 3.8

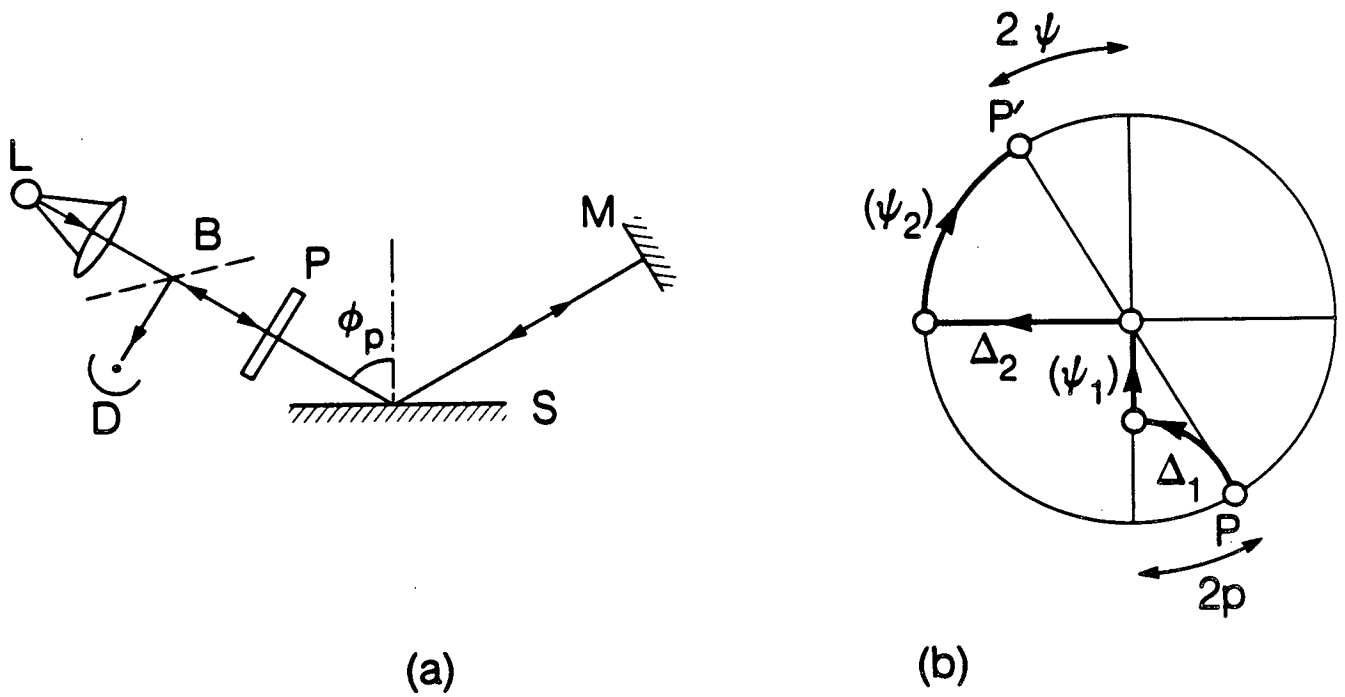

XBL 879-11168

Fig. 3.9

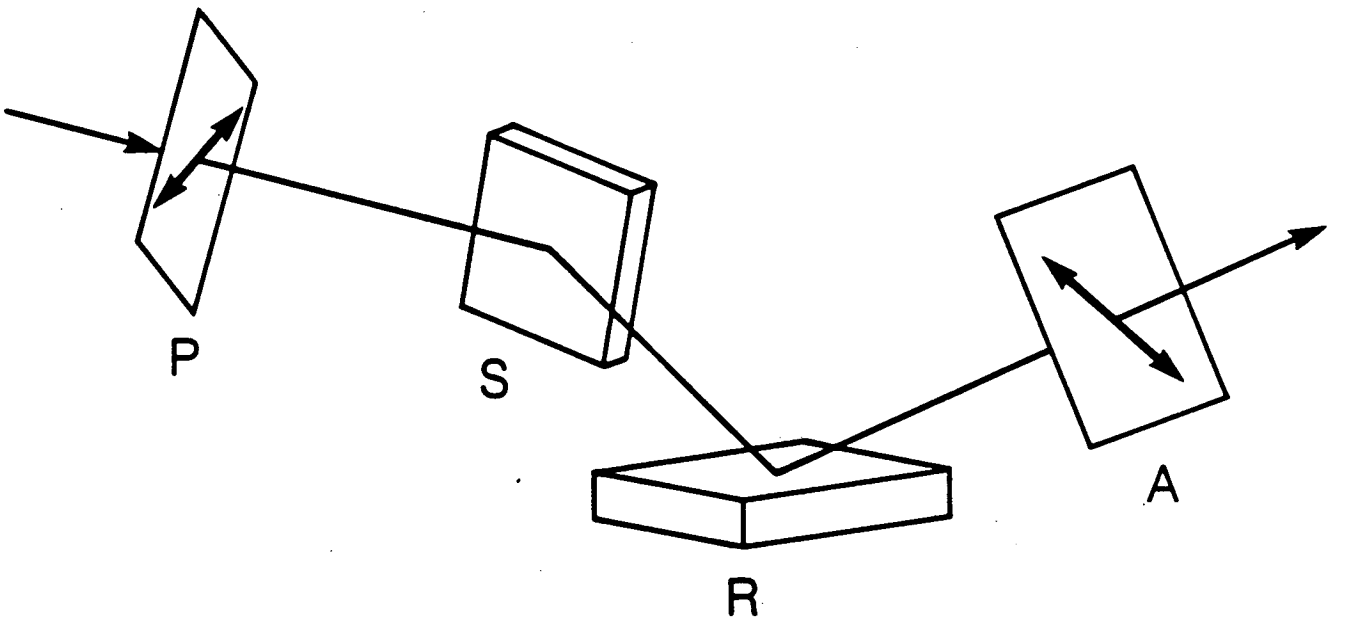

XBL 879-11145

Fig. 3.10

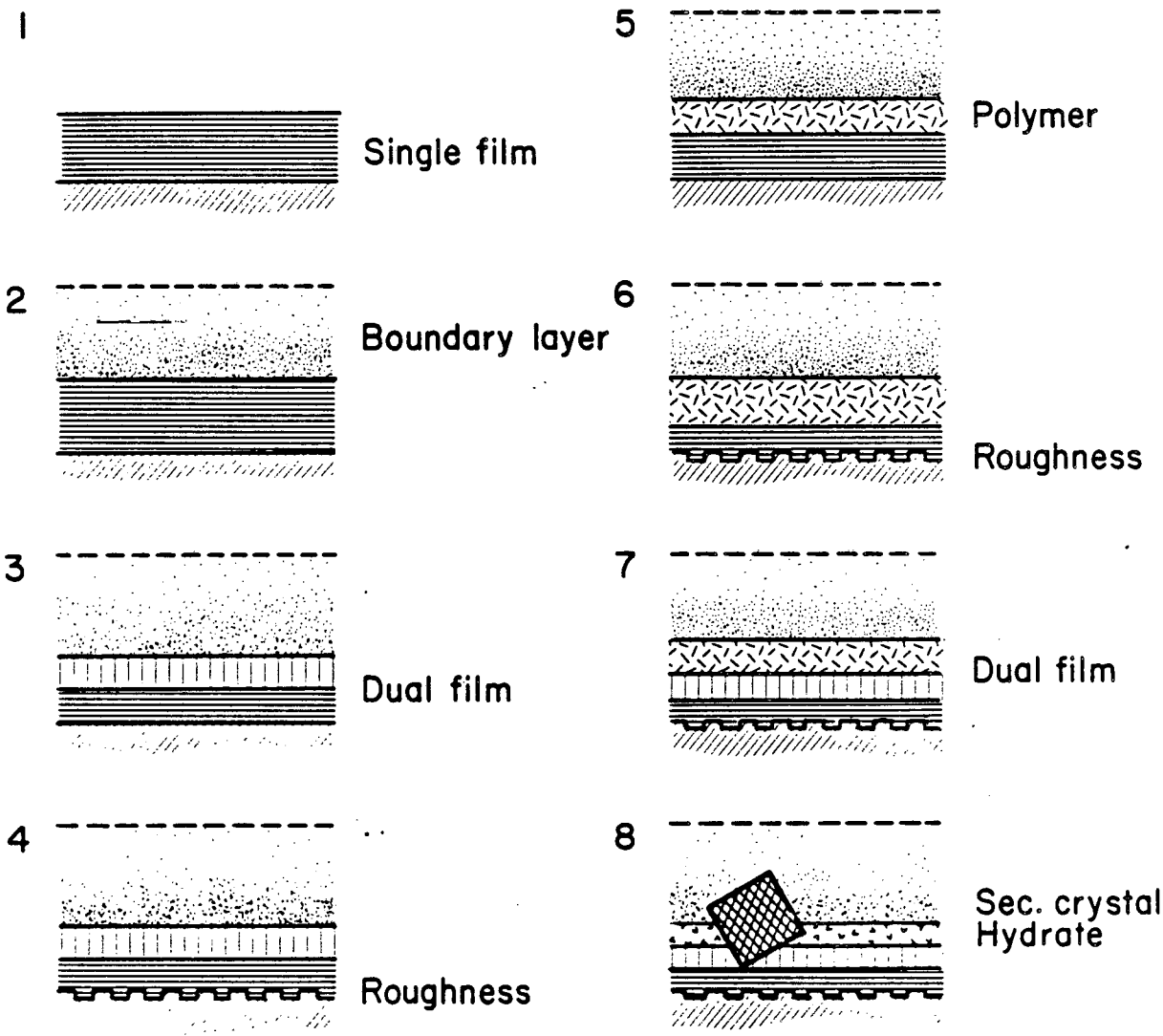

MODELS FOR ANODIC FILM FORMATION

XBL 785-871

Fig. 4.1

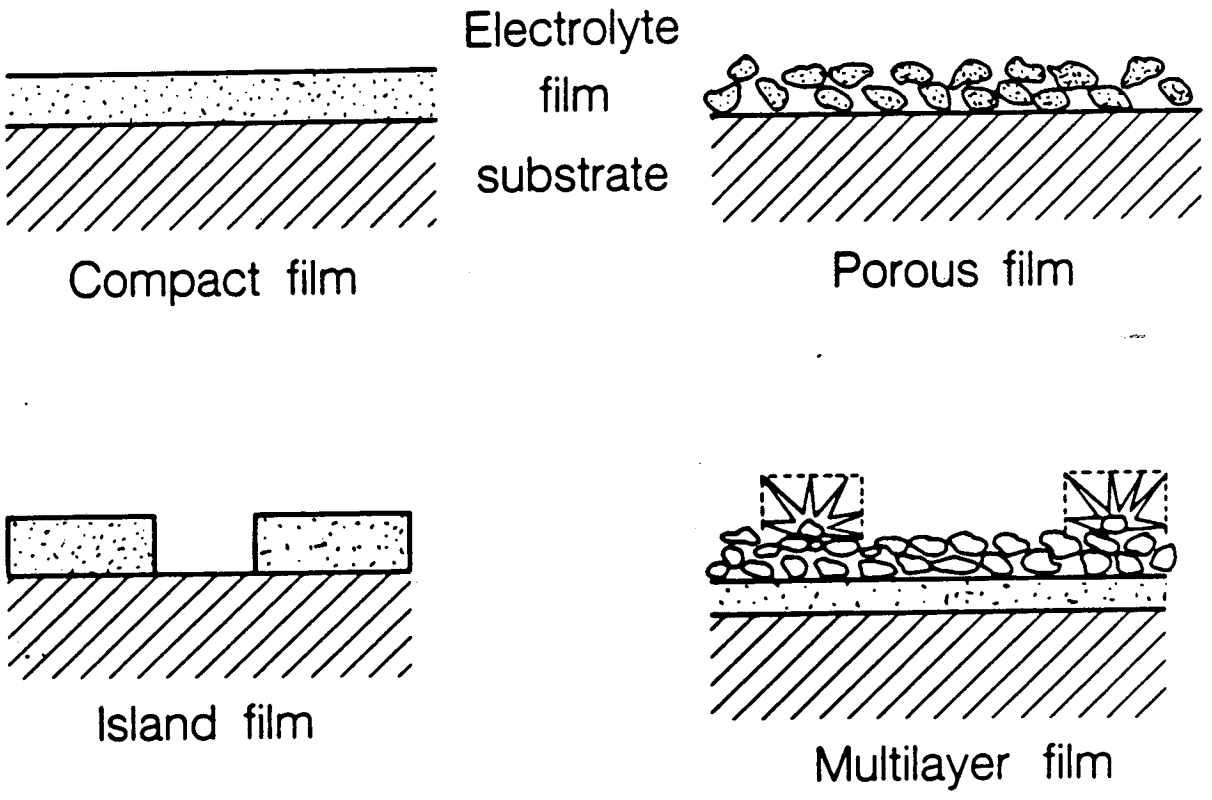
Electrolyte
film
substrate
Compact film
Porous film
Island film
Multilayer film
XBL 854-9812

Fig. 4.2

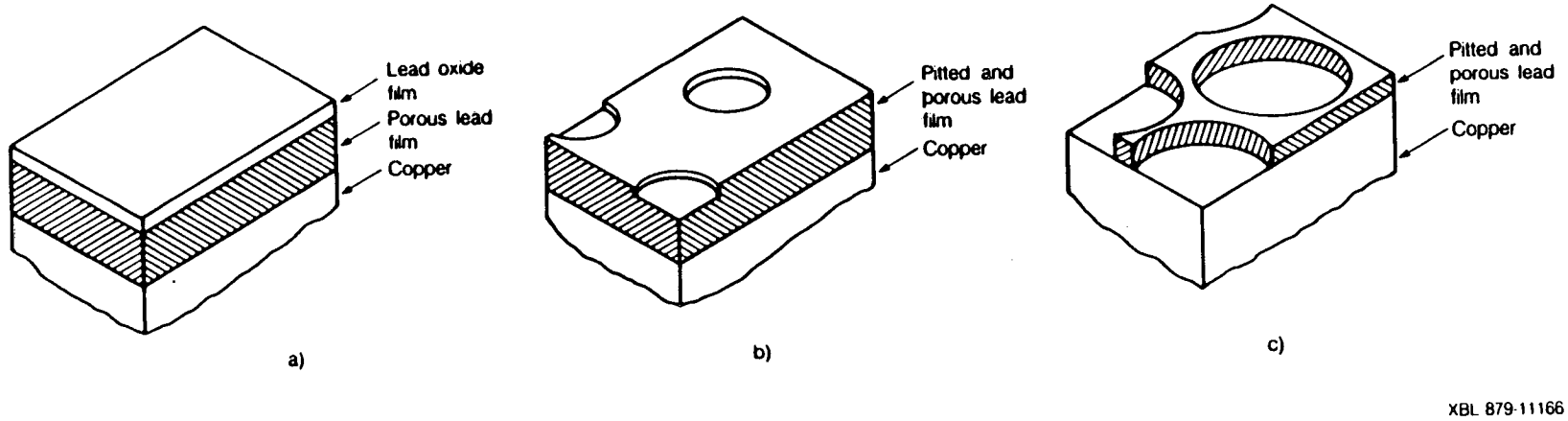
Lead oxide film
Porous lead film
Copper
a)
Pitted and porous lead film
Copper
b)
Pitted and porous lead film
Copper
c)
XBL 879-11166

Fig. 4.3

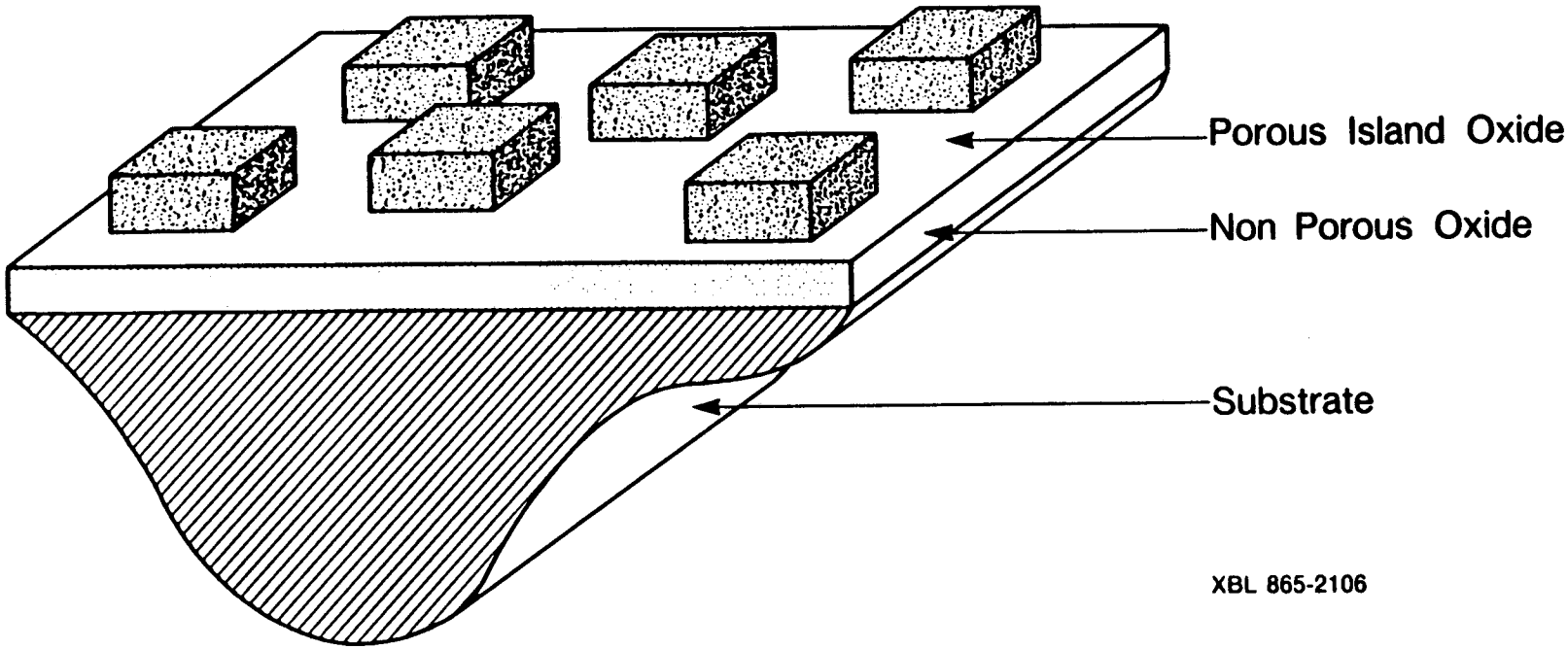
Porous Island Oxide
Non Porous Oxide
Substrate
XBL 865-2106

Fig. 5.1

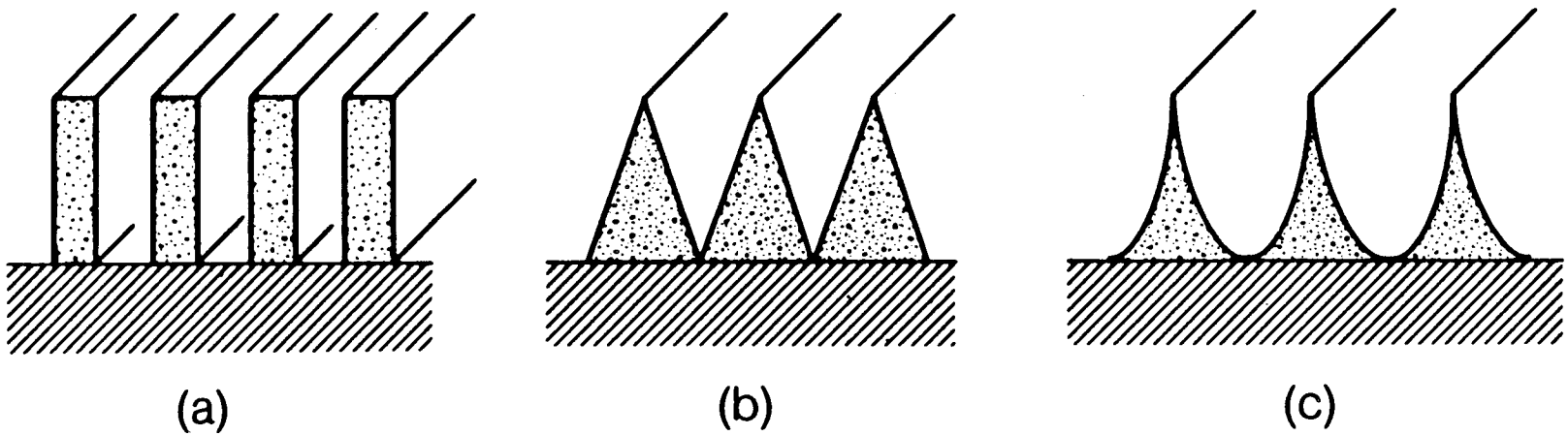

XBL 893-946

Fig. 5.2

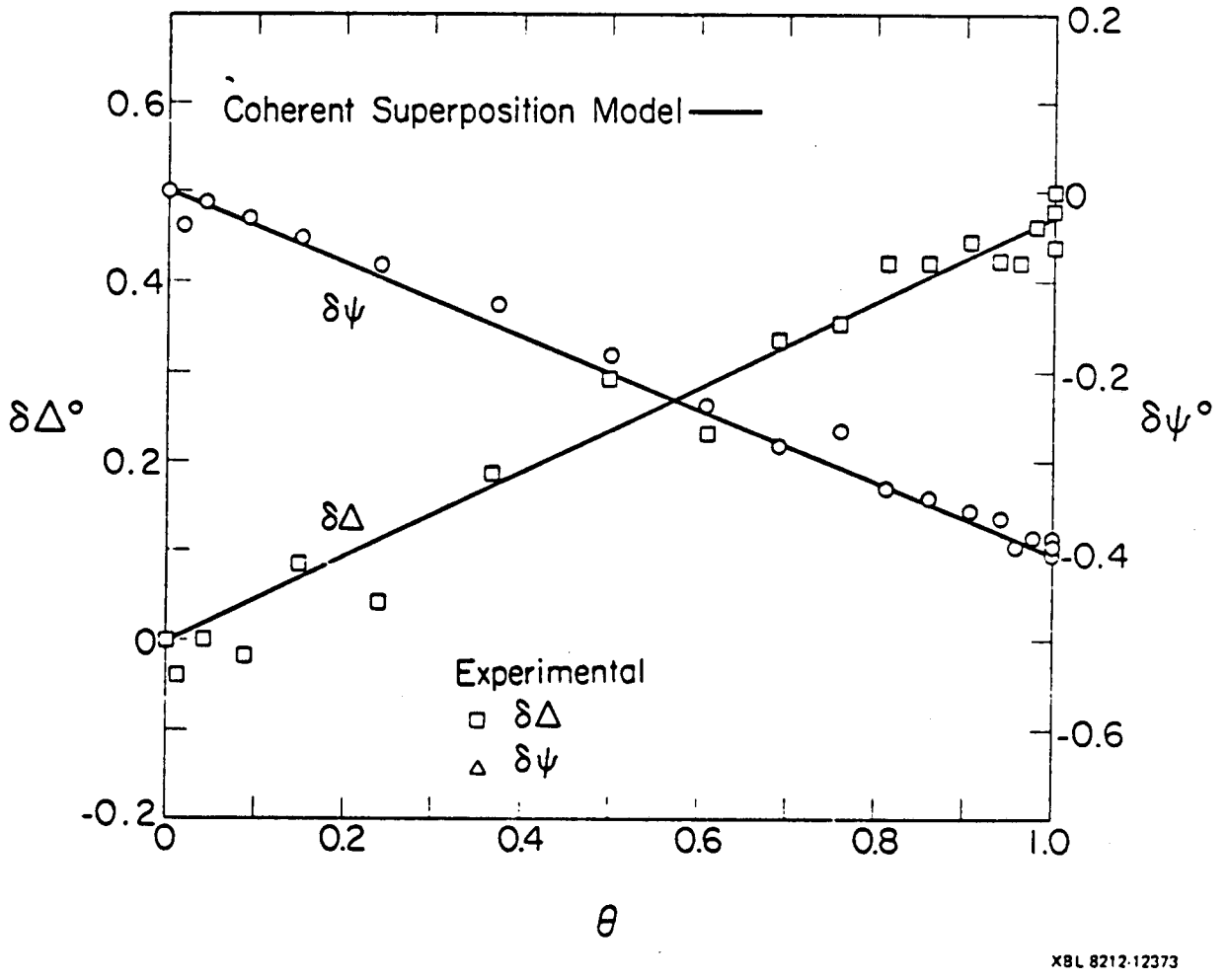
Coherent Superposition Model
δψ
δΔ
Experimental
δΔ
δψ
δΔ°
δψ°
θ
0.6
0.4
0.2
0
-0.2
0.2
0
-0.2
-0.4
-0.6
0
0.2
0.4
0.6
0.8
1.0
XBL 8212-12373

Fig. 5.3

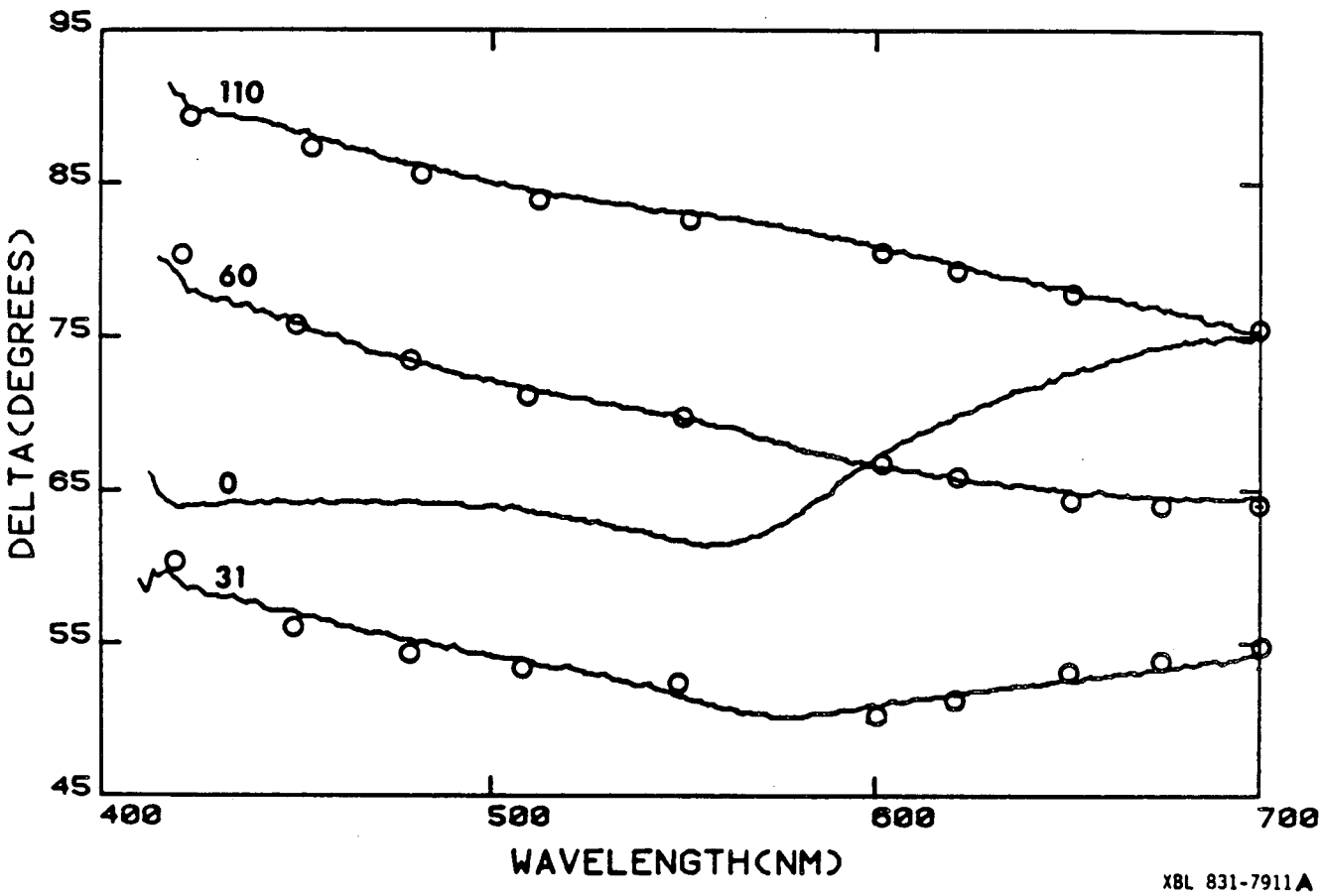
95
85
75
65
55
45
DELTA(DEGREES)
110
60
0
31
400
500
600
700
WAVELENGTH(NM)
XBL 831-7911A

Fig. 5.4

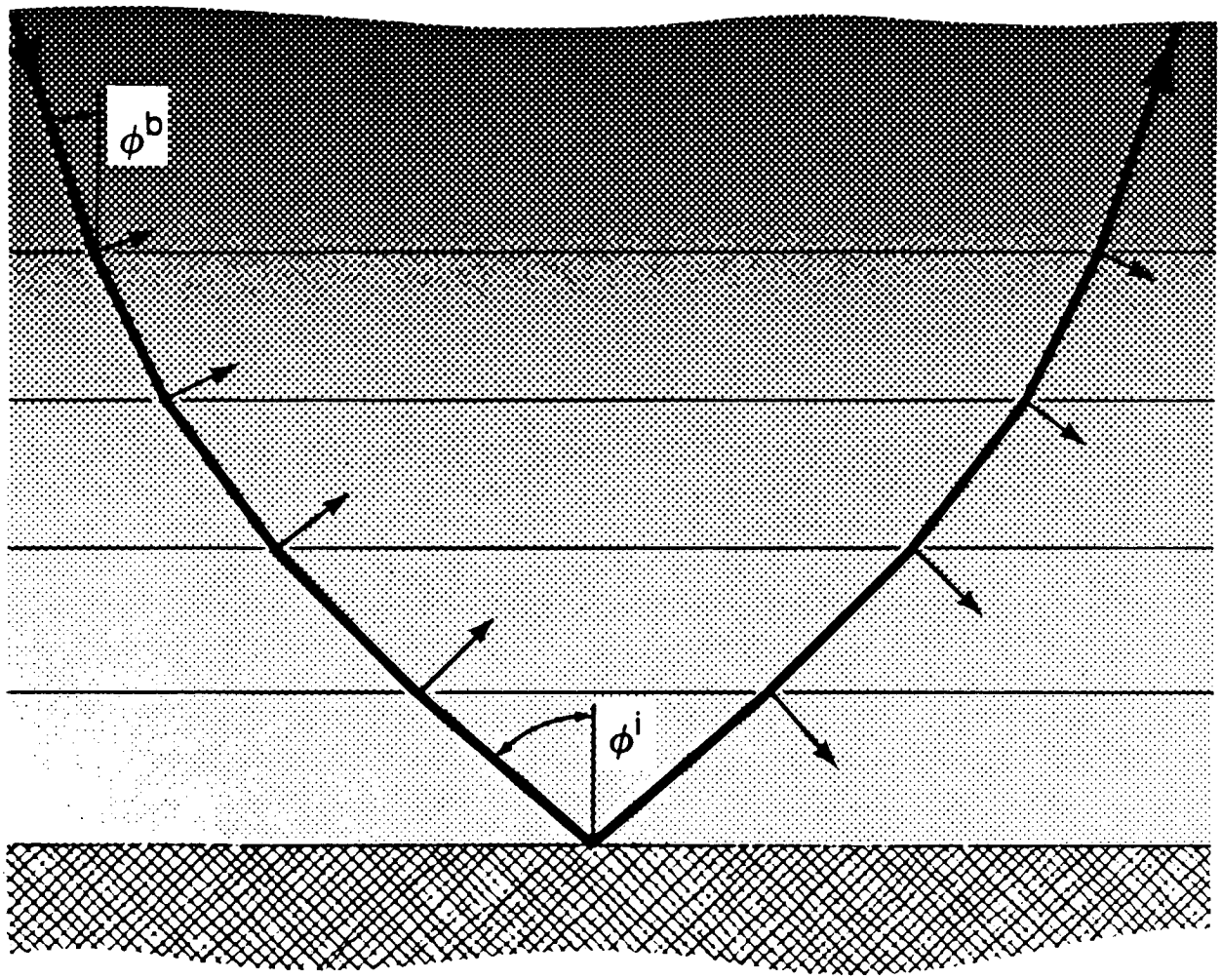

XBL 7611-4369 C

Fig. 5.5

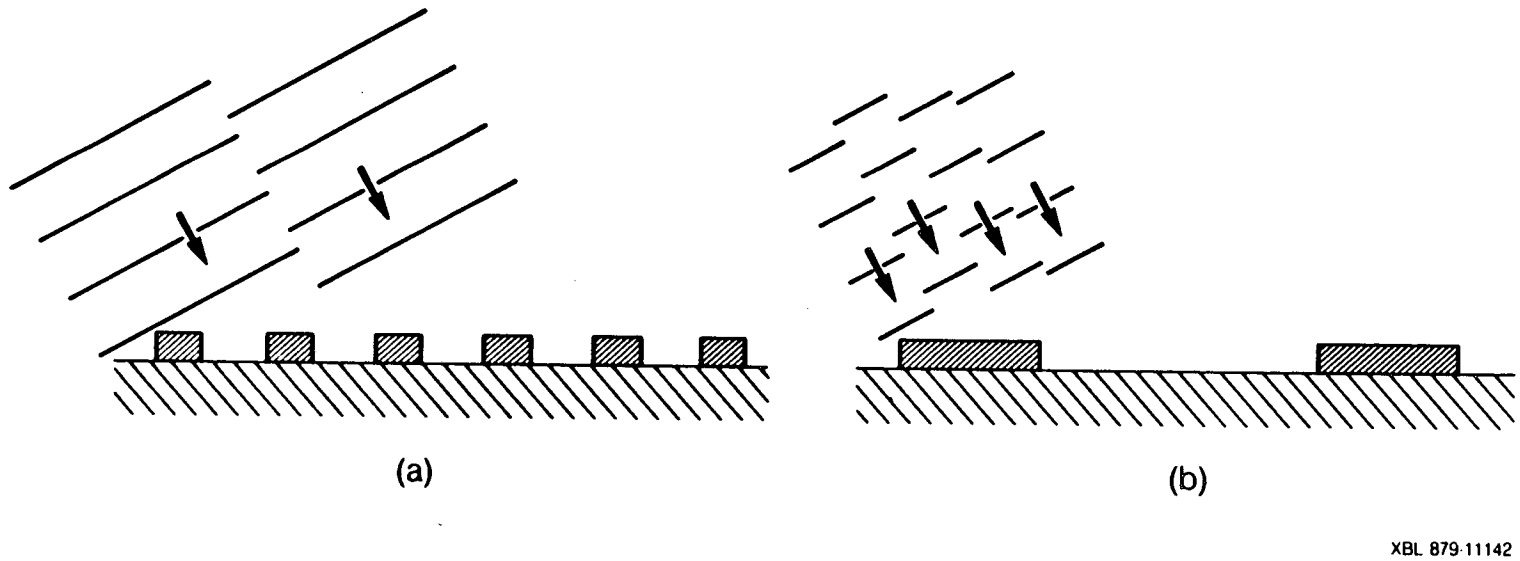

Fig. 6.1

LAWRENCE BERKELEY LABORATORY
TECHNICAL INFORMATION DEPARTMENT
1 CYCLOTRON ROAD
BERKELEY, CALIFORNIA 94720